NANOMATERIALS FOR PREGNANCY DETECTION

A DISSERTATION FOR THE DEGREE OF DOCTOR OF PHILOSOPHY SUBMITTED TO IMPERIAL COLLEGE LONDON

By Nawal Albilal

October 2014

Declaration of originality

I declare that I am the sole of author of the written work of this thesis and it is all written by my own words. This thesis has not been submitted for any degree, I also confirm that the referenced work has been cited and all assistance, which have been received to complete this work, has been acknowledged

Declaration of copyright

‘The copyright of this thesis rests with the author and is made available under a Creative Commons Attribution Non-Commercial No Derivatives license. Researchers are free to copy, distribute or transmit the thesis on the condition that they attribute it , that they don’t use it for commercial purposes and that they do not alter , transform or build upon it . For and reuse or redistribution, researcher must make cleat to others the license term of work’

Acknowledgment

Many people have a contribution in this thesis to be complete. I would like to thank all of those people who have supported me during my PhD journey. First and foremost, I would like to thank prince Banderi Al-Faisal for her finically support this project .An enormous thank you must go to professor Tony Cass for his help, gaudiness and patience.

I would like also to express my deepest gratitude to my husband as well as to my family for their encouragements. I am also grateful for all lab mates and post docs in Cass group for their help. Moreover, I am very thankful to Claudio zuliani from the department of Electrical and Electronic Engineering at Imperial College for his great contributions for this project in respect of his knowledge, experience, as well as for his time.

Last and certainly not least, thanks are given to Dr. Chaker Adra, Huda al-Mosallam, Lama Sultan and Arwa Faydh from king Faisal specialist hospital and research centre for their kindness and their support to facilities all the difficulties I have faced during my PhD period.

Abstract

Point of care (POC) is a powerful tool as a diagnostic test because of its advantage of being small, portable device and rapid results obtained. One major class of POC is the lateral flow assay (LFA), which is widely used for protein determinations. A home pregnancy test is the most successful example of the LFAs. A limitation of being quantitative or at best semi quantitative assay leads to improve the assay performance and to enhance its sensitivity. Hence, for this project, a switch from visual detections to electrochemical measurements is the primary goal, which occurred by developing the assay' concept with keeping the ease and robustness of the traditional LF assay. The integration of streptavidin lateral flow with electrochemical measurements (in particular voltammetric techniques) is the key element to introduce an electrochemical lateral flow assay (ELFA). This concept was based on the amplification of the polymer nanoparticles. A pH responsive eudragit S-100 was synthesized by nanoprecipitation process. These PNPs are encapsulated with redox active probe such as hydroxylmethyl ferrocene. Eudragit S-100 is dissolved at pH > 7 and it is insoluble in an acidic condition. This dissolution mechanism is preferable since the release of entrapped probe can be controlled until it is being detectable at the test line. Our findings summarized as follows; nanoprecipitation process is able to synthesis PNPs encapsulated both hydroxylmethyl ferrocene and methylene blue. These small-sized particles (~200 nm and ~300 nm) have a highly value negative zeta potentials (-34 mV and -29 mV). These two proprieties respectively, are important in enhancing the probe loading efficiency and in efficient adsorption with the antibody. From our data, it was found that more than 50% of the probes were encapsulated. Further characterizations were performed to investigate the probes' electroactivity as well as their electrochemical behavior. These voltammetric techniques include cyclic voltammetry and square wave voltammetry, the results suggested good electrochemical behaviors of both probes in respect of their release form the PNPs in immobilized format as well as in the aqueous phase. Importantly, an electrochemical lateral flow assay (ELFA) was investigated the FcMeOH-PNPs and was successfully demonstrated in the presence of varied concentrations of hCG compared to the control (absence of hCG). This indicates that the applied approach was proven. However, further improvements are needed. This led to move toward the screen-printed technology to realize a point of care device.

Table of Contents

Declaration of originality 2

Declaration of copyright 3

Acknowledgment 4

Abstract 5

List of table 8

Chapter 1 Introduction 9

1.1 Preamble 9
1.2 Point of care as diagnostic tools 11
1.3 Lateral flow assay (LFA) 12
1.3.1 Concept and layout of lateral flow assays 12
1.3.2 Limitations of LFAs and recent developments 16
1.4 A historical journey of pregnancy testing 18
1.5 The role of hCG 19
1.6 Nucleic acid aptamers 20
1.6.1 Aptamers as diagnostic reagents 20
1.6.2 SELEX process 21
1.6.3 Modification of RNA aptamers and ELONA 22
1.6.4. Spectroscopic studies of conformational of the RNA nucleic acid aptamers 24
1.7 Nanomaterial 25
1.7.1 Polymeric nanoparticles as a carrier system 25
1.7.2 Antibody conjugated polymeric nanoparticles. 26
1.7.3 Synthesis of the polymer nanoparticles via nanoprecipitation 27
1.7.4 Characterization of the nanoparticles 28
1.8 Electrochemistry 29
1.8.1 The electrochemical cell 30
1.8.2 Voltammetric techniques 31
1.9 Screen-printed electrode on paper substrate 32
1.10 The aim 33

Chapter 2 Experimental 35

2.1 Chemical and materials 36
2.2. Molecular Biology' experiments 38
2.2.1. 2nd strand synthesis 39
2.2.2. Chloroform extraction and ethanol precipitation 39
2.2.3. In vitro transcription 39
2.2.4. Urea polyacrimde gel electrophoresis 39
2.2.5. The quantification of RNA/DNA 40
2.2.6 Biotinylation of RNA aptamer 40
2.2.7. ELONA assay 41

2.2.8. Circular dichroism (CD) of RNA aptamer 42
2.3. Nanoparticles experiments 42
2.3.1 Synthesis and characterization of the polymeric nanoparticles (PNPs) 42
2.3.2. The purification of redox probe-encapsulate beads 43
2.4 Characterization of PNPs 43
2.5 Electrochemical experiments 44
2.5.1 Screen-printing based on NC membrane 45
Chapter 3 Results and discussion: Characterization of anti-hCG aptamer 46
3.1 Aptasensors 46
3.2 Size analysis of RNA aptamer 48
3.3. The conformational structure of RNA using CD 48
3.4 ELONA 53
3.6 Discussion 56
3.7 Summary 56
Chapter 4 Synthesis and characterization of the polymer nanoparticles 57
4.1 Nanoparticles synthesis 57
4.2 Purification of the PNPs by centrifugation 59
4.3 Size analysis by dynamic light scattering (DLS) 62
4.4 Zeta potential 63
4.5 Loading efficiency 64
4.6 Discussion 73
Chapter 5 Release of entrapped redox probes as a function of increased pH 75
5.1 Release of redox probes under alkaline conditions 76
5.2 Dissociation of PNPs via the enzymatic reaction 86
5.3 Discussion 91
Chapter 6 An electrochemical lateral flow assay (ELFA) and screen printing technology 92
6.1 An electrochemical lateral flow assay (ELFA) 92
6.2 Discussion 94
6.3 Screen printed NC membranes 95
6.4 Discussion 96
Chapter 7 Conclusion and recommendation for the future work 98
7.1 Conclusion 98
7.1 Future work 99
Bibliography 100

List of table

Table 2-1 Chemical and supplier _____ 36
Table 4-1 The properties of five chosen redox probes _____ 58
Table 4-2 The parameters of eudragit S100 nanoprecipitation _____ 59
Table 4-3 the concentration of the entrapped ferrocene methanol _____ 66
Table 4-4 the concentration of the entrapped of Methylene blue _____ 68
Table 4-5 Nanoprecipitation conditions to synthesis (150-250nm)-particles _____ 73

Chapter 1 Introduction

1.1 Preamble

In the 21th century the identification of analytes using wearable and portable devices rather than laboratory methods can offer several advantages such as real-time outcomes, reduced costs, the ease of performance and the production of reliable and accurate results[1]. The sensing devices would be beneficial not only for the healthcare sector, but also for the industrial and environmental-protection industries. Particularly, the use of non-laboratory based medical devices in the context of biomedical analysis has generated the concept of the thus called point of care (POC), i.e., a diagnostic test performed near to the patient care[2]. The advantages of POC are both economical and clinical, since these systems allow cutting the public expenditure associated with the traditional lab-based analytical testing, providing outcomes in real-time and empowering people in self-managing their health. The majority of medical devices lately-introduced have been developed for the home-market in response to the demand of the public for low-cost analysis and self-medication[3]. Indeed, in our houses we have become increasingly accustomed to glucose, cholesterol test, and pregnancy-detection. Immunosensors such as that for HIV and hepatitis B virus have become available at the clinics[4]. Point of care devices play an important role in improving the healthcare for example a rapid and accurate diagnosis of the disease at an early stage provides the appropriate and timely treatments for the patients[5]. For example, an early diagnosis of the pregnancy helps to pay more attention for the developing fetus by providing the mother with special needs and stopping her from taking harmful medications. In return, avoids the loss of the pregnancy and results in a successful delivery[6]. Considering these facts and some other criteria regarding the device specifications (such as cost, and size), many efforts have been made to provide the markets with more advanced and accurate devices for several analytes. Thus the aim for this thesis is: to enhance the performance of exiting point of care and to provide an accurate numerical device. This is achieved by developing a novel concept based on lateral flow assay (LFA) to use at a point of care.

For the work presented in this thesis, two detection strategies have been employed. Both of these methods are based on electrochemical measurements, which provide

quantitative data as well as to enhance the assay sensitivity. The first strategy aimed to develop an aptasensor by using an anti-hCG aptamers. This aptamer was synthesised in vitro and then was characterized to determine its binding affinity (K_D). The RNA conformational structure was also investigated using a spectroscopic technique. It is quite challenging to use RNA aptamer to detect hCG since more efforts have been made in developing an immunosensor rather than aptasensor. These applications were varied from quantitative detections in particular an electrochemical immunosensor to colorimetric detections. For example, an electrochemical immunosensor has been developed for the detection of hCG by introducing nanolabel, which was based on prussian blue-carbon nanotubes /gold nanoparticles (GNP-PB-CNTs). This strategy showed a low detection limit of 0.023 mlU/ml[7]. Additionally, a gold-linked immunoassay (GLIA) with single wall carbon nanotubes (SWCNT) was able to detect dawn to 0.024 ml/Uml of hCG[8]. The second strategy was the development of an electrochemical lateral flow assay (ELFA). This was achieved by the amplification of the polymer nanoparticles, which were able to encapsulate and release redox active molecules. This novel concept of hCG detection can also be applied for various analytes. Moreover, the integration of the screen-printing technology with LFA would provide markets with a cheap numerical, disposable, and accurate point of care devices with keeping the simplicity of the traditional LFA. This thesis is divided into seven chapters. The first chapter delivers a literature review of POC with special emphasis on pregnancy detection. This chapter presents also a brief history regarding the evolution of pregnancy detection systems together with an overview of the pregnancy hormone. The second chapter describes materials, methods, and experimental protocols employed in this work in order to develop the investigated assays. The chapter also contains a brief description of the techniques and instrumentation employed. The third chapter describes the preparation and the characterization of RNA aptamer in terms of its binding affinity to hCG and its conformational structure under different conditions (temperature and salt concentrations). The fourth chapter lays the foundation for the ELFA and describes the synthesis and properties of the redox molecule-loaded nanoparticles such as size and zeta potential analysis, loading efficiency and electrochemical behaviours. The fifth chapter demonstrates the pH-triggered release of the encapsulated probes performed either by alkaline condition or by the enzymatic reaction. The sixth chapter concerns the results regarding the performance of the

ELFA as well as the performance of the screen-printing is demonstrated. The thesis concludes with a summary of the main results and the recommendation for the future work.

1.2 Point of care as diagnostic tools

A rapid and accurate diagnosis is the most important factor for any diagnostic testing. They facilitate making the right diagnostic decision, which helps to provide patients with appropriate, timely treatments and shorten the patient time[9]. Point of care system compared to the polymer chain reaction (PCR) and the enzyme-linked immunoassay (ELISA), as diagnostic techniques, offer several advantages because they are affordable, portable and accessible in resource-limited setting as they are not laboratory based[10]. What is more, these devices are easy to operate even by non-trained people that make them ideally suited near the patient care[11]. Point of care categorized in several classes depends on the detection system. Glucose assays are the major classes of POC. Although their assays are running on the strips, they are not classified as LF because of the difference in the analytical detection method that applied[12]. These self-testing devices are based on electrochemical measurements, which are based on redox couple mediator either by glucose oxidase or glucose dehydrogenase. More details of glucose measurements, which are beyond the scope of this thesis, are explained in the article reviewed by Yoo et al (2010)[13]. Lateral flow assay is the second major class of the point of care (where the membrane or paper strip is used). It is used to detect the presence of the analyte most commonly proteins and more recently nucleic acid[14]. Since 1990, and based on this format many diagnostic tests (patient' self-testing) have become available in the market include the pregnancy test[15]. More details regarding the development of LFA and its principle are presented in the following sections since it is the main area of interest for this project. The integration of the point of care with the microfluidic technology has a significant contribution in the development of POC assay testing. The idea of microfluidic technology is to control the fluidic network. These referred to the lab on chip (LOC) technologies[16] .Furthermore, the thus called 'iSTAT' tests, which were introduced in 1983 are based on microfluidic technology. They are available for the UK company called Abbott point of care since 2004. They are an example of a successful introduction of a small portable analyser, which is used in emergency departments (ED). These microsensor devices contain disposable cartilages, which

measure blood chemistries include sodium, potassium, chloride, urea glucose, gasses, and haematocrit. In addition, iSTATs measure some cardiac marker as troponin 1. The sample, which is required, is only 150 μL of bloods[13].

1.3 Lateral flow assay (LFA)

1.3.1 Concept and layout of lateral flow assays

Lateral flow assay (LFA), for the use of point of care, is commonly based on immunoassay, i.e., the determination of biomarkers in the diagnosis of immunological or physiological conditions of an individual[17,18]. The first reported an immunoassay for the LFA was by the immobilizing of an antibody on a chromatographic paper[19]. The use of nucleic acid (DNA/RNA) instead of antibodies in LF is increasingly exploited. This is due to the fact that the nucleic acid aptamers may offer several advantages such as their great ability for diagnosing various diseases. The employment of nucleic acid in the paper-based assay is more sensitive than the solution-based as there is no background interference. In addition, the isolation of RNA/DNA aptamers is relatively cheap. The common examples of the nucleic acid based LF are the development of biosensor of food-borne bacteria (Salmonella), which is based on DNA aptamers and dipstick-type DNA as well as a biosensor, which was developed to detect HIV[19] .A lateral flow assay (LFA), is also referred to as an immunochromatographic assay or a strip test. It is a qualitative or semi-quantitative assay for clinical diagnosis. These assays are primarily designed for a single use of the point of care, which give a rapid result, within 10 to 20 minutes. The first reported LFAs were comparable to two sites (sandwich) immunoassay, which was called an immunography with the difference of using a chromatographic paper instead of the microplate (a substrate that is widely used in ELISA). The assays, which are used for LF, have been adapted in various formats to fit different applications as well as to enhance the LF performance. The lateral flow assay (LFA) consists of four different zones as is presented in Figure 1-1 the sample pad, the conjugate pad, the membrane, and finally the absorbent pad. Each of these components has a particular function and together leads to more enhanced LFA performance[20].

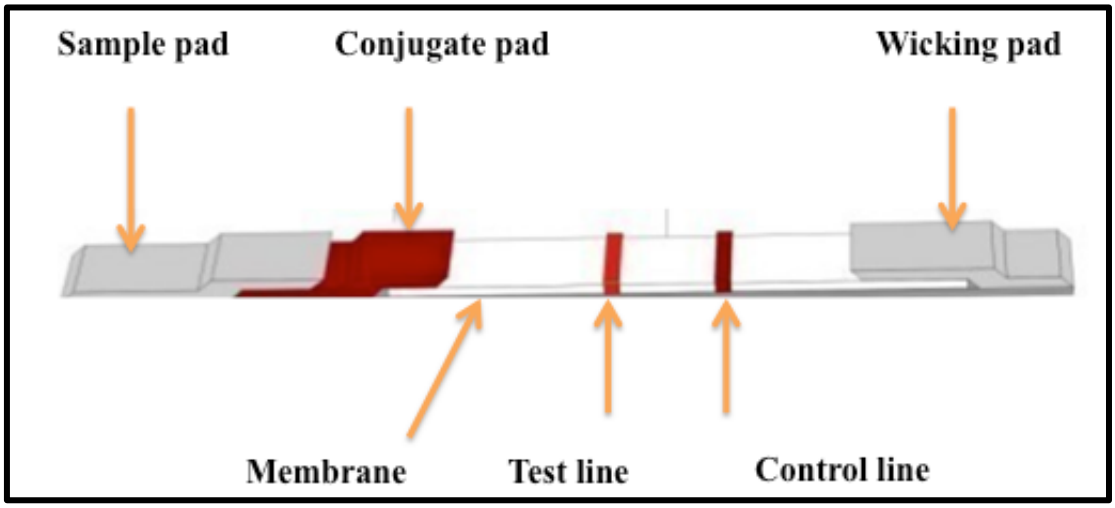


Figure 1-1 The standard layout of lateral flow assay (LFA), which consists of four different zones, which has the following order; the sample pad, the conjugate pad, the membrane and the wicking pad. Each of these parts has a particular function.

- The sample pad: is the dedicated area for the loading of the sample. This pad is treated with materials such as viscosity enhancers, protein, or salts. These materials increase the sample flow rate, thus help in reducing the reaction time.
- The conjugate pad: the labelled antibody is immobilized into the conjugate pad. The type of the label depends on the application, gold colloids and colored latex beads are among the most common materials. In this area, the binding reaction occurs between the labelled antibody and the corresponded antigen if presents in the sample.
- The membrane: is an important part in LFA, since it assists the immobilization of protein by the capillary action imparts a flow, which helps transporting the sample from the sample pad to the test line. The membrane can be made of various materials such as nitrocellulose, nylon, and polyethylene. The advantages of the commonly use of the nitrocellulose membrane over other types are; the absorption of the protein on NC is very high, this absorption is not affected when the NC is wet by buffer addition[21].
- The absorbent pad: is also referred as the wicking pad, prevents the excess liquid from flowing back into the membrane, thus providing uni-directionality of the flow.

The assay, which is used for lateral flow is either a sandwich or competitive, this depends on the type of the analyte. In fact, competitive assays are often preferable for low molecular weight targets, while the sandwich assay is used for proteins as they have several epitopes and thus can apply two different antibodies[22]. Figure 1-2 shows an example of a sandwich assay in the form of the pregnancy test. According to this figure, and after loading of the urine specimen to the sample pad, the specimen moves to the conjugate pad. In this area the human chorionic gonadotropin (hCG), eventually presents in the sample, reacts with the labelled anti-hCG antibody, which is immobilized on the conjugate pad and thus forming an immune complex. This complex then moves along the strip to be bound by the second (capture) anti-hCG antibody, which is immobilized on specific zone on the NC membrane called the test line. Uncomplexed, labelled antibodies are captured by a second antibody where is immobilized in control line just close to the test line. This action is resulting

two visible lines, which indicate the positive results. While in the absence of hCG, only one visible line is shown and this reflect the validity of the assay. In case if there is no visible line is appeared, that indicates that the assay is not working.

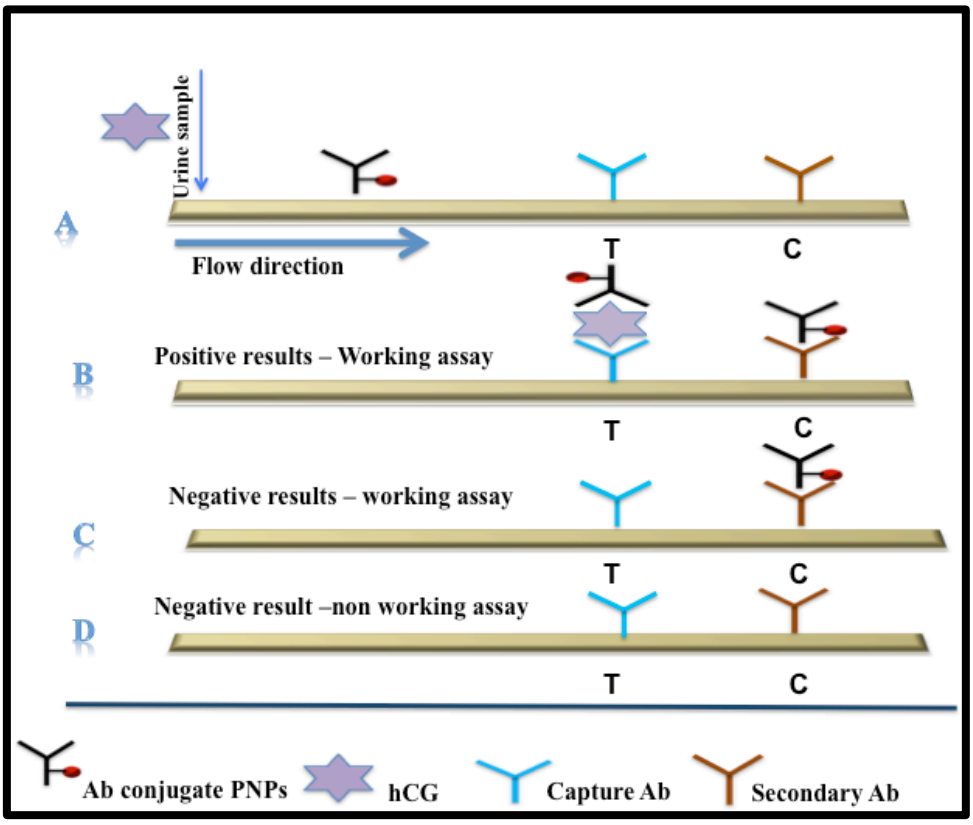


Figure 1-2 The figure demonstrates the concept of lateral flow assay to detect hCG (pregnancy test), which is explained as follow A: demonstrates the format of LFA and the flow direction. B: due to the capillary flow, the urine sample moves to conjugate pad zone and then hCG (when presents in the sample) binds to the immobilized labelled Ab. The immunocomplex then captures by primary Ab at the test line. As a result a red visual line is shown, which indicates a positive result. The excess of labelled Ab moves to be captured by the secondary Ab at the control line, as a results another red visual line is shown, which indicates a valid assay C: in the absence of hCG in the urine sample, no binding reaction occurs, which results of a red visual line at the control line (due to the binding between labelled Ab and the secondary Ab) that reflects the negative result. D: Nonappearance of the red line at the control line indicates that the assay is invalid.

1.3.2 Limitations of LFAs and recent developments

Lateral flow assay LFA, which is used for a wide range of point of care testing systems (POCTs), has several advantages[23]. These benefits include; simplicity, not only in the manufacturing of the equipment but also in its use, where they can be used even by non-trained people. This makes them ideally suited to near the patient testing. In addition, the cost is relatively low. In the spite of the above-mentioned advantages of POCTs. They also have some limitations. On one hand, most LFA applications are qualitative or at best semi quantitative, for many analytes a quantitative measurement is needed with sufficient precision to be useful. On the other hand, the poor colour discrimination as a result of inefficient reaction between the particles and the analyte resulting in low assay sensitivity[24]. Another major challenge is related to the amount of sample required by the LFA, especially in relation to the analysis of blood or saliva in order to cause minimum discomfort to the patient. However, past research has tackled some of these weaknesses. These improvements have been made either by the developing a range of the new detection materials/labels or by linking LFA with electrochemistry. For instance, to enhance the assay sensitivity, europium chelate-loaded silica nanoparticles were introduced; these particles were conjugated with antibody using dextran as a linker. Their finding of LOD was 0.03μg/L, which was 100 times lower than these obtained individually from both gold nanoparticles-LFA and ELISA[25]. Another reported strategy for enhancing the LFA sensitivity was by using of the aggregates particles rather than individual particles. This was achieved by using magnetic iron oxide Fe_3O_4 nanoparticles as a label. The advantages of using Fe_3O_4 nanoparticles rather than AuNPs are: the aggregation of Fe_3O_4 does not changes the absorption proprieties compared to Au aggregation, which is due to the electronic coupling between Au particles. Also, the detection of the analyte can be traced (via magnetic single measurement) when Fe_3O_4 particles are used[23]. Moreover, the introduction of the enzyme in particular horseradish peroxidase (HRP) has a significant effect on the enhancement of LOD[26].

Meo and his group showed LOD of 0.5 nM when a nucleic acid (DNA hybridization) reaction was used on LFA. The sensitivity was enhanced as lower as 50 pM LOD when HRP-Au-NPs dual nanoparticles were used for DNA target. Whiteside pioneered the research in microfluidic based paper analytical devices (μPAD). The

2D/3D format devices prevent cross contamination when sample of multiple analytes are used. Moreover, they are also reduced cost, do not required external pumps. They are lightweight devices (0.15 $g \cdot cm^{-2}$) and simple in their fabrication[27]. Additional improvement has been performed in order to quantify the concentration of various analytes by linking μPAD with the electrochemical detections. In particular, glucose, which was based on glucose oxidase in artificial sample, was detected using chronoamperometric measurements with LOD of 0.22 mM, This result was much lower compared to LOD obtained from glucometer and colorimetric detection as 1.0 mM and 0.5 mM respectively[28]. Independently, Dung chai and his group demonstrated a microfluidic paper based on an electrochemical detection of glucose, lactate, and uric acid for the analysis of serum samples. The novelty was by using the electrochemical paper based microfluidic device applying real biological samples. The employment of screen-printed paper was characterized using cyclic voltammetry while the detection of the analytes was performed using chronoamperometric[29]. In addition, a streptavidin capture lateral flow assay is a modified format of traditional lateral flow assay, which was developed in order to increase LFA sensitivity. In this modified format of LFA, there is a biotin labelled antibody and an immune complex being formed during the LF before it is captured on immobilized streptavidin at the test line as shown in the Figure 1-3**.**

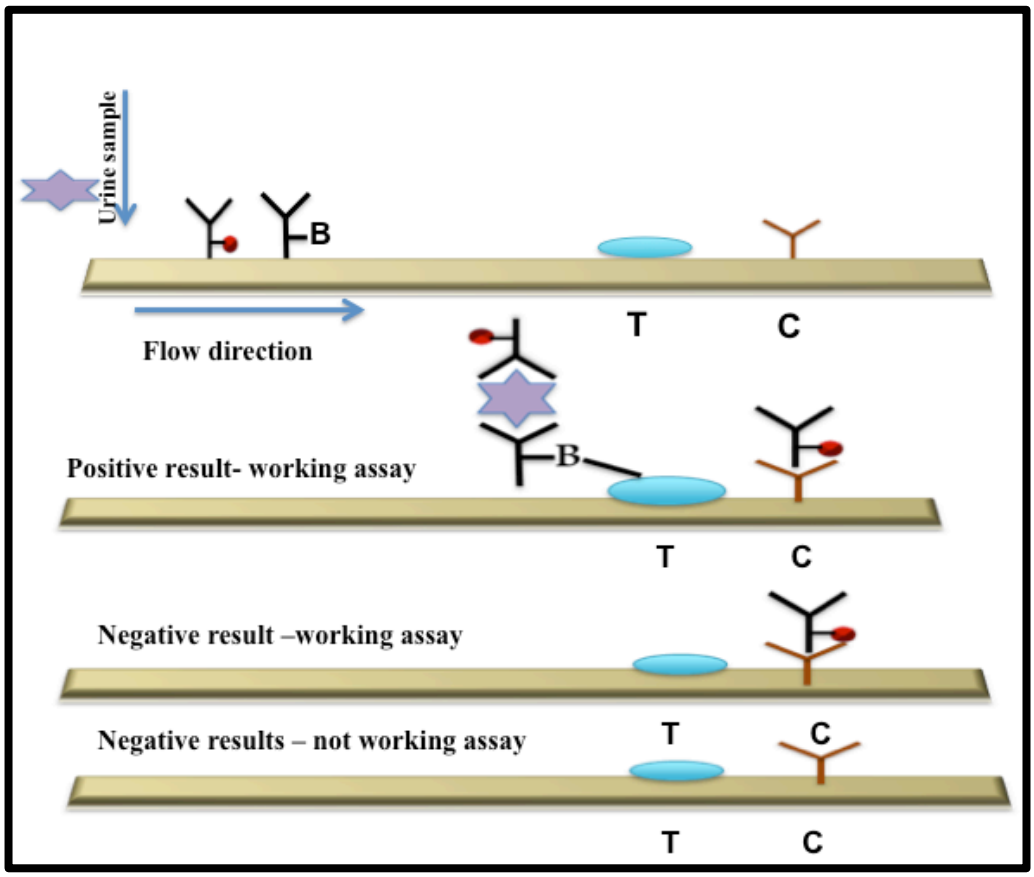


Figure 1-3 Streptavidin-capture LFA, the figure presents the adopted format of LFA using biotin streptavidin detection system. This format was developed by the US company Church & Dwight and is the basis of their first response ™ products. In this format, biotinylated-Ab is immobilized near the labelled Ab and then the sandwich immunocomplex is formed. The immunocomplex is then bound strongly to the streptavidin at the test line due to the high affinity between the biotin and streptavidin.

1.4 A historical journey of pregnancy testing

The history of pregnancy test has reviewed by Haarburge, (2011)[30] and summarized as follows: over thousands of years, urine based pregnancy tests have been developed through different cultures. The first simple pregnancy test was recorded in 3000 years ago in ancient Egypt. The Egyptians used barley and wheat to predict the pregnancy and the sex of the fetus. The primitive principle was that the growth and the type of barley growth in the urine sample indicated the sex of the new born. If barley grew in the urine over several days, the expected child will be a male, while if wheat grew that meant a female fetus was expected. On the other hand, non-growth

reflected sterility[31]. The ancient Greeks believed that urine must be examined for its colour, clarity, aroma, and taste for determining whether a woman was pregnant or not. Significantly, these last two properties may have been related to the incidence of gestational diabetes, which may occur in some pregnancies. In 1831, Nauche and Tanchuo developed an assay for pregnancy detection based on chemical reaction using urine samples. The authors claimed that Kyesteine (perpetrated casein, a milk protein), which indicates pregnancy, is developed when urine from a pregnant woman was collected and kept standing for 30-40 h. In the early twentieth century, Ludwig Fraenkel identified was discovered the corpus luteum and the pregnancy hormone progesterone in urine samples discovered In 1927, gonad stimulating hormone, which presents in pregnant blood and urine, was believed to be produced by the anterior pituitary. However, in 1943, Seegar-Jones proved that the placenta produces this hormone following the implantation of the fertilised egg in the uterus. The discovery of the antibody specific for hCG by Sam Brody and Gun Carlstrom in 1959 seems to represent the key point in the development of immunoassays for pregnancy. In fact, the immunological pregnancy tests were introduced in 1960 and these tests relied on coated latex beads radioimmunoassay (RIA) was presented in 1996. With the start of lab-production of monoclonal antibodies, home pregnancy tests based on an enzyme-labelled immunoassay became available in the 1970s. Currently, pregnancy tests are considered to be one of the easiest, over the counter, consumer tests available.

1.5 The role of hCG

Although pregnancy is a complex physiological process yet not fully understood, several stages of this process have been unravelled. These stages include implantation, decasualization and placentation and each stage is vital for the following one for a complete pregnancy and for a successful delivery[32]. The human chorionic gonadotropin (hCG) is a key hormone during all stages of pregnancy. The growing embryo initially secretes the hCG hormone as early as the eight-cell stage. The secretion of hCG is summarized as follows: after conception, the corpora luteal (CL) is produced and become responsible for secreting the progesterone (P4) and estrodial (E2). These hormones are important for inducing the uterine epitheliums to allow the efficient interaction with blastocyst. This action is essential for embryo implantation and then introducing the trophoblastic cell, in return it helps to secret

hCG. The produced hCG helps CL to continue producing P4 and E2 in addition to start producing estrone E1 until the placenta become able by itself to secrets the progesterone. Additionally, hCG also promotes the invasion of the trophoblastic cell to the uterine walls[33]. Therefore an increased hCG level in the urine sample is a good indicator of pregnancy. Human chorionic gonadotropin (hCG) is a glycoprotein hormone comprised of two identical subunits α (92 amino acid in length) and ß (145 amino acid in length) Although the β subunit in hCG is responsible for the specificity to the hormone It is also linked to trophoblastic invasion of the maternal endometrium in some pregnancy cases, which can lead to some serious complications[34]

1.6 Nucleic acid aptamers

1.6.1 Aptamers as diagnostic reagents

LFA's as described in the previous section use antibodies as the molecular recognition elements. However, they have some limitations, which leads to the search for substitutes. For instance, in some cases, it is difficult to obtain an antibody against a specific target. This is because the production of antibodies often requires the use of animals and in the case where the targets have high homology to an endogenous protein or where the targets are toxic to the host animal this fails[35]. As an alternative, nucleic acid aptamers have been used because of their temperature stability, low cost and the possibility of generating in vitro highly sensitive and specific molecular recognition molecule[29]. In spite of these advantages in using aptamers, they have potential drawbacks in terms of degradation by nucleases, especially with RNA aptamers. However, a chemical modification increases their stability in this respect[36]. Nucleic acid aptamers comprise short sequences (usually between 25 to 90 bases long), which can be generated through the process of systematic evolution of ligands by exponential enrichment (SELEX)[37]. Due to their ability to adopt stable three dimensional, sequence-dependent, structures, these artificial ligands can show highly specific binding affinity to different targets, including amino acids (e.g. L-arginine), other small molecules (e.g. ATP ligands and neomycin) and proteins (e.g. protein E, M. tuberculosis ESxG and protein-stress induced phosphoprotein[38,39]. Nucleic acid aptamers can be easily screened and evolved in vitro, which makes them good candidates as recognition elements in

analytical and diagnostic assays. They have also been exploited as therapeutic agents because of their capabilities to block or interrupt the functions of the targets. Aptamers are also used in the field of the drug delivery, in particular with those that can bind to the cell surfaces[40].

1.6.2 SELEX process

The SELEX procedure, which was first reported in 1990 by Tuerk and Szotack independently, is the main technique for the generation of aptamers. By applying this method, isolation of either RNA or DNA aptamers requires iterative rounds of selection, partition, and amplification. To begin with, a randomized nucleic acid sequence library is incubated with the target of interest. The library is synthesized chemically and consists of about 10^{10} to 10^{15} different sequences that are flanked by two defined primers sequences (around 25 bases each), which allows for PCR amplification of the selected sequences[37]. After incubation, the sequences that bind to the target molecules are then separated from unbound sequences. For that purpose and because the separation method could affect the binding features of the selected aptamers, several different partition methods have been used, including nitrocellulose membrane filtration, the use of affinity capture, gel electrophoresis and capillary electrophoresis. The bound sequences are then dissociated from the target and amplified by PCR. The generation of the RNA aptamers requires the additional steps of *in vitro* transcription using T7 polymerase and reverse transcription. As PCR products are double stranded, single stranded DNA needs to be produced using digestion, affinity capture using biotinylated primers or asymmetric PCR. Efficient generation of ssDNA from dsDNA products is crucial, since only ssDNA can be capable of binding to the target molecules. After performing several rounds of SELEX, the generated nucleic acid aptamers then can be cloned, sequenced and further characterized. This process is demonstrated in the Figure 1-4**.**

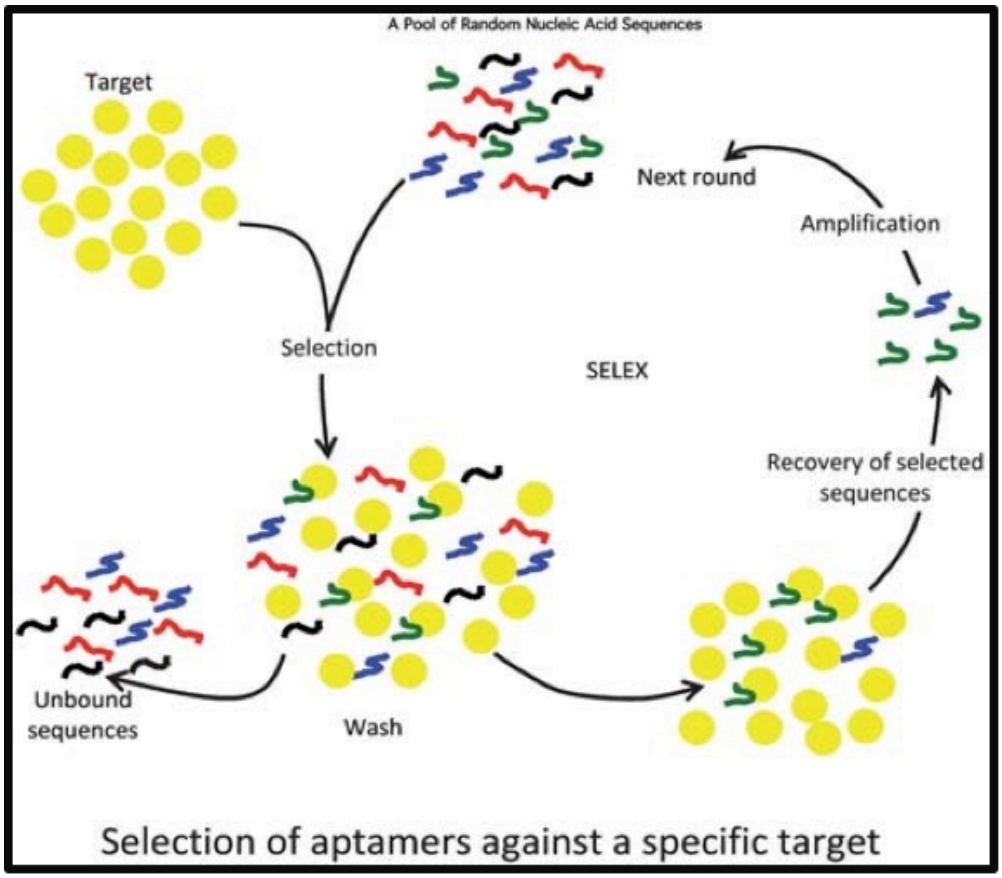


Figure 1-4 The process of SELEX, which involves several rounds include selection, partition, and amplification. By this method nucleic acid aptamers (RNA/DNA) is generated from random sequence library. This figure was published by (Cass and, 2011)[41]copyright © 2010, royal society of chemistry (with permission).

1.6.3 Modification of RNA aptamers and ELONA

The selected aptamers obtained from SELEX can be modified and then characterized with respect to aptamer/ligand interactions. Post SELEX aptamers could be used either in their native or modified state. In the case of RNA, molecules can be modified post SELEX either chemically or enzymatically. It is important to ensure the position of the modification to avoid the changes in the proprieties of the original molecules[42]. Many possible modifications could be made, however, in this thesis, one example of the modification of RNA is presented, as this is relevant to the subsequent experimental work. This modification method is the biotinylation of RNA aptamers. Modification with biotin permits a specific tight binding to streptavidin and is a useful tool for detection. The biotin-avidin or streptavidin interaction has several advantageous features, which make them preferable to many

other detection applications. These characteristics are summarized as follows: The non-covalently binding affinity between biotin and avidin/streptavidin is around 10^{15} $Lmol^{-1}$. This formation constant is very high and makes the reaction stable and dose not disrupted under different changes in the surrounding conditions like a change in pH. Highly specific binding between avidin/streptavidin and biotin ensures non-interference with the binding reaction to the target under investigation. In addition, the small size of the biotin (244.31Da) makes it ideal for various biologically active macromolecules and will not affect their biological activity. The term ELONA stands for an enzyme-linked oligonucleotides assay. The first report of ELONA was to characterize the binding of an anti-human vascular endothelial growth factor (VEGF) aptamer to its target by Drolet et al 1996[43]. The aptamers, which are employed in this method, could be either as a capture or detector molecule and they fulfil the same role as antibodies in immunoassay. Typically, ELONA is performed in order to study the interactions between aptamers and their targets, especially determination of the dissociation constant (K_D) of the aptamer/target complex. Knowing the (K_D), is important in designing the analytical aptamer assay. Generally, these binding affinities range from micromolar to picomolar and the best conditions for each aptamer and target complex is optimized depending on the properties of the target of interest. A typical ELONA assay for a macromolecule target (e.g. protein) is shown in Figure 1-5**.**

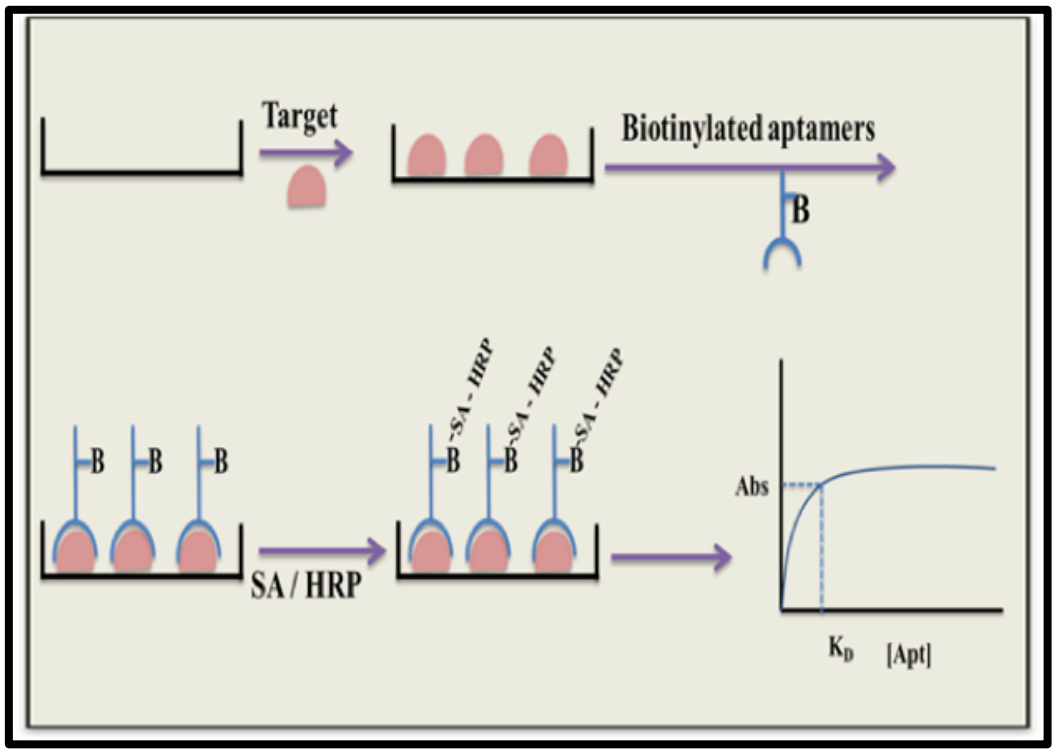


Figure 1-5 The scheme of ELONA assay, which is used for the determination of the K_D to study the binding affinity of the aptamer and its target. In this assay, the microplate well is coated with fixed concentration of target (hCG), after incubation for an hour, several washing were preformed with BPST, the plate were blocked with 1% albumin serum bovine. Vary concentration of biotinylated aptamer were then added. After several washing with BPST, substrate was then added. Followed by adding (1:1000) diluted streptavidin conjugate HRP. A blue green colour was developed as a result of the oxidization. The absorbance was measured at 450nm.

1.6.4.Spectroscopic studies of conformational of the RNA nucleic acid aptamers

Information regarding the secondary structure of DNA/RNA aptamers is often determined by spectroscopic studies such as the circular dichroism technique (CD). Circular dichroism is a sensitive method, which provides valuable information on the molecule conformation. The fundamental principle of the CD is based on measuring the difference in molar extinction coefficients for left and right circularly polarized light. This difference is termed as ellipticity. Comparison of the CD spectra with reference spectra gives an indication of the aptamers conformational state. In

addition, it can be employed to study the effect of different ionic compositions and aptamer concentrations.

1.7 Nanomaterial

The field of nanotechnology is wide and it links between the disciplines of science and engineering. Several applications have been involved in the field of nanotechnology include; drug delivery, biomaterials and electronics[44].

1.7.1 Polymeric nanoparticles as a carrier system

Polymeric nanoparticles (PNPs) have been exploited widely in drug delivery. This is due to the fact that polymeric nanoparticles have several properties that make them ideal in encapsulating/releasing drugs at different areas of the body. The polymers used are either naturally occurring or synthetic. They are often pre-designed in such a way that they release material under specific conditions. Synthetic nanoparticles are more attractive than natural polymers since the latter require cross-linking which could inactivate the encapsulated drugs, they vary in their purity[45]. Nanoparticles either in dispersion or as the solid particles is defined as being in the size range from10 to1000 nm. Depending on the preparation method of the nanoparticles, drugs and other active agents can be entrapped in or attached to them. Polymeric nanoparticles are also capable of being conjugated to various recognition elements, which are useful for different applications. These elements include proteins[46], peptides, antibodies and most recently aptamers .The synthesized polymers, which are designed to mimic biopolymers are also known as ‘‘smart polymeric materials’’, since they respond to significant changes in their environment. The change that occurs in their structure is often a reversible transition. These responses are often displayed as a change in shape, surface characteristics, solubility, and finally the formation of an intricate molecular assembly. While the environmental changes involve, for example changes in temperature, pH, ionic strength, and the addition of an oppositely charged polymer, light, and radiation. Chitosan, alginate, and eudragit are common examples, which have been widely used in such applications. eudragit S-100 has many desirable features in encapsulating and controlled release of materials in several drug delivery applications[47,48]. These various methacrylate polymers offer a range of physicochemical features including water permeability as well as pH solubility in term of the dissociation and coating behaviour[49]. The key

property of these series of copolymers is the surface chemistry. Eudragit S-100 (ES) consists of methacrylic acid and methylmethacrylate monomer (1:2 MW= 135.000) and it is very sensitive to pH, which makes it widely exploited in various applications. It was reported that the combination of eudragit with other polymers helps to stabilize the loaded drugs and provides a more controlled release of them[13]. The solubility of the ES-100 occurs with increased pH due to the electrostatic deprotonation of the repulsion when carboxylic acid groups overcome the attractive force between the polymers backbone. Hence ES-100 is insoluble at low pH and dissolves above neutral pH. The solubility of ES-100 and EL-100 depends upon the ratio of the carboxyl to ester group, which is being 1:1 in the former and 1:2 in the latter. This ratio has a direct effect on their solubility and pH sensitivity[50].

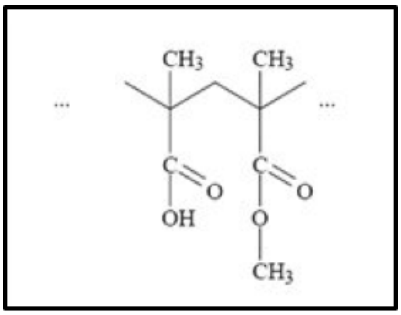


Figure 1-6 The chemical structure of eudragit S-100, which consists of methacrylic acid and methylmethacrylate monomer in the ratio of 1:2.

1.7.2 Antibody conjugated polymeric nanoparticles.

Immunoglobulin G is a glycoprotein consisting of two identical heavy and light chains bound by disulphide bridges. IgG's comprises two identical antigen binding domains (Fab region) and an aneffector domain (Fc region)[51]. The conjugation of the antibody with nanoparticles provides a product, which combines features of both. For instance, the small size of nanoparticles and their physicochemical properties make them ideal for the conjugation to antibodies. The conjugate retain the selectivity and specificity of the antibody towards it antigen[52]. Although production of the NP-antibody conjugate through adsorption is a straightforward method,which is done by direct incubation with desired concentratin Figure 1-7, the molecular forces involoved are not yet fully understood.

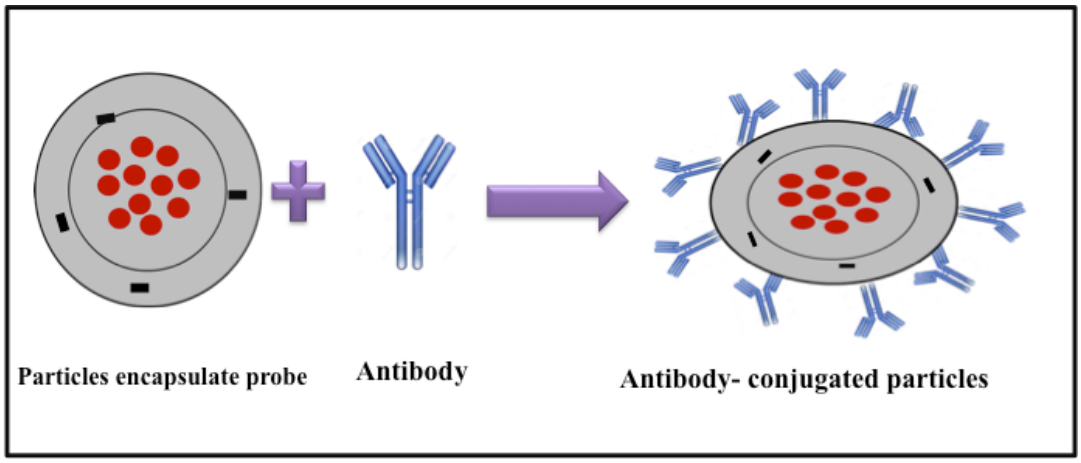


Figure 1-7 Adsorption process, which is used for conjugation of the antibody with the nanoparticles. Mainly, the desired concentration of the Ab and PNPs are overnight incubated. The negatively charged polymer nanoparticles PNPs is electrostatically interacted to the antibodies. Adsorption at pH6.5 keeps PNPs insoluble and gives the IgG the positive charges (probably a distribution of orientation of IgG on the surface).

1.7.3 Synthesis of the polymer nanoparticles via nanoprecipitation

Many methods have been described for the preparation of the polymeric nanoparticles (PNPs). In the work described in this thesis, nanoprecipitation was used and so is described as follows: it is a simple, economical and rapid method compared to many other techniques. Nanoprecipitation is also referred as solvent displacement or as interfacial deposition. According to this method, synthesis of the nanoparticles requires two phases to be prepared. These phases are the solvent in which the polymer is dissolved and a solvent in which the polymer is insoluble. typically water. The solvents in which the polymer is dissolved such as ethanol. Common polymer solvents include ethanol,acetone and hexane,either individually or as a mixture .The aquous phase often contains surfactant,which prevents aggregations of the nanoprticles. Adding the polymer/solvent phase slowly with moderate stirring to the aqueous phase forms a colloidal suspension,which is called then a nanoparticle .Chapter 2 describes the method in more detail. Importantly, there are several variables in the nanoprecipitation process. Each of which has a direct effect on the nanoparticles' sizes and shapes. It is important to control these variables when preparing nanoparticles, especially in applications in which small size particles

are crucial, and when it is necessary to synthesize particles with uniform size and shape from different batches of polymer. These variables include injection flow rate, type and concentration of the surfactant, and stirring speed during the injection[53].

1.7.4 Characterization of the nanoparticles

Several parameters should be characterized after the formation of the nanoparticles. These parameters include; surface charge, size, and shape. The study of the surface charge is important for the chemical modification of the particles. On the other hand, the size and the shape of the particles have an impact on the carriers' function and the loading efficiency[54].

1.7.4.1 Size analysis

Several methods are available for measureming the nanoparticles'size for examples:atomic force microscopy (AFM), analytical ultracentrifugation (AUC), dynamic light scattering (DLS) and nanoparticles tracing analysis (NTA). Regardless of the performed method, the size distribution of particles is measured in either the dried form or in suspension. Each of these methods has pros and cons,which have been reviewed in detail in XU et al, (2008). Dynamic light scattering (DLS) was the primary method used in this project and is based on the interaction between light and the particles. Briefly, DLS measures the light scattering of the laser beam when it passes through the suspension and then the modulation of the scattered light intensity as a function of time is analyzed, and the hydrodynamic size of particles determined. According to Brownian motion, the particles have a random movement in the suspension due to the fluctuation in their thermal energy and that of solvent molecules.The light is scattered in all directions in which called (Rayleigh scattering) and scattering intensity varies with time as described above.The fluctuations of the intensity are then analysed and are dependent on the particle' sizes. Thus the hydrodynamics are then determined using the Stokes-Einstein Equation.

$$D=k_BT/(6\ \pi\eta r)$$

Where: D is the diffusion constant, k_B is Boltzmann's constant, T is the temperature, η is the viscosity and r is the radius of the spherical particle[55].

1.7.4.2 Zeta potential

Information regarding the electrostatic properties of the particles in solution as well as their stability is usually obtained from measuring the zeta potential. The determination of the zeta potential occurs by measuring the electrocophoretic mobility, which is defined as the velocity of the particles when an electric field is applied. Charged particles will move with constant velocity to the electrode of the opposite charge. When the solution containing the particles is put in the zeta potential cell, the fluctuation intensity of the scattered light that occurred is proportional to the electrophoretic mobility and hence the charge. This technique is called laser doper velocimetry.

1.8 Electrochemistry

Electrochemistry, as an analytical technique, is very widely used because of its cost effectiveness, accuracy and sensitivity as well as instrumental simplicity. There are many electrochemical methods that have been described, this thesis makes use of those where the applied potential at an electrode is controlled and the current measured. Measurements where the applied potential is varied are called the voltammetric methods and those where the applied potential is controlled are called amperometric methods. The common electroanalytical methods have been reviewed by Dogan (2011)[56]. Two voltammteric methods include cyclic voltammetry (CV) and square wave voltammetry (SWV), were applied in this work, hence they are described in detail next. Electrochemistry studies the transfer of the charge between the electrode, which is most commonly a metal or carbon, and the solution, which contains a molecule that can be oxidized or reduced. The transfer of the charge can be represented in the redox reaction as shown in the equation below :

$$\mathbf{O} + \mathbf{n}\mathbf{e}^{-} \leftrightarrow \mathbf{R}$$

Where O is the oxidised form and R is the reduced form of the molecule under investigation, n is a integer and is the number of the electrone transfered. In a conductore (e.g. gold or graphite) the energy levels of the electrones are so close togather that they form a continuum. The highest energy point of this continuum is called the Fermi level. The energy of the Fermi level is influenced by the application of a voltage. In reduction proceses, electrons in the Fermi level transfer from the electrode to the lowest unoccupied molecular orbital (LUMO) of the molecule in

solution. While in the oxidation reaction, the electron is tranferred from the highest occupied molecular orbital (HOMO) to the Fermi level. Potential,which is often measured when appling a potential to an electrode, the value is always with respect to a reference electrode as it is demonstrated in Figure1-8 .

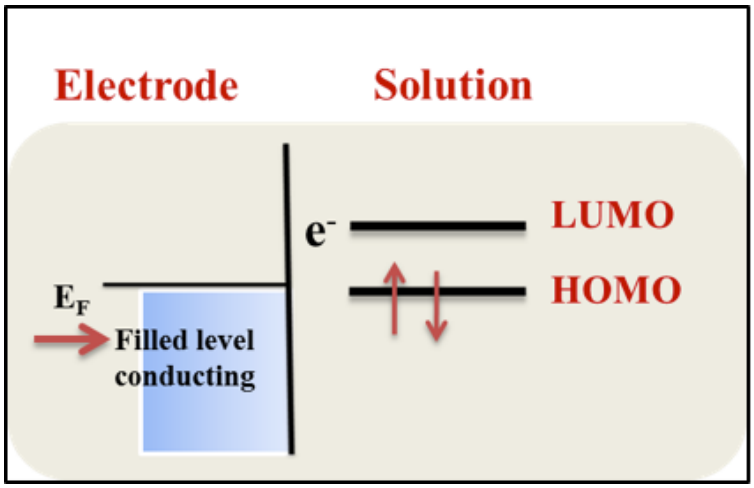


Figure1-8 Electron transfer between electrode/solution interface facilitating reduction and oxidation**.**

1.8.1 The electrochemical cell

The simplest electrochemical cell consists of two electrodes, the reference electrode (RE), and the working electrode (WE) as shown in Figure 1-9**.** The important consideration that should be taken into account when choosing a reference electrode is that it should be non-polarizable i.e. it has a stable potential, which does not change when a current flows through it. Although redox potentials are quoted with respect to the standard hydrogen electrode (SHE), which has its potential defined as OV, it is not practise to use SHE as a reference electrode. Instead, alternative reference electrodes such as saturated calomel electrode (SCE) or the silver/silver chloride (Ag/AgCl) are used. The SCE is not widely used as it requires toxic mercury salts and cannot be fabricated in a planer format. However, The redox reaction that occurs at the Ag/AgCl electrode is shown bellow:

$$\mathbf{AgCL(s) + e^- \leftrightarrow Ag(s) + Cl^-}$$

The working electrode (WE) is where oxidization/reduction of the redox molecule occurs and the material of the WE must be a good electrode conductor.

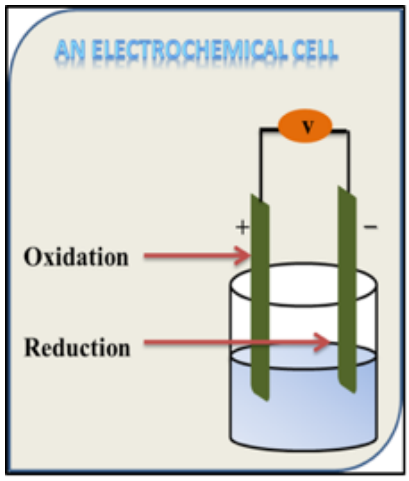


Figure 1-9 The simplest electrochemical cell, which is comprised of reference and working electrodes.

1.8.2 Voltammetric techniques

Voltammteric techniques are based on the measurement of the currents that flow when there is an alteration of the applied potential at the working electrode due to the oxidation or reduction of the molecules in solution[12].

1.8.2.1 Cyclic voltammetry

Cyclic voltammetry (CV) and square wave voltammetry are the two of the most common voltammetric methods. Cyclic voltammtery is a widely used technique in modern analytical chemistry. It is often the first method to be used for electrochemical experiments since it is simple and provides valuable information regarding the system under investigation. However, the information obtained from this method includes stability of the oxidized/reduced states and the rate of electron transfer between the electrode and the redox species. Other valuable information that can be obtained by CV includes the number of redox states of the electroactive species and its concentration. Although historically cyclic voltammetry used an analogue voltage ramp and continuouse current measurements, the modern digital potentiostats instead apply a linear staircase waveform and sample the current at the end of each step, providing the step and step duration are sufficiently small, this is a good approsematric to CV illustrated in the Figure 1-10.

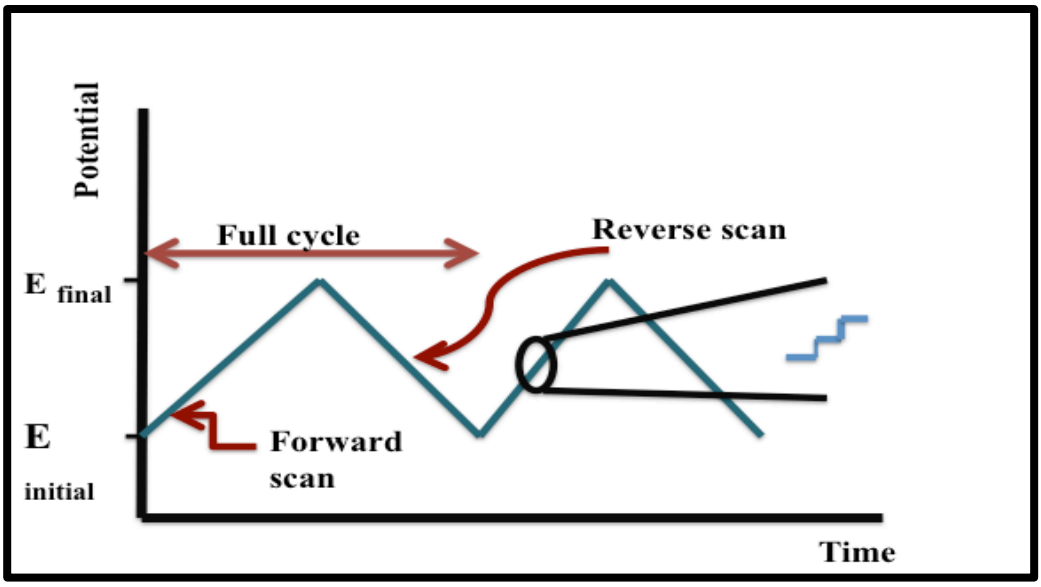


Figure 1-10 a full cycle potential triangular waveform, which is an example of potential vs. time for a typical voltammetry experiment.

1.8.2.2 Square wave voltammetry

Although CV is very useful technique to characterise electrode/molecule reactions, it has limitations in detection of low concentrations. There two reasons for this: the first is the capacitance contribuation to the current-voltage curve, which makes it difficult to identifiy the faradaic peaks. The second reason is that when an electron transfer is slow the peaks broaden and separate again making low concentrtation measuremental difficult. Both these limitations can be overcome by using pulse voltammetric methods such as square wave voltammetry.The widespread availability of modern digital potentiostats make these techniques very easy to implement.

1.9 Screen-printed electrode on paper substrate

Traditionally, electroanalytical methods use solid disk electrodes (typically 2-4 mm in diameter). However, such electrodes are expensive; require often-elaborate cleaning procedures, and separate reference electrodes. They also require sample volume >500 µl. In order to reach the objectives of this work, there is a need to design a platform to use as a final device that is both cheap enough to be disposable and compatible with lateral flow assay. In developing inexpensive, portable, disposable and simple diagnostic platforms, paper based microfluidic or lab on paper

has been used. Screen-printing has been widely reported and used for the fabrication of electrodes on a suitable substrate for diagnostic applications including those based on the LF[57]. Disposable screen-printed electrodes (SPEs) have none of the disadvantages of traditional electrodes described above. Generally, the electrodes are made on inexpensive substrates by printing either carbon or gold inks as the working electrode and a silver /silver electrode inks as the reference electrode[52]. Typically SPEs are made on impermeable plastic or ceramic substrate however, papers particularly cellulose fibres are very attractive materials as liquids can penetrate within the matrix with no need for an external pump. Filter paper has been widely used in this respect as fluid can flow rapidly between the fibres (wicking or capillary action) without undue swelling. Modified papers are also exploited in this field, for example hydrophobic nitrocellulose papers have minimal non-specific binding and can be modified for better immobilization of the reagents[58].

1.10 The aim

This thesis introduces a new concept of the lateral flow assay to use at the point of care. One of the main goals of this project was to switch from the visual detections (traditional pregnancy test) to the electrochemical measurements whilst keeping the ease and robustness of traditional LFAs. The second goal is to enhance the performance of the lateral flow assay by developing a new concept based on pH responsive nanaoparticles. Hence a combination of streptavidin captures lateral flow assay (already established) and the use of the polymer nanoparticles (a new concept to be developed), were used to develop a pregnancy test (a model example). For this work, to begin with the AuNP labels were replaced with stimuli responsive polymers encapsulated redox reporter molecules. The electrochmical measurement was performed (at the test line) once the redox proes released from pH responsive nanaoparticles. The realse of this moleculae occurs because of a change in the pH, which resilts from an enzymtic reaction spesifically urease, which is immoblized at the test line. This enzyme hyrdolyes urea in the urine sample into ammoina, which leads to an incearse in the pH so that, polymers nanoparticles then disolve and release the probe which is detected electrochemically. In the case of sample that are not urine, the urea can be derid into to the pad and reducation in the sample. This is iluustred in the Figure 1-11.

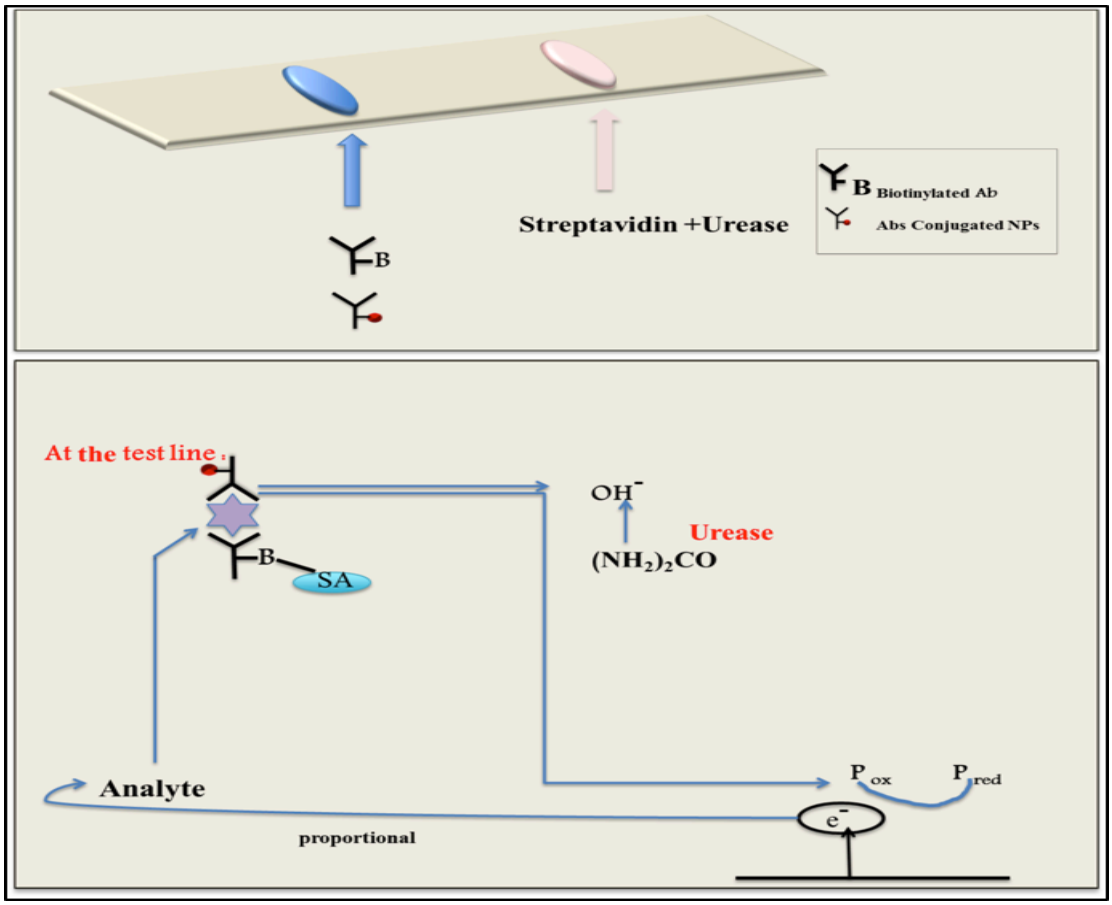


Figure 1-11 The concept of an electrochemical lateral flow assay (ELFA), which is a combination of SA capture LFA and an electrochemical detection .The electrochemical detection occurs with redox active molecule be entrapped in polymers nanoparticles PNPs, which are released by a pH change.

Both amplification of the nanoaparticles and the electrochemical detections were sucssfully achieved. Polymer nanopartciles in partcuilar eudragit S-100 were able to efficient encapsulte FcMeOH and contollred rlease the probe at the desired location (test line). The emplyment of the enzymatic reaction was a realiable method to increase the envirmental pH on NC membrance. In addiation FcMeOH has a good and reproducable electrochmical signal. However , all the material, which were used, are retavilay cheap and have reaiable and reproducable resuilts regarding the sysnthesis of PNPs (polymer size, zeta potential, loading effciency and controlled release of the encapsualted probe) and also in term of electrochmical measurments.These features are very impoartant factors for the product industry.

Chapter 2 Experimental

According to the flow work of this project, this experimental chapter is divided into three parts. The methods related to the characterization of anti hCG-RNA aptamers in the first part, while the second part concerns polymeric nanoparticles fabrication and characterization. The final part is related to the electrochemistry and screen-printing applications. The main part of this work was the developing of an electrochemical lateral flow assay, the main stages are illustrated in the Figure 2-1.

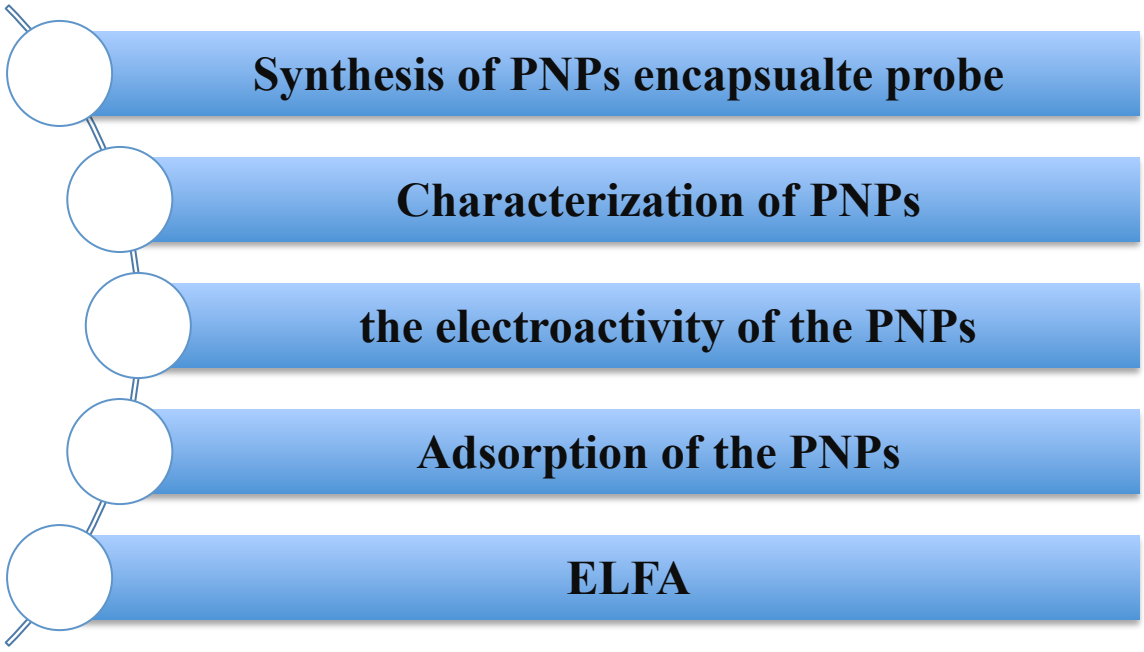


Figure 2-1 The flow work of developing an electrochemical lateral flow assay

2.1 Chemical and materials

Table 2-1 Chemical and supplier

Chemical	**Supplier**
(2X) Loading dye.	Invitrogen
3, 3', 5, 5'-Tetramethylbenzidine liquid substrate, supersensitive.	Sigma
30% Acrylamide/bis solution.	Bio-rad
Ampliscribe ^{TM} T7-flash transcription kit.	Epicentre
Ampliscribe^{TM}T7-flash biotin-RNA transcription kit.	Epicentre
Anti-hCG alpha antibody [ME.109].	Abcam
Biotin quantitation kit.	Fisher scientific
Carbon paste (C2130814D).	Gwent electronic material
Cassette 1mm.	Invitrogen.
Dura scribe™ transcription kit.	Epicentre
Eudragit ES-100	(Evonik Röhm GmbH, Pharma polymers)
EZ-link^{TM}NHS-PEG$_4$ - biotinylation	Thermo scientific
EZ-Link Hydrazine Biotins.	Thermo scientific.

Chemical	**Supplier**
Hexaammineruthenium chloride.	Sigma-aldrich
High Sensitivity Streptavidin-HRP.	Pierce®
Hydroxyl methyl Ferrocene 97%	Sigma, Aldrich
Methylene blue.	Fisher scientific
Nitrocellulose membrane.	Millipore
Novagen perfect RNA marker 0.1-1Kd.	Life technology
Oligos.	Integrated DNA technologies (IDT)
PCR buffer.	Invitrogen
Sliver /sliver chloride paste (C2130905D3).	Gwent electronic material
Sodium acetate.	Sigma-aldrich
Sodium citrate.	Sigma-aldrich
SYBR gold nucleic acid gel stain.	Invitrogen
Taq DNA Polymerase.	Invitrogen
TBE running buffer (5X).	Invitrogen

2.2. Molecular Biology' experiments

Initially, the sequences of the oligos, which were used, are given below: First, the sequence of DNA complementary primers, which was attached to T7 promoter at its 5` end, is shown below:

5`- GATAAT ACGACT CACTAT AGGGGG AGGACG ATGCGG GTTTCA CTTCAA GTTGAA CGATCC TTCTTG GCTTGC GCACAG ACGACT CGCCCG A-3`

Second, The sequence of the T7 complementary primers is shown below:

5`- TCC TCC CCC TAT AGT GAG TCG TAT TAT C-3`.

The diagram below shows the flow work of studying the binding affinity of hCG-RNA aptamers; it will be discussed in more details subsequently in the following section:

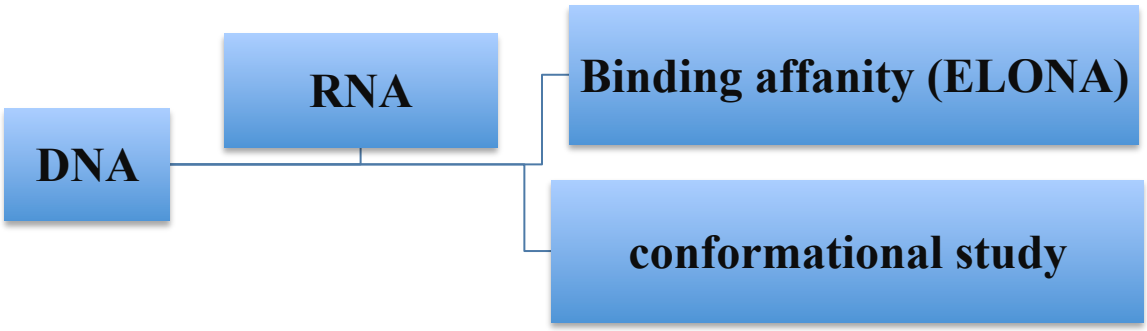


Figure 2-2 The diagram demonstrates the flow work of the production and the characterization of anti hCG-RNA aptamer.

2.2.1. 2nd strand synthesis

The ssDNA (36 µg) and the complementary primer (72 µg) were dissolved in 100 µl of TEM buffer (10 mM Tris-HCl 0.1mM EDTA at pH6.5). The mixture was then heated up at 95ºC for 10 minutes and then annealed at 52ºC for 7 minutes using the thermal cycle. After that the dsDNA was purified and precipitated by chloroform extraction and ethanol precipitation as described below.

2.2.2. Chloroform extraction and ethanol precipitation

The volume of the DNA solution was adjusted up to 200µl with TE buffer (10 mM Tris, 0.1M EDTA pH8) and then 200 µl of chloroform was added to the DNA solution. The DNA sample was mixed gently by pipetting up and down. After that, the sample subjected to centrifuge at high speed (12000 rpm) for two minutes. After centrifugation, the aqueous layer was transferred to another eppendorf tube and 1:10 of the volume of 3M of sodium acetate (pH5) was added. Followed by adding 2.5 volumes of absolute ethanol, the sample then centrifuged (12000 rpm) for two minutes at 4^{o}C. After that, 5 µl of 5mg/ml linear acrylamide (life technologies) was added. After overnight-incubation at -20ºC, the sample was centrifuged at 12000 rpm for 40 minutes. The pellet was washed with cold 70% ethanol and centrifuged for further 10 minutes. Finally, the pellet dried for two minutes at RT and then it was re-suspended in TE buffer. Sample stored at -20ºC for the next step.

2.2.3. In vitro transcription

The transcription reaction mixture was prepared by mixing the following components: 2µl of ampliscribe T7-flash 10X reaction buffer, 1.8 µl 100mM ATP, 1.8 µl 100 mM, 1.8 µl 100mM CTP, 1.8 µl 100mM GTP, 1.8 µl 100mM UTP and 2µl DTT, 0.5µl of riboguard^{Tm} RNase inhibitor and 2 µl of ampliscribe T7-flash enzyme solution. This mixture was incubated for 30 minutes at 37ºC. After that 1 µl of RNase free DNase was added to the previous mixture. RNA was extracted and precipitated using chloroform /ethanol precipitation as previously described.

2.2.4. Urea polyacrimde gel electrophoresis

The urea polyacrylamide gel was prepared as follows: pure urea (4.8g) was dissolved in either 3.5ml of 30 % or 2.5ml of 40% polyacrylamide/bis and 2.5ml of 1X TEB

buffer (Tris/Borate/EDTA) for one minute in the microwave. The mixture cooled at room temperature for half an hour. After that 100 µL of 1 % (W/V) ammonium persulfate and 4 µL of TEMED (N, N, N, N-tetramethylethylenediamine were added respectively. The mixture was purred immediately in a 1mm gel cassette and left to polymerise for 40 minutes at RT. The RNA sample (10 µl) was mixed with an equal volume of 6X loading buffer. After gentle mixing 12 µl of the sample was loaded in each well. The gel was run with constant voltage 200V and current at 400 mA for 35 minutes. The gel stained in 50 ml of 1X TBE buffer contains 5µl of SYBR®gold nucleic acid gel stain, the gel was covered and kept agitated with gentle shaking for half an hour. The gel imaged using a diversity image system.

2.2.5. The quantification of RNA/DNA

Absorbance measurements were carried out using ND-1000 (nanodrop) using 1µl of the sample for each measurement. Both ssDNA/RNA were measured at 260nm absorbance. The extinction coefficient, which was used for DNA and RNA, were 0.025 mL cm^{-1} μg^{-1} (or 40 ng cm μL^{-1}), 0.027 mL cm^{-1} μg^{-1} (or 37 ng cm μL^{-1}) respectively while the extinction coefficient for dsDNA was 0.02 mL cm^{-1} μg^{-1} (or 50 ng cm μL^{-1}).

2.2.6 Biotinylation of RNA aptamer

2.2.6.1 Biotinylation of RNA via transcription

The transcription reaction mixture was prepared by mixing the following components: 2µl of ampliscribe T7-flash 10X reaction buffer, 8µL of NTP/ biotin-UTP premix, 2µl of 100mM DTT, 0.5µl of riboguard^{Tm} RNase inhibitor and 2µl of ampliscribe T7-flash enzyme solution. The linear dsDNA (prepared via 2nd strand synthesis) was added up to a total volume of 20µl in the transcription reaction. Following that, the mixture was incubated for 4 hours at 37ºC. The RNA was extracted and precipitated using chloroform /ethanol precipitation method.

2.2.6.2. Chemical biotinylation of RNA aptamer

The RNA sample was diluted in 0.1 mM sodium acetate at pH4.5 to make 1mM solution. Then the solution of 100 mM of sodium periodate was freshly prepared before use. After preparation, 10 µl of the periodate solution was added to each 90µl of the RNA and were mixed well. The mixture was incubated for an hour at RT in

the dark. The reaction stopped by adding 5 µl of the 3 M sodium acetate (pH5.2) and 0.3ml of ethanol and after that the RNA sample was centrifuged at 10000xg for 15 minutes. The pellet washed with 70 % cold ethanol and centrifuged for five minutes at 10,000 xg. The dried pellet then was re-suspended in 70 µl of distilled water. After that, 10 µl of 3M of sodium acetate pH5 and 20 µl of biotin hydrazine solution (which was prepared in dimethyl formamide) were added respectively to the oxidized RNA sample. The mixture was incubated overnight at RT in the dark with gentle mixing. The modified RNA was precipitated with chloroform/ethanol precipitation method.

2.2.6.3. Biotin quantitation

HABA/avidin, which is provided in the HABA quantitation kit, was equilibrated at room temperature and then 100 µl of PBS buffer was added to the HABA/avidin (step 1). In microplate wall, 160 µl of PBS buffer was added in the well. 20 µl of the HABA/Avidin (prepared from step1) was added to the same previous well. The absorbance measured at 500nm. Following that, 20 µl of the biotinylated RNA was added to the pervious mixture and then the absorbance was measured at 500nm. The mole ratio of biotin to RNA was calculated as described in the provided datasheet.

2.2.7. ELONA assay

The walls of the microtiter plate were coated with 20 µl of 200 nM hCG and the plate was incubated for 2 hours at RT. The walls were emptied and raised with PBS containing 0.05% Tween 20 (PBS-T). The surface then was blocked with 200 µl of 1% (w/v) bovine serum albumin and the plate was incubated for 30 minutes. Triplicate sample of different concentrations (from 50 to 250 nM) of BRNA aptamer were added to each wall. The plate was incubated for two hours at RT. After washing the wells with PBS-T, streptavidin-conjugated horseradish peroxidases (1:1000 diluted) were added to the each wall and then the plate was incubated for 20 minutes at RT. The well was washed thoroughly three times with PBS-T. After washing, 150 µl of 3, 3', 5, 5'-tetramethylbenzidine TMB was added to the substrate solution and incubated until a blue green colour was developed. The reaction stopped with 1M sulphuric acid. The absorbance at 405nm was measured using a microplate reader.

2.2.8. Circular dichroism (CD) of RNA aptamer

The entire CD measurements were performed at 37°C using Jasco model.

2.2.8.1 CD measurement of RNA aptamer

RNA aptamer was diluted in TEM buffer to a final concentration of 5μM. Then the RNA sample denatured at 90ºC for 10 minutes. After cooling the sample at RT for 30 minute, the solution was filtered through a 0.25μm membrane immediately prior to the CD measurements. The measurements were repeated at different concentration of $Mgcl_2$ and Licl.

2.2.8.2. CD measurement of the RNA-hCG complex

The RNA sample was prepared as described above. A final concentration of 10μM of hCG was added to the RNA sample. The mixture was incubated for 2 hours at RT, and was filtered prior to the CD measurements.

2.3. Nanoparticles experiments

2.3.1 Synthesis and characterization of the polymeric nanoparticles (PNPs)

The polymeric nanoparticles (PNPs), which encapsulated redox active molecules, were produced using a nanoprecipitation process. The synthesized nanoparticles were purified in order to remove un-entrapped redox active molecules. Size and zeta potential were determined using dynamic light scattering (DLS) (zeta seizer from Malvern). While the voltammetry techniques were performed in order to confirm that the beads were electroactive. The dissociation study under alkaline and acetic condition was conducted to ensure efficient releasing of the encapsulate probe. The synthesis of the polymers nanoparticles encapsulated redox active was done by nanoprecipitation method. The redox molecules, which were investigated in this pace of work, were: hydroxylmethyl ferrocene (FcMeOH), methylene blue (Mb), potassium ferricyanide, Tris (2,2`bipyridyl) ruthenium (II) chloridehexahydrate and hexaammineruthenium (III) chloride. The nanoparticles synthesis was performed in the fume hood as follows: 285mg of ES-100 and 130 μmoles of the redox species were dissolved in 11 ml of 96% ethanol and kept stirring at 250 rpm for three hours at room temperature. After a complete dissolving the organic phase was injected

whilst stirring at 600 rpm into 50ml emulsion buffer (100 mM citrate buffer at pH5 contains 2% tween 20 as an emulsifier) using a syringe pump at 20ml/h injection rate. This solution was left under magnetic stirring overnight at room temperature to allow the evaporation of the organic phase (ethanol). The beads were collected by centrifugation at 1000 rpm for 10 minutes.

2.3.2. The purification of redox probe-encapsulate beads

2.3.2.1 Centrifugation

The purification of the nanoparticles, for removal of the un-entrapped redox probe, was conducted as follows; post synthesis, 30 ml of the suspended beads was centrifuged, After that 30 ml of the acetate buffer (pH5) was added to the pellet and ultrasonicated (this step was repeated five times). Following that, the square wave voltammetry was performed of the supernatants, which were obtained from each washing cycle. The pallet, from the last cycle, was re-suspended in 5ml of 10 mM acetate buffer pH5. Finally, the PNPs kept in covered glass vial at 4ºC to be protected from the light.

2.4 Characterization of PNPs

2.4.1 Size and zeta potential

Dynamic light scattering (DLS) was used for the measurements of the size and zeta potential. The synthesized particles were dispersed in water (100µl of the freshly synthesized PNPs suspension was diluted in 5ml distilled water) and dispersed by ultrasonication for two minutes to make a homogenous suspension.

2.4.2. Loading efficiency

The concentration of encapsulated probes was estimated indirectly. Initially, a calibration curves for the redox active molecules (in particular FcMeOH and Mb) was obtained from the UV/Vis spectrum. Supernatants after purification were collected and its spectra were measured to obtain the corresponding concentrations. After calculating the amount of un-entreated redox active molecules, the difference between the concentration of un-entrapped and original probe concentrations determined the concentration of the encapsulated probes.

2.4.2 Antibody-conjugate nanoparticles

Adsorption was the process, which was used for the conjugation of the antibody with the nanoparticles. This occurred by mixing anti-hCG antibody with the nanoparticles at the ratio of 10:1 (w/w) of PNPs to the antibody. The incubation was performed in pH 6.5 solution (SME) at room temperature with gentle shaking. After overnight incubation, the PNPs coated antibody was subjected to centrifuge for washing and removal the excess of unbound antibody.

2.4.3 Coating efficiency

In order to calculate the concentration of the antibody, which were bound to the surface of the nanoparticles (PNPs). The concentration of the antibody before incubation was measured from its absorption and the absorbance of the supernatants, which was collected from each washing cycles, were also taken .The equation below was used to calculate the adsorption efficiency:

$$\frac{\mathbf{Ab(added)} - \mathbf{Ab(supernant)}}{\mathbf{Ab(added)}}$$

2.4.3.1 Release of the encapsulated probe

The electrochemical behaviours of the encapsulated probes were determined after dissolution of the PNPs and release of the probes. The PNPs dissolution occurred in two ways: Firstly, by adding alkaline buffer (Tris buffer at pH9), to the immobilized PNPs on NC membrane. Secondly, by the enzymatic reaction between the urea, which was added to the NC membrane, and urease, which was immobilized on NC as the second layer at the top of the immobilized beads.

2.5 Electrochemical experiments

Amperometric techniques such as cyclic voltammetry (CV) and square wave voltammetry (SWV) were performed in order to study the electrochemical behaviours of the released redox active molecules. These techniques were performed in either solution phase or on nitrocellulose membranes as required (the use of nitrocellulose membrane was to create a similar condition for LFAs). The buffers, which were used, are A) Tris buffer at pH9 for PNPs dissolution and releasing of the encapsulated probe and B) Acetate buffer at which was used to keep the polymeric nanoparticles (PNPs) insoluble. The electrochemical measurements were carried out

using Ivuium potentiostat. A saturated silver /silver chloride as a reference electrode was used with 2 mm gold wire disk used as working electrode. The working electrode was polished prior to each measurement using alumina suspensions with decreasing particle sizes (1.0 mm, 0.3 mm, and 0.05 mm) on flat polishing pads. In between each polishing step, the electrode was rinsed with water and left to be dried at RT. A platinum wire was used as a counter electrode.

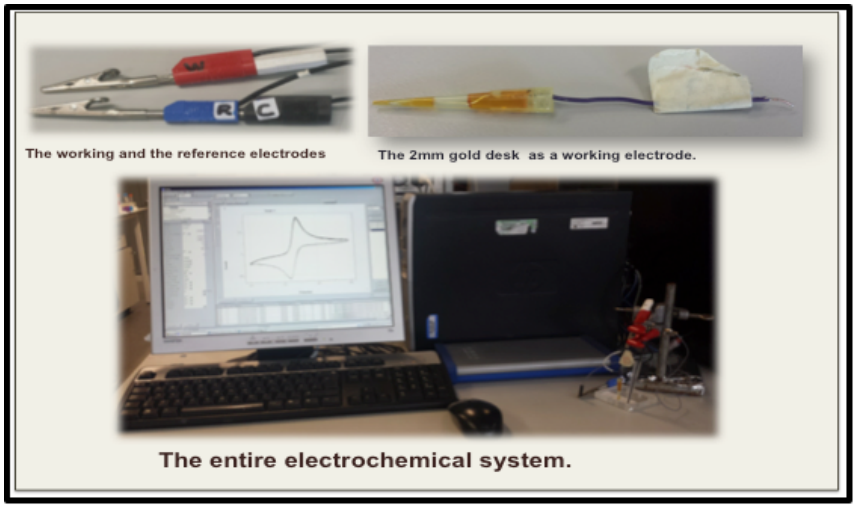


Figure 2-3 The electrochemical experiments set up, the entire electrochemical experiments were conduct on nitrocellulose membrane using sliver /sliver electrode as a reference electrode and 2mm gold disk as working electrode.

2.5.1 Screen-printing based on NC membrane

A screen-printing template of silver/silver ink and carbon ink on NC membrane is designed by Gwent electronic material Ltd.

Chapter 3 Results and discussion: Characterization of anti-hCG aptamer

3.1 Aptasensors

In recent years, the integration of aptamers with the electrochemical sensing has been drawn a lot of attentions. Generally, aptamers, which are used for sensor applications, are modified commonly with thiol group at its 5` end and with redox active molecules at the 3`end. Common redox active modifications include methylene blue and ferrocene derivatives. These modifications respectively assist the aptamers to be attached to a gold electrode and to generate a current via electron transfer. In such applications DNA aptamers have been used more than RNA aptamers and this might because the degradation of RNA occurs more easily. A second reason for most electrochemical aptasensors being based on DNA, rather than RNA is that the SELEX process is less complex for DNA (no reverse transcription and no in vitro transcription steps). Moreover, modified DNA is cheaper than the complementary RNA.

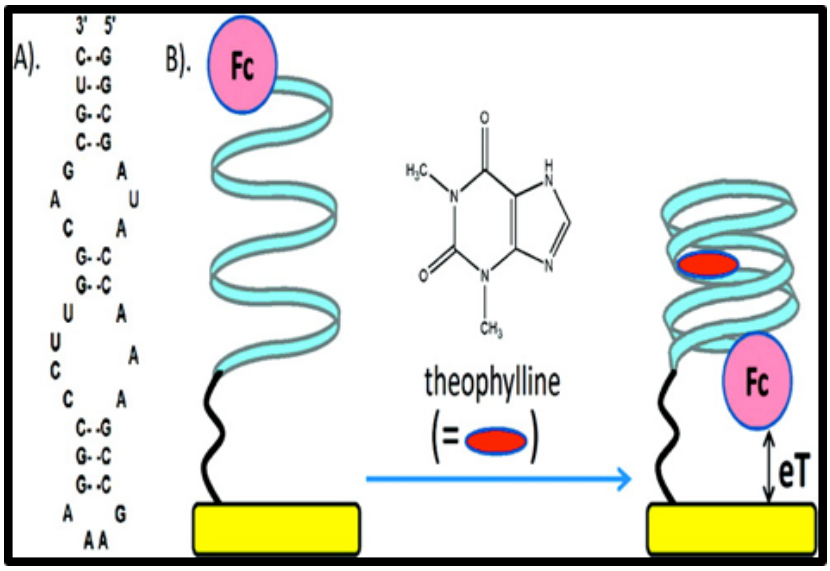


Figure 3-1 A) Theophylline-binding RNA aptamer sequence and (B) schematic representation of the electrochemical RNA aptamer-based sensor for theophylline (Fc = ferrocene). Reproduced from Elena E. Ferapontova; Eva M. Olsen; Kurt V. Gothlf: J.am. Chem Soc, 2008, 130 4256-4258 Dol G10.1021/ja711326bCopyright © 2008 American Chemical Society (with permission).

The first reported RNA aptamers based electrochemical sensor was developed for theophylline detection. The theory behind its operation was that, when RNA is modified and attached to the electrode surface, the open extended conformational structure of RNA yields a long distance between the redox couple and the electrode surface, which results in slow electron transfer and hence low current. In the presence of the target, the RNA is folded and the resulting structure decreases the distance and consequently increases the electrochemical signal. This concept is illustrated in the Figure 3-1**.** In recent years, the integration of aptamers with the electrochemical sensing has been drawn lot of attentions. Generally, aptamers, which are used for sensor applications, are modified commonly with thiol group at its 5` end, and with redox active molecules at the 3`end. Common redox active modifications include methylene blue and ferrocene derivatives. These modifications respectively assist the aptamers to be attached to a gold electrode and to generate a current via electron transfer. In such applications DNA aptamers have been used more than RNA aptamers and this might because the degradation of RNA occurs more easily. A second reason for most electrochemical aptasensors being based on DNA, rather than RNA is that the SELEX process is less complex for DNA (no reverse transcription and no in vitro transcription steps). Moreover, modified DNA is cheaper than the complementary RNA. However, the first reported RNA aptamers based electrochemical sensor was developed for theophylline detection. The theory behind its operation was that, when RNA is modified and attached to the electrode surface, the open extended conformational structure of RNA yields a long distance between the redox couple and the electrode surface, which results in slow electron transfer and hence low current. In the presence of the target, the RNA is folded and the resulting structure decreases the distance and consequently increases the electrochemical signal. This concept is illustrated in the Figure 3-1**.** Based on the reported results of Ferapontova et al, development of an aptasensor for hCG detection would be promising tool to improve the quality of pregnancy tests by providing a quantitative measurement. An anti-hCG RNA aptamer had previously isolated though SELEX a process and has the following sequence-SEQ ID No.126 (Gold patent).

GGGAGGACGA **UGCGGGUUUC ACUUCAAGUU GAACGAUCCU UCUUGGCUUG AGCACAGACG ACUCGCCCGA (N70).**

The aptamer was calculated to have a KD of 430 nM using a filter-binding assay. In this chapter, results regarding the further characterisation of the anti-hCG-aptamer are discussed.

3.2 Size analysis of RNA aptamer

A synthetic DNA oligonucleotide was used to produce the RNA aptamer by in vitro transcription as described in chapter 2. Chemical synthesis of RNA is costly compared with DNA synthesis and so *in vitro* transcription offer a convenient and lower cost route. After transcription, the linear dsDNA template was digested using RNase free DNase. The size of RNA aptamer was determined using urea polyacrylamide gel electrophoresis (Urea PAGE), which is widely used for this purpose. The urea denatures any secondary structure in the RNA aptamer and so the migration though the polyacrylamide gel matrix is according to its molecular weight (29 KD). The size of RNA is 91 including the priming sequence. A clear single band indicates that RNA was not degraded and ready to use for further experiments as it can be seen from the Figure 3-2.

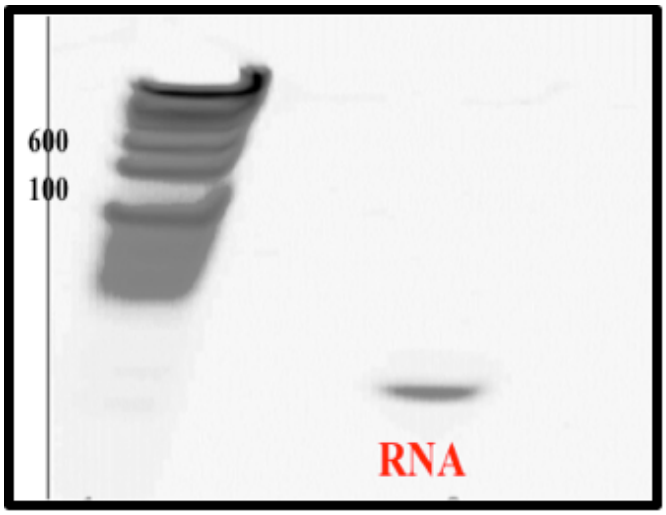


Figure 3-2 7M Urea polyacrylamide gel electrophoresis for the size determination of RNA aptamer synthesized via *in vitro* transcription and purified by ethanol precipitation. After that, 12 µl of the mixture (RNA+ loading buffer) as loaded into the gel wall, the gel was stained in SYBR gold and imaged using the Diversity system.

3.3. The conformational structure of RNA using CD

Circular dichroism (CD) was employed to study the conformational structure of anti hCG-RNA aptamer in its native state and in the presence of hCG. The conformational structure of RNA aptamer under different conditions (temperature and ionic strength) was also investigated. This helps to explore the changes in RNA spectra under various conditions, which reflects the changes

in its structure. The CD spectrum of 5 µM RNA aptamer at 37°C is shown in Figure 3-3**.** This spectrum has a maximum positive peak at 265 nm and two weak negative peaks at around 240 nm and 220 nm.

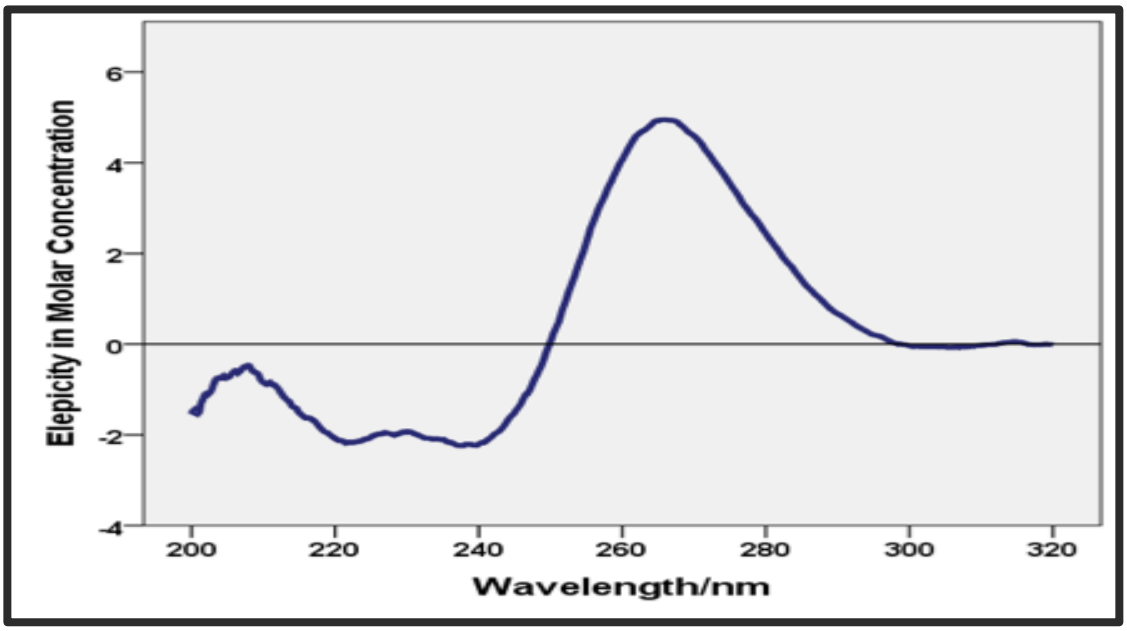


Figure 3-3 The CD spectra of 5 µM of RNA aptamer in TEM buffer at 37° C. The maximum negative peak at 265nm and the weak negative peak at 235nm suggest that the RNA aptamer might have A-form structure.

A similar positive peak is observed at the same wavelength for RNA in the complex of aptamer and hCG (5 µM RNA aptamer and 10 µM hCG) as shown in **Figure 3-4.** These RNA spectra are similar to one reported by Bozza et al (2006), who assigned the positive peak at around 265 nm and the weak negative peak at 235 to a mismatched hairpin structure where the duplex region contained the mismatches indicating a normal A- form structure. Additional results show a shift in the positive peak from 265 nm to 270 nm and another shift from 220 nm to 210 nm in the negative peaks. There was also change in the relative intensities of the positive at negative peaks. These spectra probably reflect structural change in the RNA as a result of binding to hCG. No contributions to the CD spectra arise from hCG since it has negligible ellipticity above 200 nm even at the concentration of 20 µM.as it can be seen from the Figure 3-5**.**

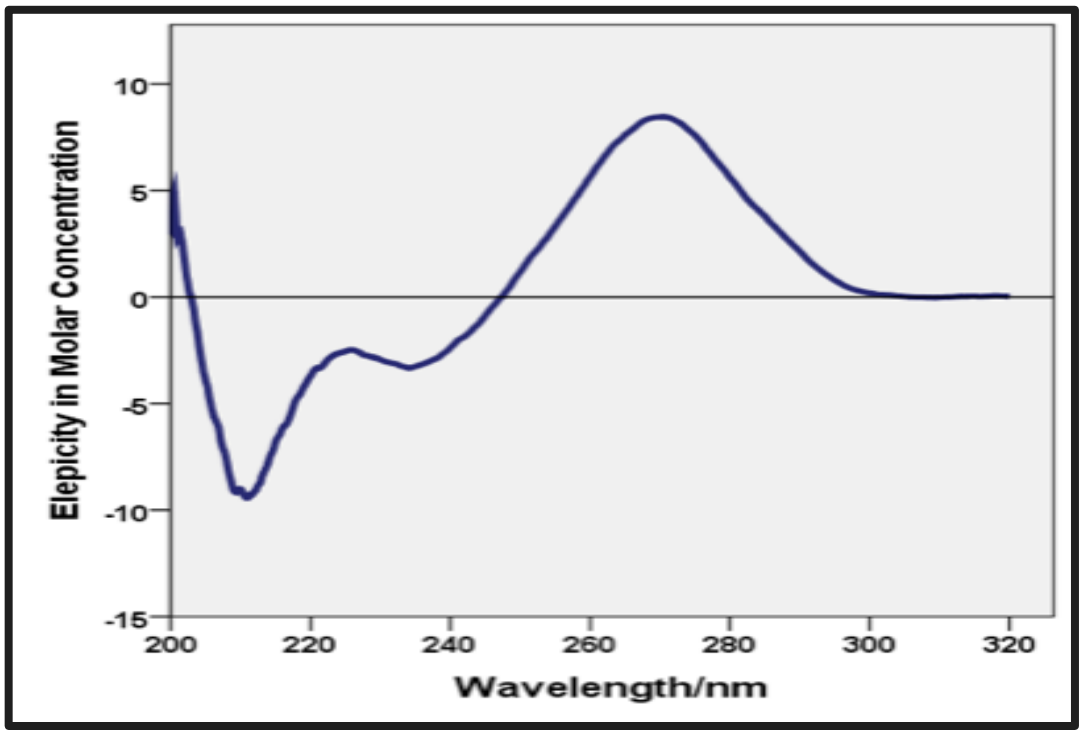


Figure 3-4 The CD spectra of the complex of 5 μM RNA aptamer after binding to 10 μM hCG. This mixture was incubated for 2 hours and filtered prior to the CD measurement.

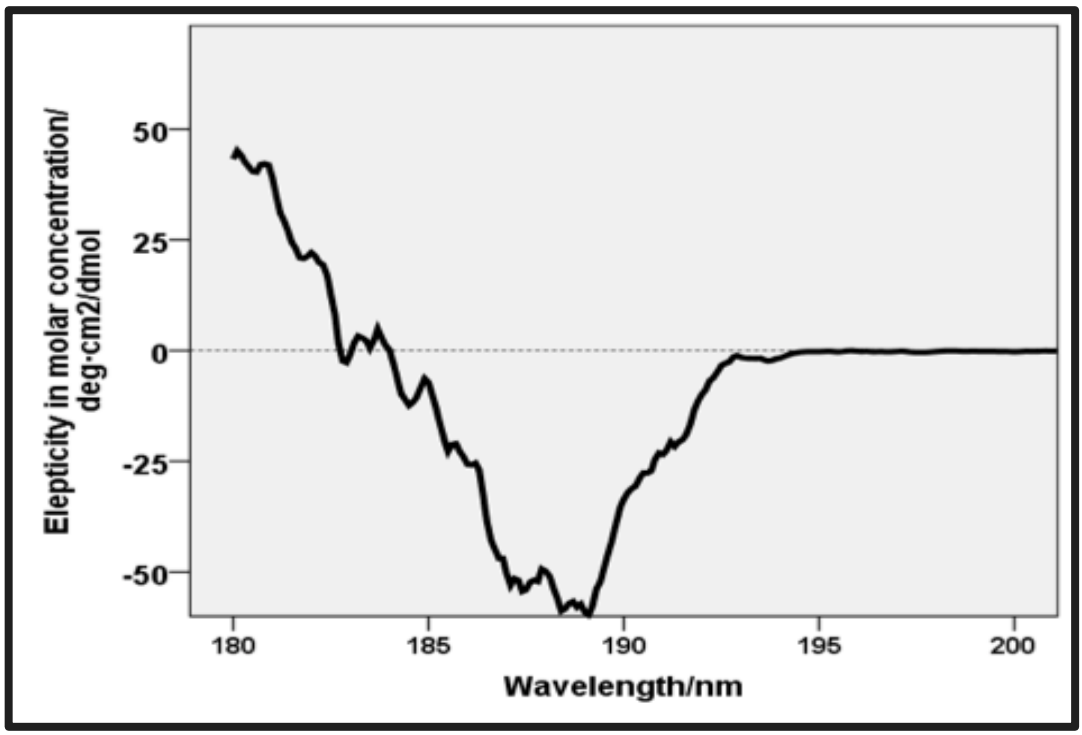


Figure 3-5 the CD spectra of hCG shows a maximum negative peak at 189nm.

The major sequence-dependent forces drive the helix formation such as base stacking and hydrogen bonding is affected by environmental conditions such as temperature, pH and the type and the concentration of the salts present. Here it was decided to investigate the conformational change of RNA aptamer at different temperatures (range from 20º C to 90º C.

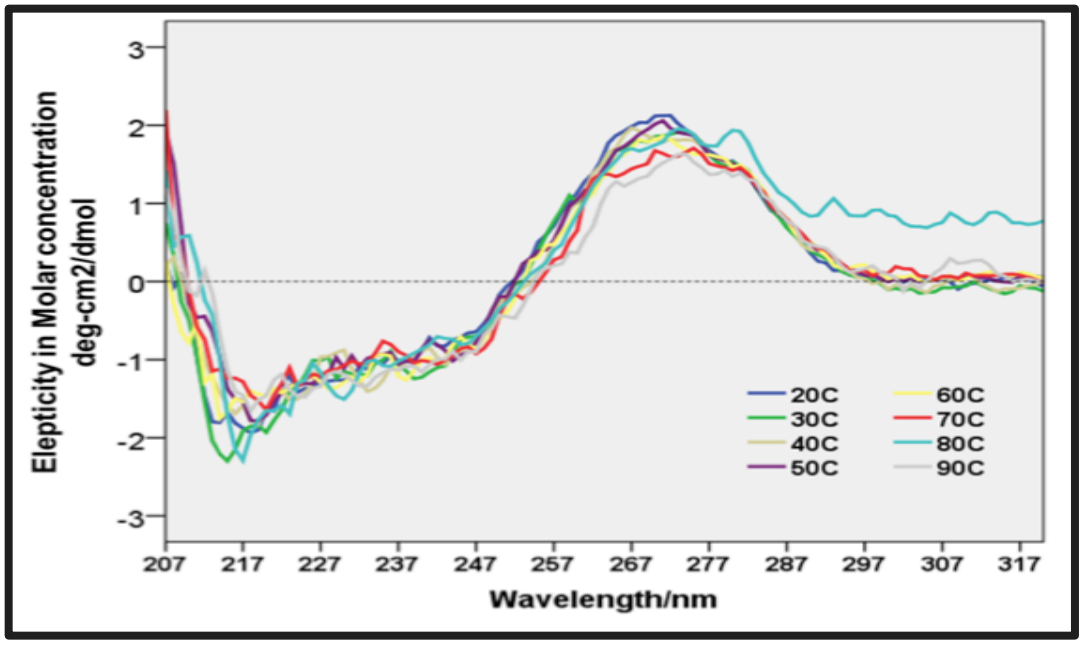


Figure 3-6 The CD spectra of 2µM RNA aptamers under different temperature ranging from 20ºC to 90ºC to investigate the RNA stability.

The results indicate that there is no detectable change in the conformation of RNA aptamers with increased temperature which might reflect the highly stability of the secondary structure which is not easily converted to the linear form. This is demonstrated in the Figure 3-6**.** It is also can observed from the figure that the intensity of the CD measurements is shifted from 265 nm to 270 nm at it is maximum positive peak compared to previous CD RNA spectra. Finally, different salts at different concentrations were also evaluated to study the effect of these salts on the conformational structure of RNA aptamers. In two separate experiments LiCl and $MgCl_2$ at different concentration (10-50-100 mM) were added separately in TEM binding buffer and CD was performed at 37ºC as can be seen respectively from Figure 3-7 and Figure 3-8**.** The results show that there is a shift in the wavelength of the maximum peak from 270 nm to 265nm when decreasing the concentration of the LiCl (10 mM), whilst there is no difference in the CD spectra with the addition of Mg^{+2}.

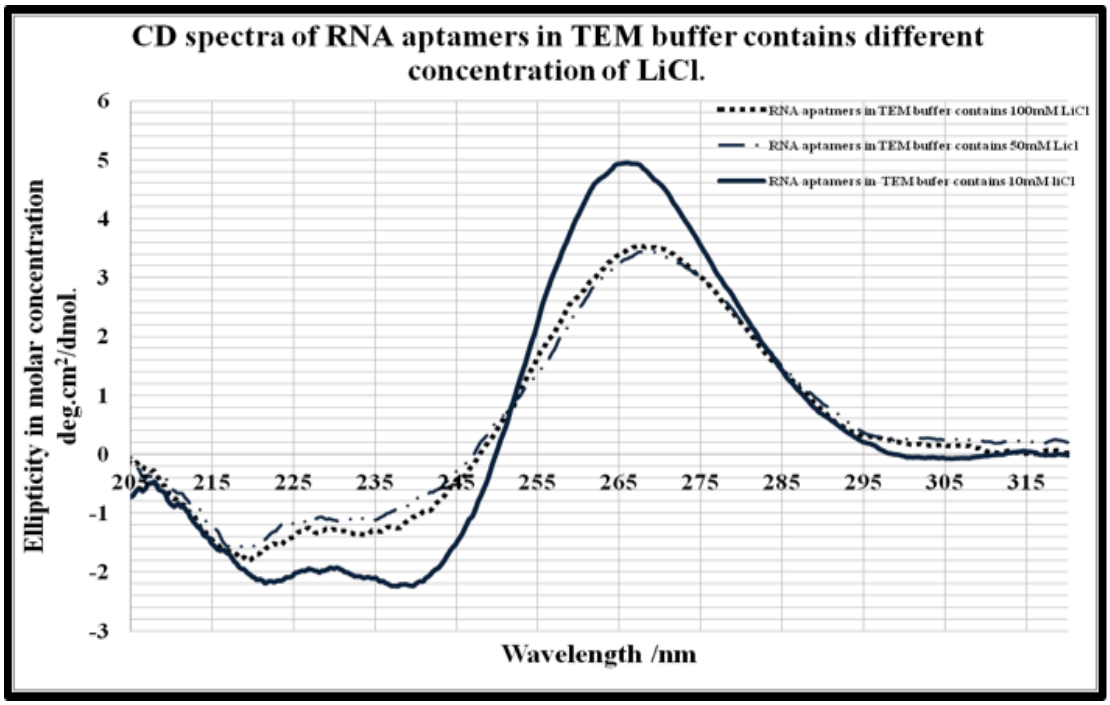


Figure 3-7 the CD spectra of 5 µM RNA aptamer in different LiCl concentration (10-50 and 100 mM)**.**

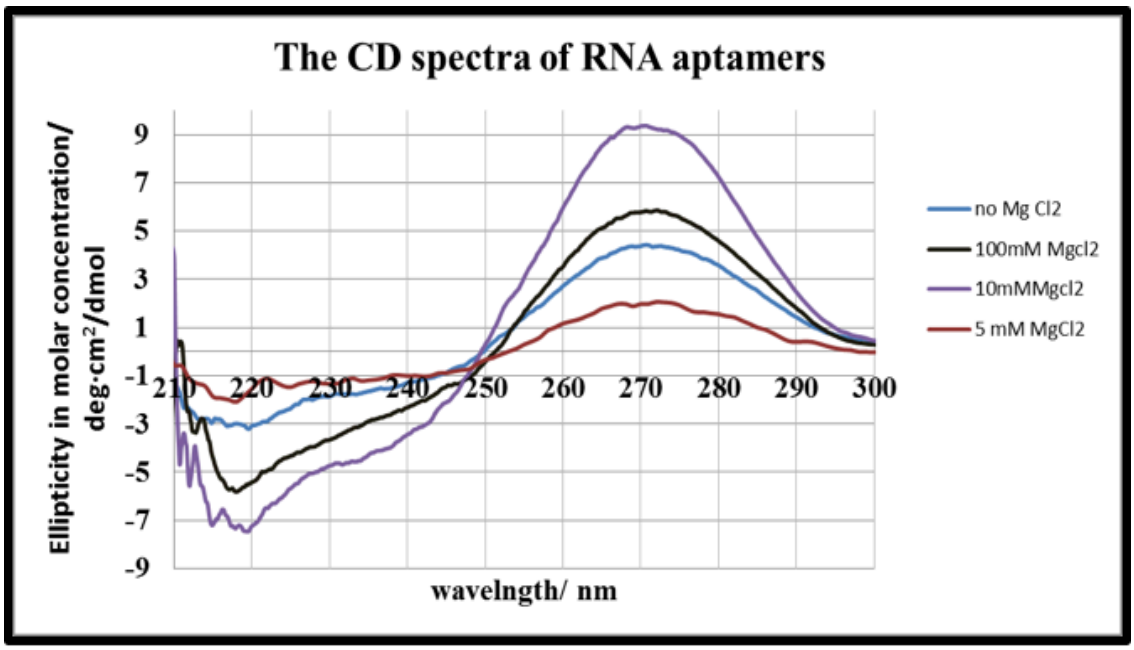


Figure 3-8 the CD spectra of 5 µM RNA aptamer in different $MgCl_2$ concentration**.**

In the light of the results above, almost all obtained CD spectra of RNA aptamers under investigated condition showed similar behaviour of their conformational stricture, which suggests that the secondary structure of RNA to a certain extent is stable under these specific conditions.

3.4 ELONA

An ELONA assay was used to evaluate the binding affinity between the RNA aptamer and hCG. A fixed concentration of hCG (50 nM) was absorbed in the wells of a microplate walls of a microplate and various concentration of biotinylated RNA aptamer were titrated in as shown in as shown in Figure 3-9.

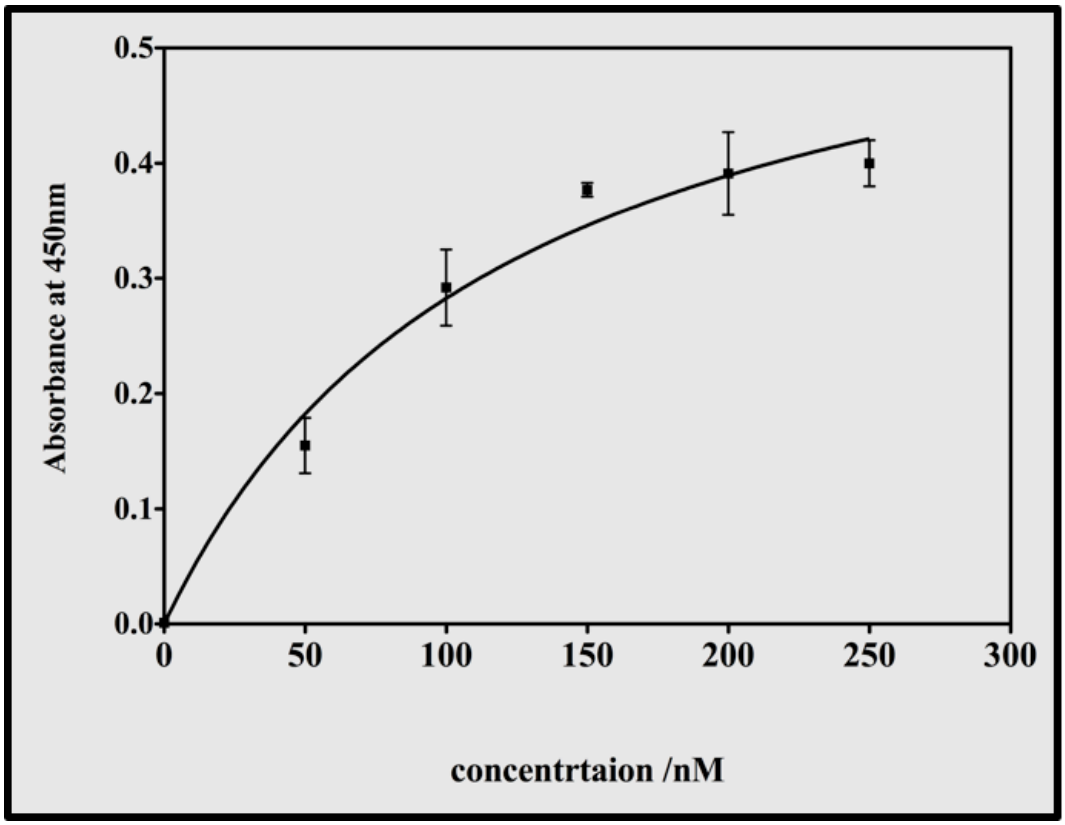


Figure 3-9 An ELONA assay for difference concentration of B-RNA aptamers and 50 nM of hCG.

During the course of running these assays it was found that there was significant variation in the dose-response curves and this may have been due either to the variable properties of different biotinylated RNA preparation or different efficiencies of immobilization of hCG on the plates .To

test the latter, the concentration of hCG in the immobilization solution was varied and the results are shown in Figure 3-9. The amount of hCG adsorbed was relevantly constant suggesting that 50nM was sufficient to completely coat the plastic wall. As a second control, the assay was repeated with a biotinylated anti-hCG antibody rather than the aptamer and the results shows in the Figure 3-10 and Figure 3-11 are broadly consistent with those for the aptamer as can be seen from Figure 3-12. It was concluded after many repeated assays that both chemical and enzymatic biotinylation of the aptamer gave very large batch-to-batch variation making the use of these reagents problematic.

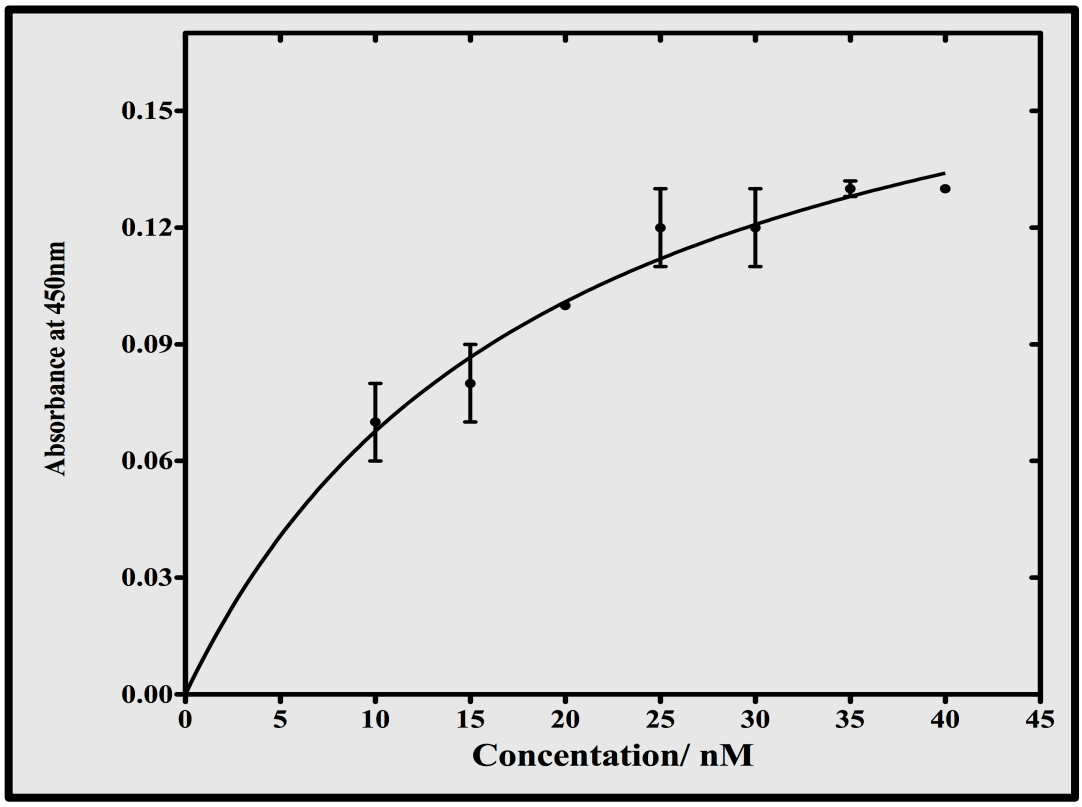


Figure 3-10 an ELISA assay, different concentrations of hCG was immobilized on the walls and (1:1000) diluted biotinylated antibody were added to hCG.

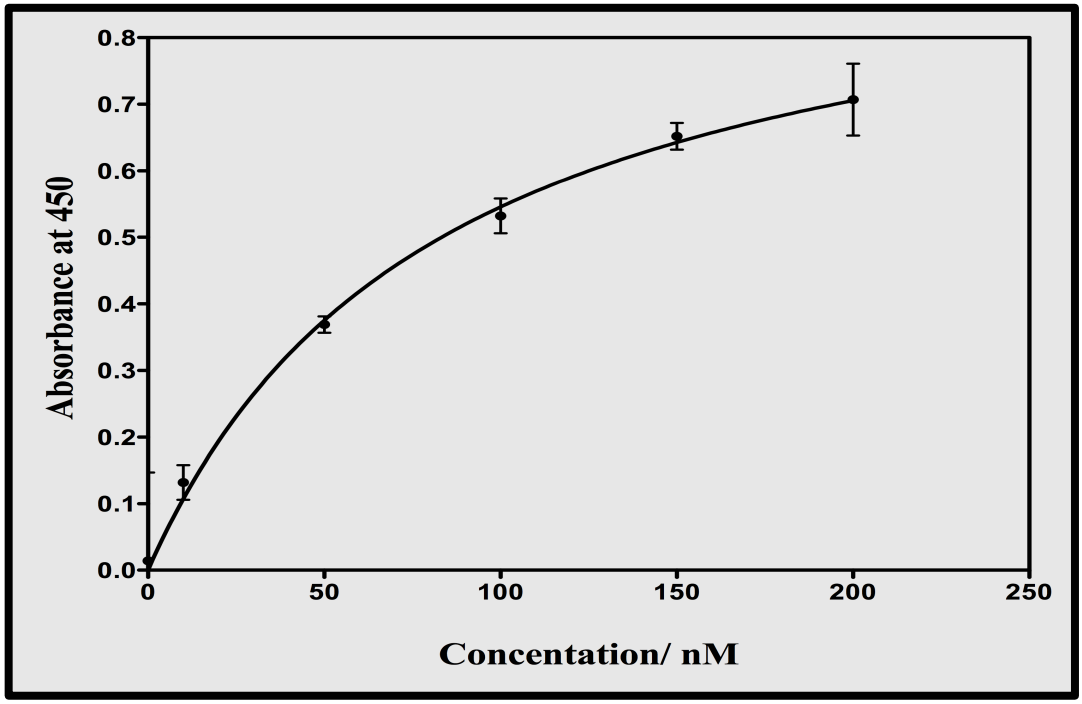


Figure 3-11 an ELISA assay, different concentrations of hCG was immobilized on the walls and (1:1000) diluted biotinylated antibody were added to hCG.

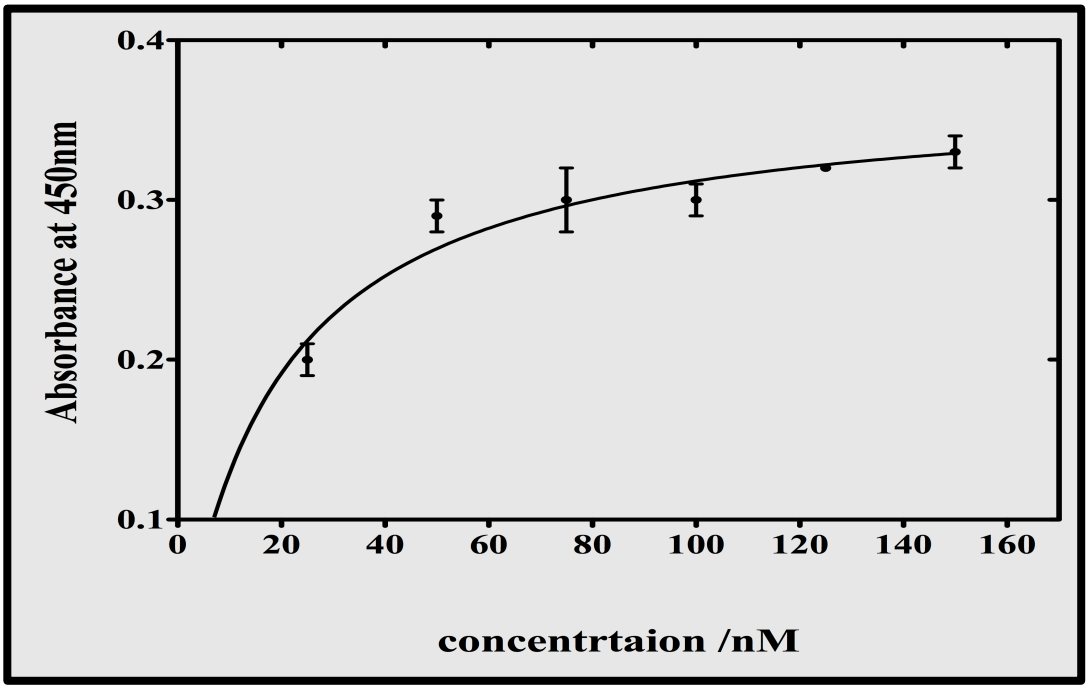


Figure 3-12 An ELONA assay for different concentration of B-RNA aptamer.

3.6 Discussion

In this section, a comprehensive study of RNA aptamers, which was selected against hCG is demonstrated. The production of RNA aptamers was performed via *in vitro* transcription from dsDNA. The size of RNA aptamer was confirmed by urea polyacrylamide gel, which also showed good quality of the product. A spectroscopic technique in particular CD was performed in order to investigate the conformational study. The CD spectra showed similar secondary structure regard less of the condition variables, which were under investigation.

3.7 Summary

The original aim of this work was to use the anti-hCG aptamer in sensor however, the substantial batch-to-batch variation in the properties of the biotinylated aptamers make it likely that similar variability would be been in other chemical modification and so make producing a reliable aptasensors very difficult. For that reason, selection a second approach to quantitative hCG was considered and this is discussed in more details in the next chapter.

Chapter 4 Synthesis and characterization of the polymer nanoparticles

This chapter presents results regarding the synthesis and the characterisations of the polymer nanoparticles (PNPs), with five different probes encapsulated. A variety of redox probe was used to give a range of electrochemical behaviour. The nanoparticles were characterized in term of size, zeta potential and loading efficiency as discussed subsequently.

4.1 Nanoparticles synthesis

Nanoprecipitation, which was initially developed by Fessi et al, (1989) was chosen in order to synthesis polymer nanoparticles PNPs. Based on the literature, eudragit S-100 was chosen as a suitable material to develop PNPs that entrapped redox active molecules. These polymers are widely and successfully used as a carrier system for drug delivery and so have been very well studied. They can protect drugs from the acidic conditions of the stomach, where they are insoluble and effectively release them in the intestines where there is alkaline condition. Although eudragit S-100 is widely used for encapsulation of drugs, trapping redox probes into eudragit S-100 PNPs has to our knowledge, not been reported previously. However, the proprieties of the five-redox active molecules are summarized in Table 4-1The properties of five chosen redox probes**.** The synthesis of the polymer nanoparticles encapsulated probe was done using nanoprecipitation process. **Section 2.3.1** describes the nanoprecipitation process in detail. However, there are several variables in the process of nanoprecipitation, which individuals have an effect on the features of PNPs produced. These variables have previously been empirically optimized to give the NPs synthesis for the all-subsequent experiments as are shown in **Table 4-2** The parameters of eudragit S100 nanoprecipitation

Table 4-1 The properties of five chosen redox probes

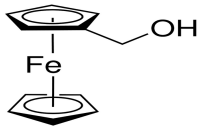
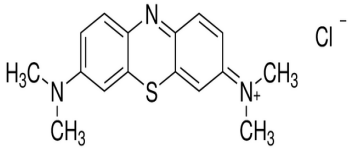
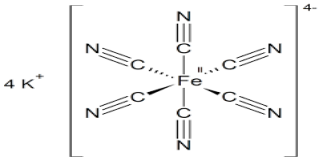
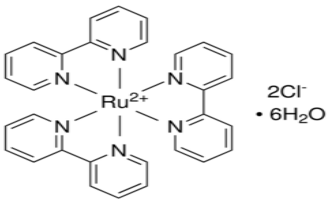
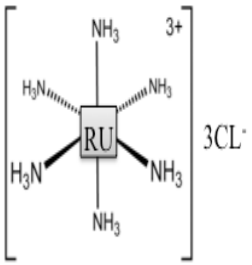
Probe name	**Chemical structure**	**Charge**	**Molecular weight\Da**
Hydroxylmethyl ferrocene		Neutral	216
Methylene blue		Positive	373
Potassium Hexacyanoferrate (III)		Negative	329
Tris (2,2` bipyridyl) dichlorouthenium (II) hexahydrate Ru (BPY) $_3$		Positive	748
Hexaammineruthenium (III) chloride [Ru (NH_3) $_6$] CL_3		Positive	309

Table 4-2 The parameters of eudragit S100 nanoprecipitation

Parameter	**Used condition**
Type and volume of organic phase.	11ml of 96% ethanol.
Volume of continuous phase.	50ml of emulsion buffer (100mM sodium citrate at pH5).
Stirring speed.	600 rpm
Surfactant	2% Tween 20
Injection rate.	20ml/ hour

The choice of ethanol as a solvent was based on the published literature Tang et al, (2011). Unlike acetone and other solvents, ethanol completely dissolves the polymers and the redox probes. It is less toxic than most solvents as well being easy to remove during the purification of the PNPs by washing with an aqueous buffer. The importance of using an acidic medium as the emulsion buffer is because the polymers are insoluble at pH5 therefore the probe becomes encapsulated until released at increased pH. The role of the surfactant (Tween 20) is to preserve the suspension of the nanoparticles and prevent agglomeration over the long storage periods. Different surfactants for example, polyvinyl alcohol (PVA) have been commonly used. However, since it was reported that PVA remains on the surface of the particles and is difficult to remove, it was avoided in this case. As an alternative, tween 20 (2% w/v) was used as a stabilizer. Moreover, it was reported that the rotating speed usually controls the size of the produced nanoparticles. Thus the rotating speed of nanoprecipitation process was set at 600 overnight at room temperature. This rotation speed might helps to achieve a complete solvent evaporation.

4.2 Purification of the PNPs by centrifugation

To avoid any interference with the electrochemical signals and to reduce the background single, removal of un-encapsulated redox probes were essential. This was carried out immediately after the nanoprecipitation process. The suspension was washed several times with acetate buffer

(pH5) and the PNPs were recovered by centrifiugation. Square wave voltammtery (SWV) was performed in triplicate on the supernatants after each wash. The results from four seperate probes are shown in the Figure 4-1,Figure 4-2**,** Figure 4-3 **and** Figure 4-4. According to the data, it is apparent that $Ru(BPY)_3$ was washed away over the course of four washing cycles. Similar results were observed with the other redox probes are illustrated in Figure 4-2 Figure 4-3 and Figure 4-4**.** Whilst most of the redox probe showed a supernatant current of 200-300 nA, Hexaammineruthenium (III) chloride was about 5-7 fold less than this, suggesting a more efficient encapsulation process and hence less redox probe remained un-encapsulated.

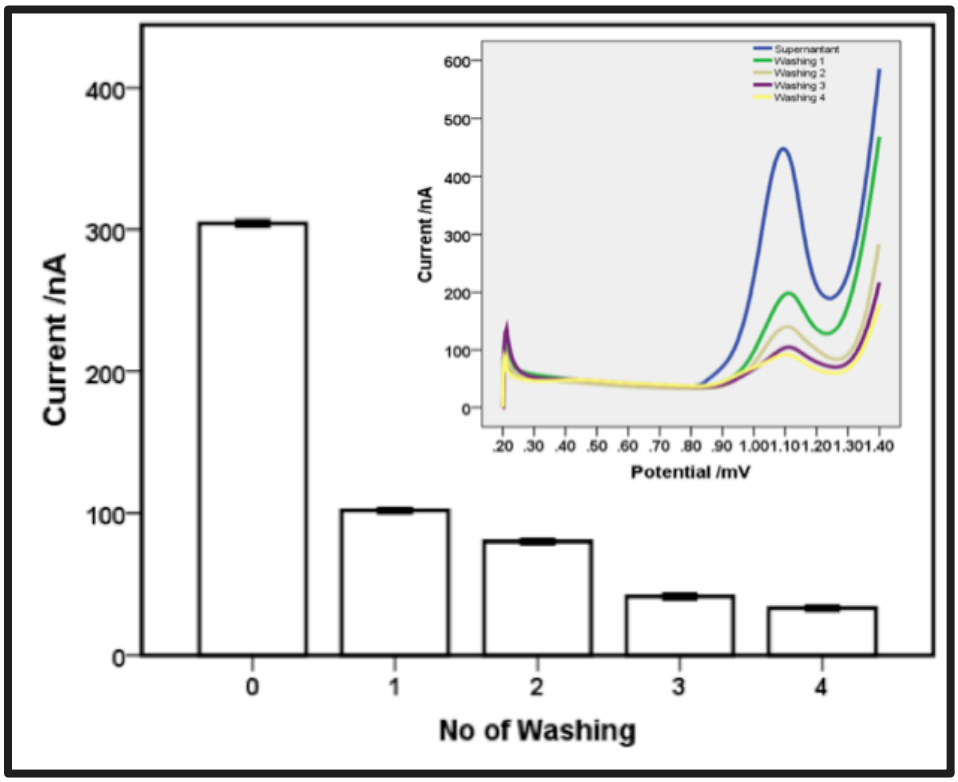


Figure 4-1 The purification of the PNPs encapsulated $Ru(BPY)^{+3}$,which was done by several washing cycles with acetate buffer (pH5) and then PNPs were recovered by centrifugation. Square wave voltammetry was performed in each supernatant in triplicate. The mean of the maximum current peak were plotted against the washing number.

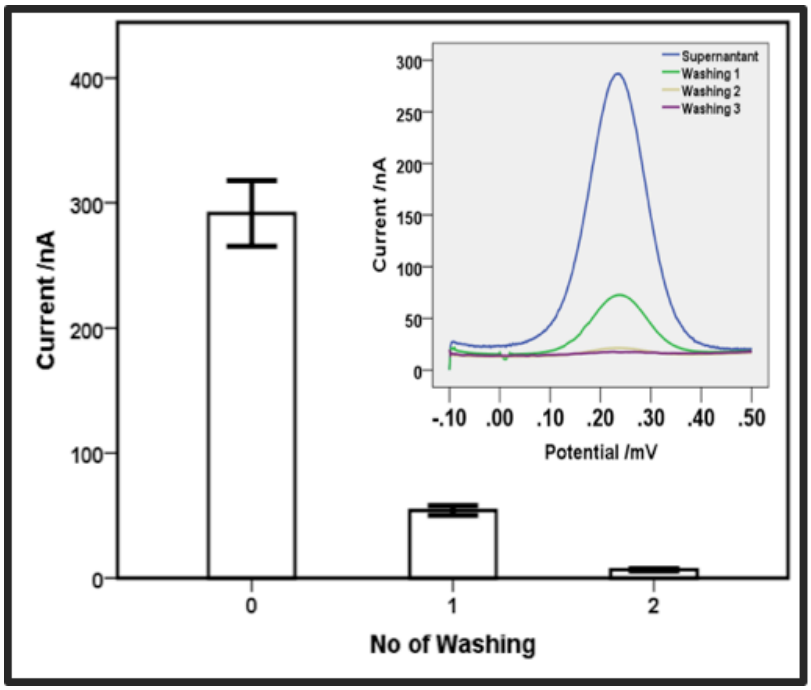


Figure 4-2 The purification of the PNPs encapsulated $K_3[Fe(CN)_6]$,which was done by several washing cycles with acetate buffer (pH5) and then PNPs were recovered by centrifugation. Square wave voltammetry was performed in each supernatant in triplicate.

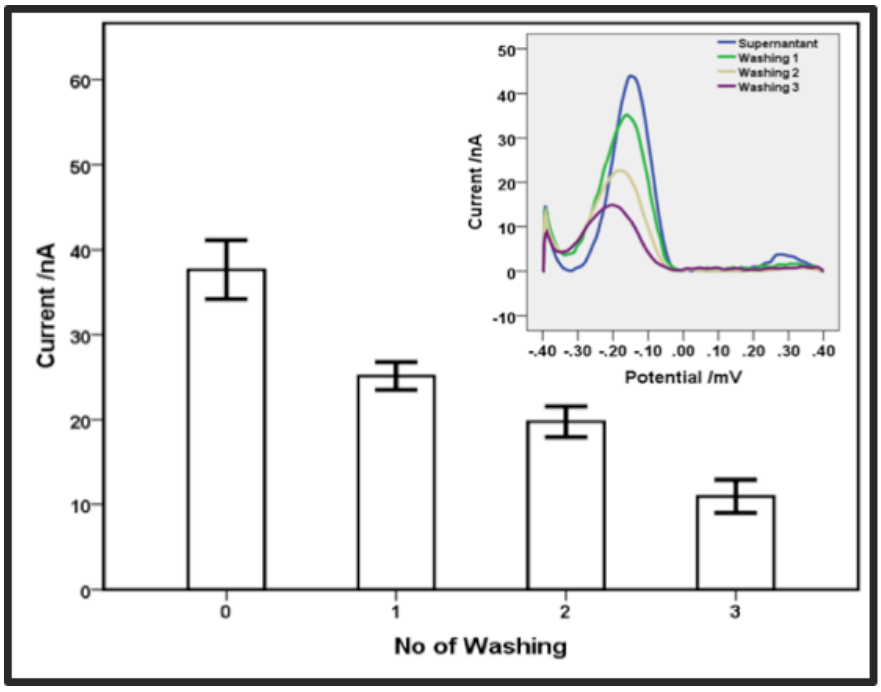


Figure 4-3 The purification of the PNPs encapsulated **[**$Ru(NH_3)_6]CL_3$,

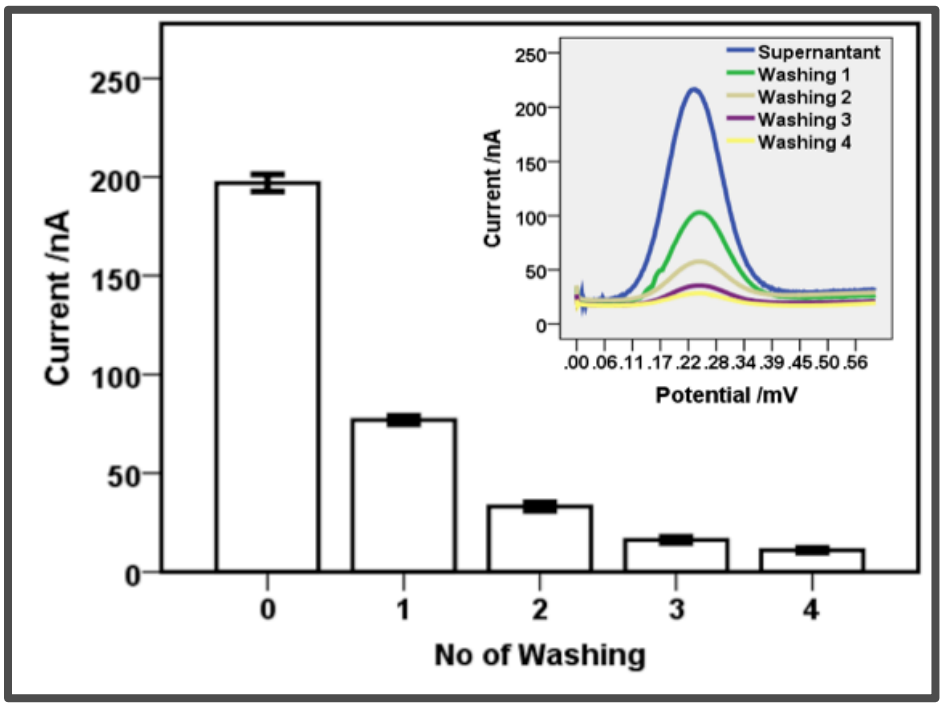


Figure 4-4 The purification of the PNPs encapsulated FcMeOH, which was done by several washing with acetate buffer (pH5) and the PNPs were recovered by centrifugation. Square wave voltammetry was performed in each supernatant in triplicate. The mean of the maximum current peak were plotted against the washing number. The un-entrapped probes were moved away after 4 washing cycles.

4.3 Size analysis by dynamic light scattering (DLS)

The size distribution (dispersity) is an important property of the nanoparticles preparation. The nanoparticles, which were prepared by the nanoprecipitation technique, showed fairly uniform appearance in term of their dispersity. The interbatch variation in mean particle diameters was around 5% showing that the batch-to-batch uniformity was good. Similarly the dispersity of the different preparation was constant. The size of FcMeOH-NPs was approximately 219.6$\pm$12 nm and the size of Mb-NPs was 316$\pm$14 nm. Theses probes-NPs have nano-scale particles in comparison to the control batch about 1000 nm (polymer with no redox probe encapsulated- data not shown). Also the micro-scale particles (almost 2631$\pm$251nm, 4000 nm and 5327$\pm$170 nm) were produced respectively, when $[K_3[Fe(CN)_6]$,$[Ru(NH_3)_6]CL_3$, and $Ru(BPY)_3CL_3$ were encapsulated. The comparison of the size for all investigated probes is demonstrated in the Figure 4-5.

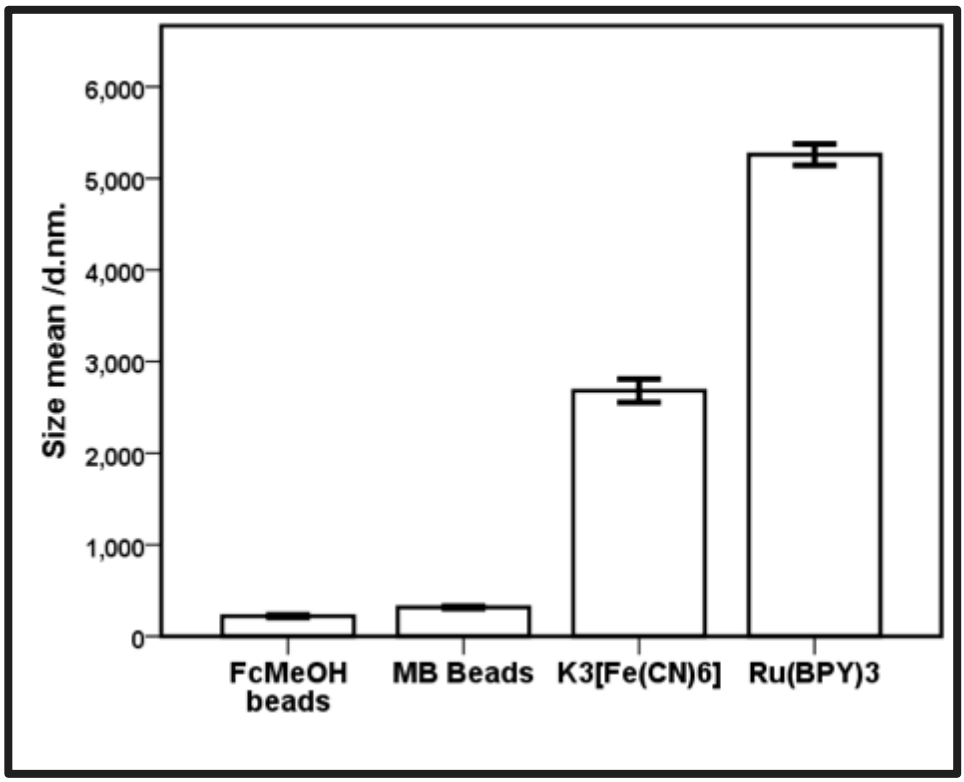


Figure 4-5 The comparison of the size mean for the probes under study.

4.4 Zeta potential

Another characteristic feature of the polymer nanoparticles of extreme interest is the zeta potential (surface charge). Polymer nanoparticles that dispersed in an aqueous medium is showing a negative charge because of the ionization of the carboxyl' groups. The surface charge provides the colloidal the stability as well as the efficient conjugation with the antibody, which occurs due to the electrostatic interaction between the negatively charged PNPs and the positively charged antibody. The DLS measurements showed that the charge surface of FcMeOH-PNPs was -43+1.5 mV, -29+1.3mV of Mb-PNPs. The zeta potential of $K3[Fe(CN)_6]$ is -27+0.8. In contrast, 0 values obtained in case of control sample (data not shown) and for both $Ru(BPY)_3$ and $[Ru(NH_3)_6]cL_3$.The comparison in zeta potential for all probes is presented in **Figure 4-6.**

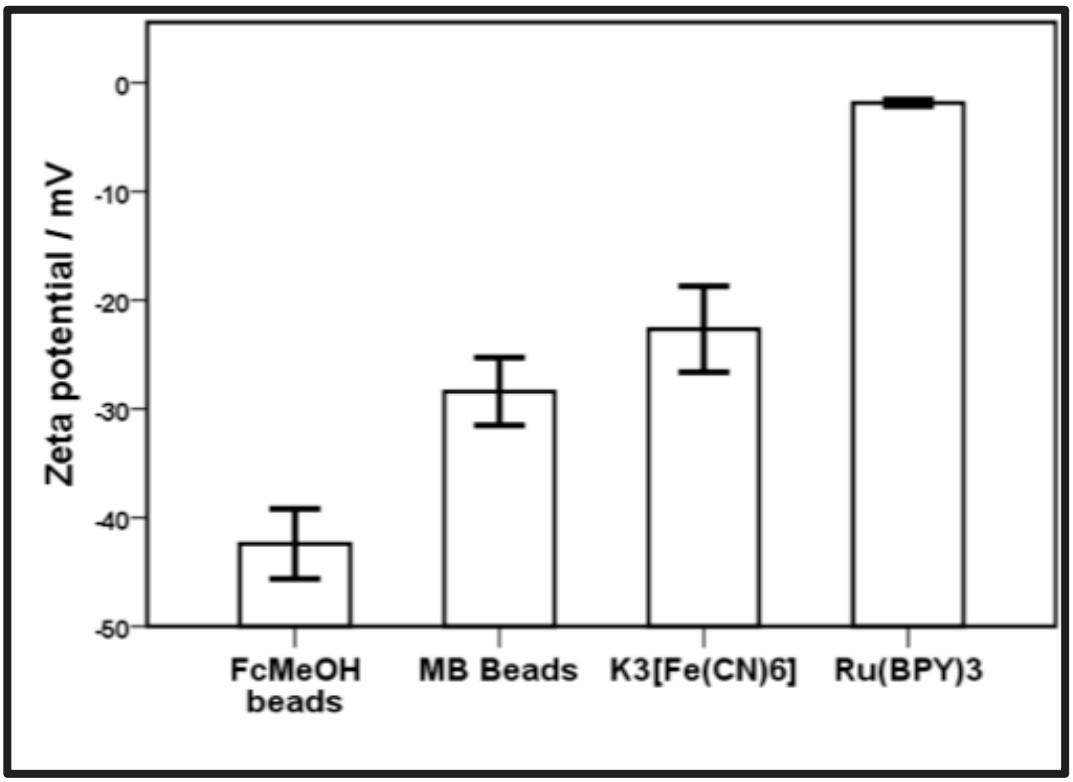


Figure 4-6 the zeta potential values for four different probes-NPs, which were under the study. The data shows highly value of negative charge NPs with all probes apart from $Ru(BPY)_3$.

4.5 Loading efficiency

The estimation of the concentration of the entrapped probe in particular, FcMeOH and Mb was calculated indirectly by calculating the concentration of the un-encapsulation, which was collected from the supernatants after NPs synthesis process. In more detail different concentration of the selected probes were prepared and then the absorbance's measurements were taken using UV/vis spectroscopy as described in chapter 2. The calibration curve was then obtained as shown in the Figure 4-7**.** After purification of the PNPs. the supernatants were collected from each washing cycle, the spectra of the supernatant were measured using UV/Vis spectroscopy and interrupted at the calibration curve to determine the corresponding concentration. The number of moles was then calculated from the equation below since the volume and the concentration are known.

$$\mathbf{concentration = mole/liter}$$

However, the amount of free probe was calculated form the equation below and then converted to the unit of mg:

$$\textbf{Mole} = \frac{\textbf{Mass (g)}}{\textbf{molar mass g/mol}}$$

The amount of the encapsulated probe is then calculated from the equation below:

$$\textbf{The amount entrappted probe} = \textbf{total probe amount} - \textbf{the amount of free probe}$$

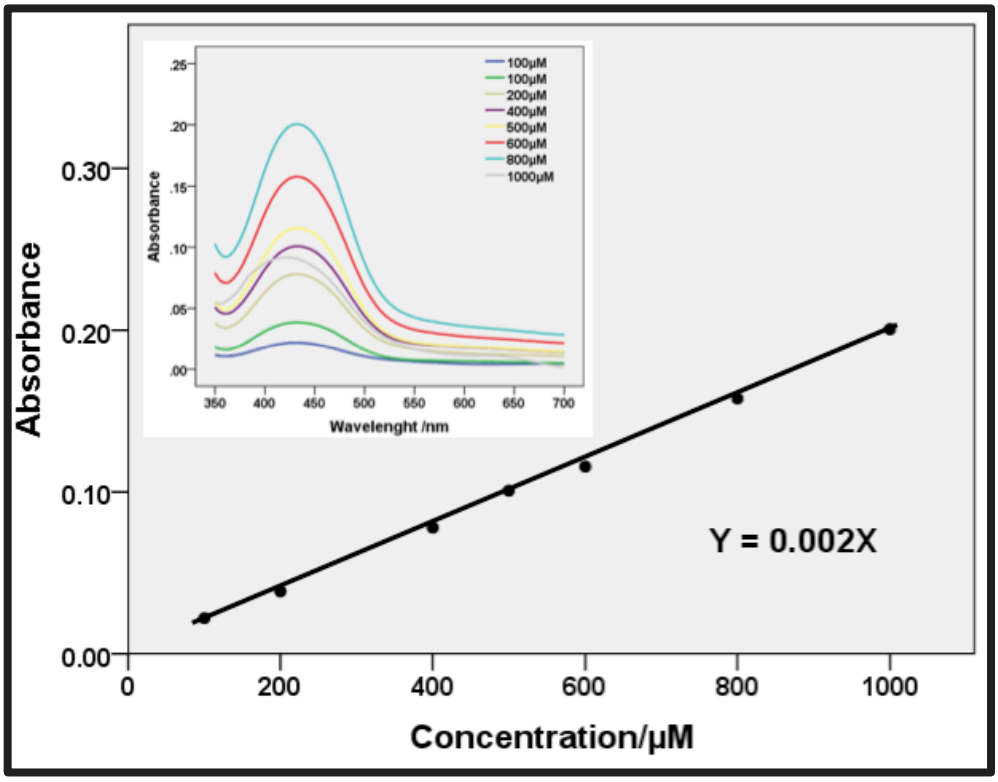


Figure 4-7 The calibration curve of FcMeOH at different concentrations, the calibration curve was obtained from plotting the maximum absorbance value against the corresponding concentration. The measurements performed using UV/vis spectroscopy.

The percentage value is determined as follows:

$$(\%) = \textbf{amount of entrappted probe/total amount} * \textbf{100}$$

Table 4-3 The concentration of the entrapped ferrocene methanol

Batch No.	**Total amount of FcMeOH (mg)**	**Amount of un-entrapped FcMeOH (mg)**	**Amount of entrapped FcMeOH (mg)**	**Percentage %**
1	28	13	15	53
2	28	12	16	57
3	28	11	19	58
4	28	15	13	43

As presented in the **Error! Reference source not found.** that the amount of entrapped FcMeOH was almost half of the initial amount of FcMeOH. This means that the encapsulation of FcMeOH into the PNPs were efficient. The variation from patch to patch was not really significant. To confirm the efficient encapsulation of FcMeOH, calibration curve was obtained by a voltammetric technique in particular square wave voltammetry as shown in **Figure 4-8**. It was found that 70 µmol out of 130 µmol of ferrocene methanol was un-entrapped. This means half of the probe was entrapped.

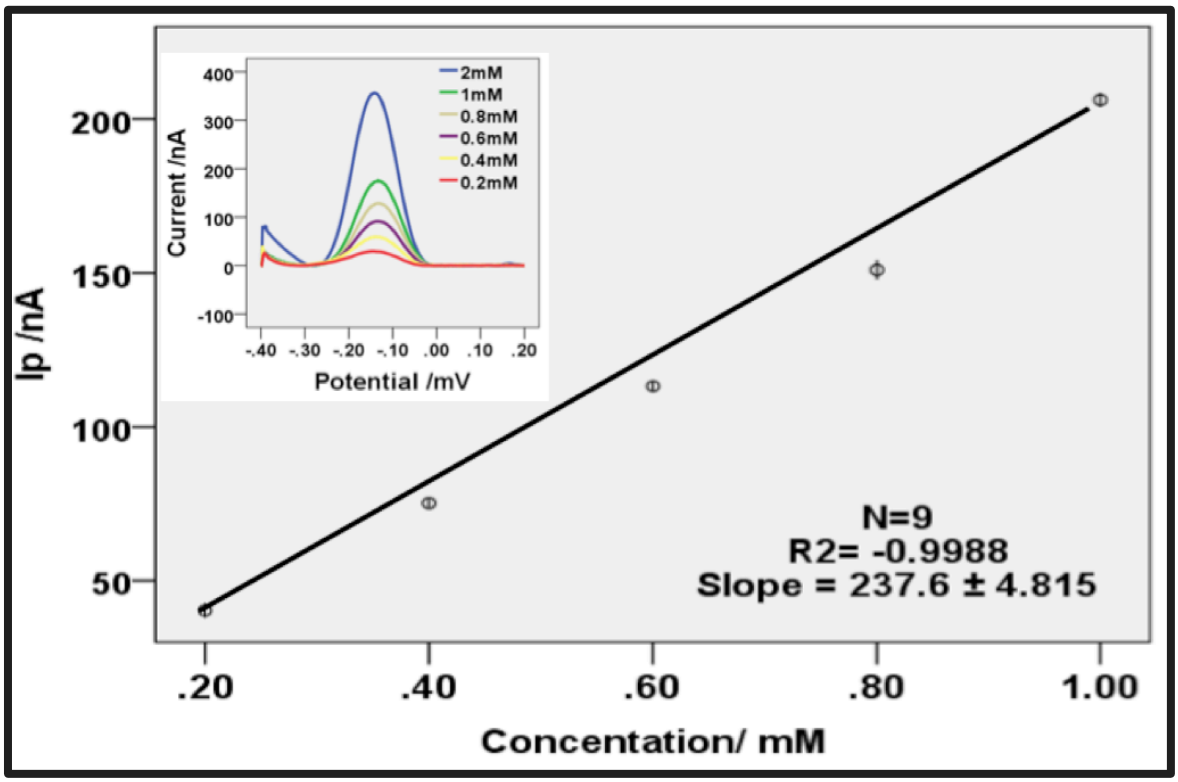


Figure 4-8 Calibration curve of FcMeOH at different concentrations obtained by applying square wave voltammetry (SWV). FcMeOH was prepared in acetate buffer (pH5).

Likewise, the concentration of the encapsulate Mb was calculated using UV spectroscopy method as described previously; the calibration curve is can be seen from the **Figure 4-9** .The encapsulation of Mb to PNPs was efficient since more than 70% of the total amount as seen from **Table 4-4**.

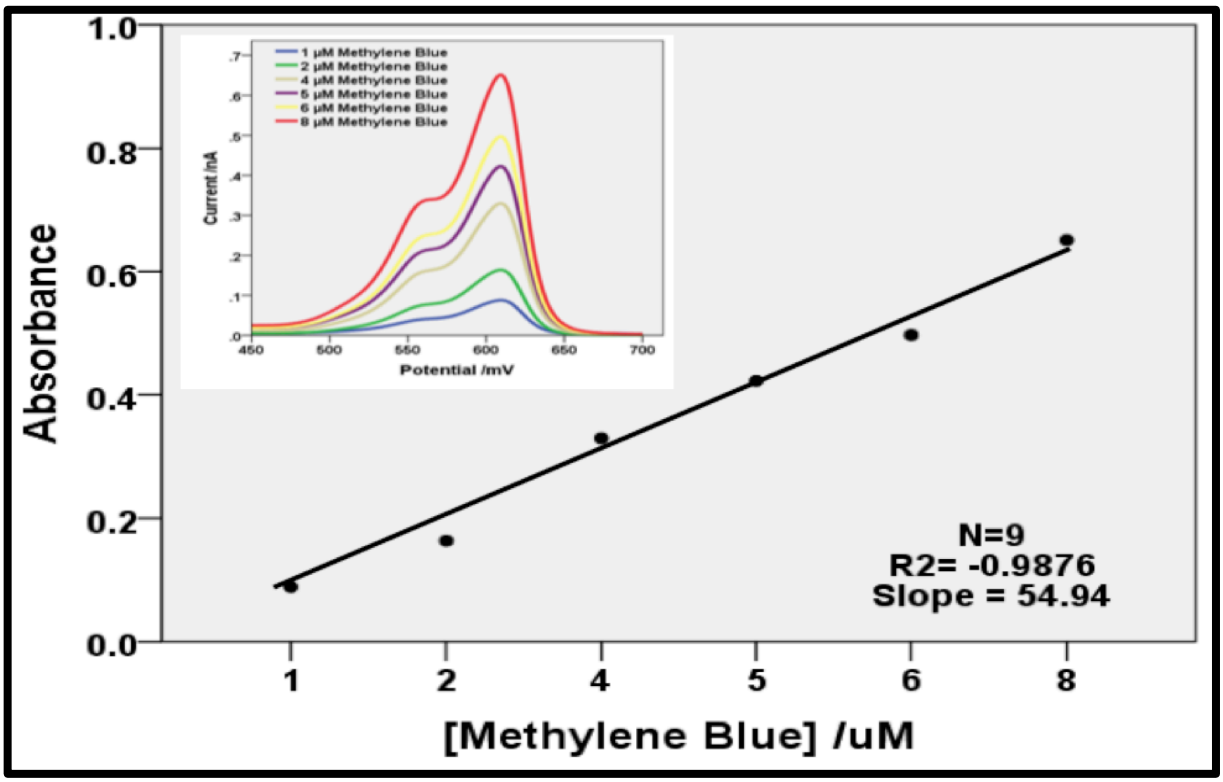


Figure 4-9 Calibration curve of Mb at different concentrations obtained by applying square wave voltammetry (SWV). FcMeOH was prepared in acetate buffer at pH5.

Table 4-4 the concentration of the entrapped of Methylene blue

Patch No.	**Total amount of MB (mg)**	**Amount of free MB (mg)**	**Amount of entrapped MB (mg)**	**Percentage (%)**
1	48	9	39	80
2	48	12	36	74
3	48	11	37	77

On the other hand only 22 µmol of $K_3[Fe(CN)_6]$ was calculated as un-encapsulated probe suggesting more than half was loaded as shown in Figure 4-10**.** In case of $Ru(BPY)_3$ data not quantitative since poor calibration curve of $Ru(BPY)_3$ was obtained (data not shown). However, apart from $Ru(BPY)_3$, the investigated probes showing good electrochemical behaviours in the aqueous solution. Further investigation of the probes electroactivity was studied by applying cyclic voltammetry for FcMeOH and Mb as shown from Figure 4-11 to Figure 5-16**.**

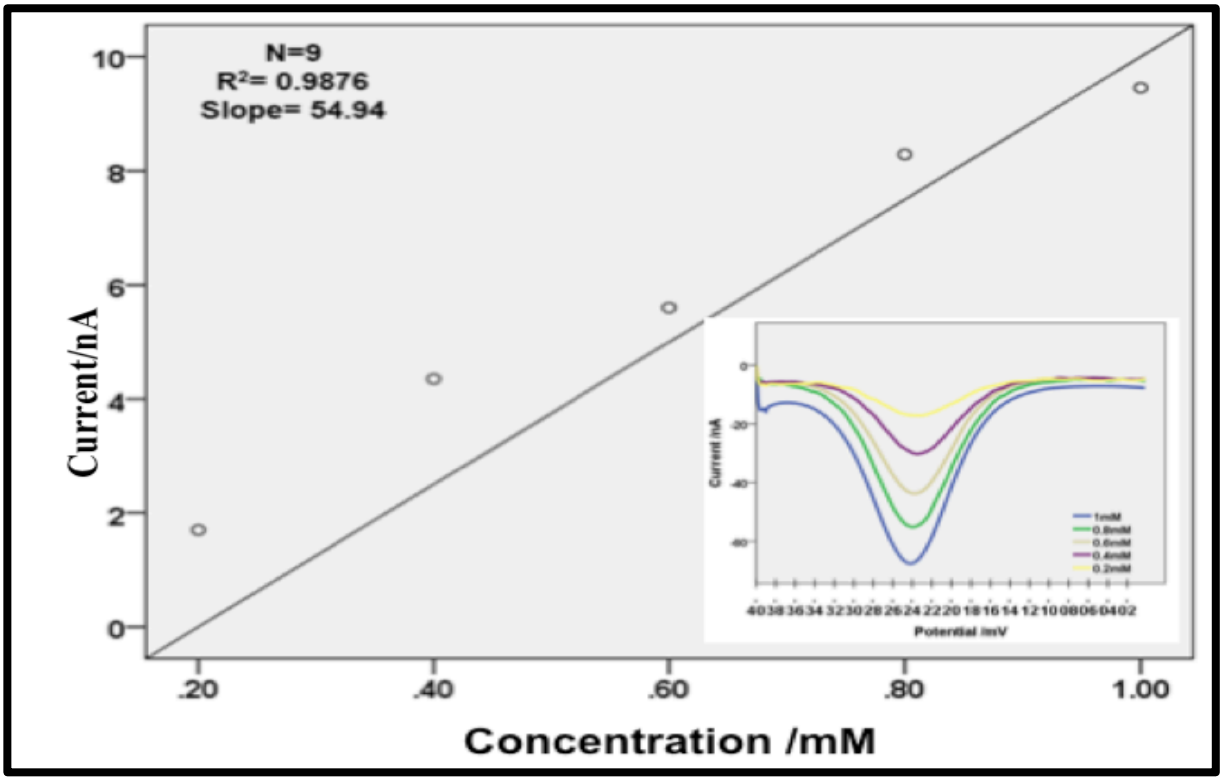


Figure 4-10 Calibration curve of $K_3[Fe(CN)_6]$ at different concentration range obtained by applying square wave voltammetry (SWV). $K_3[Fe(CN)_6]$ was prepared in ammonium acetate buffer ($CH_3CO_2NH_4$) at pH9.

It can be seen from the Figure 4-11 a pair of well-defined voltammetric peaks with catholic and anodic peak potential. This cyclic voltammograms (CV) was obtained for 1mM hydroxylmethyl ferrocene prepared in tris buffer (pH9). The scan rate was at 50mV using 2mm disk gold (Au) electrode as working and silver/silver electrode (Ag/AgCl) as a reference electrode. This obtained CV showed the reversibility reaction for hydroxylmethyl ferrocene since the potential separation

(the difference in maximum value for the oxidation and the reduction peak) is 54mV as shown in the equation below:

$$\Delta E_{p=} (Epc - Epa) = 54mV$$

However, this CV is used as a template to investigate the behaviour of the released hydroxylmethyl ferrocene from PNPs as is described in more detail in chapter 5.

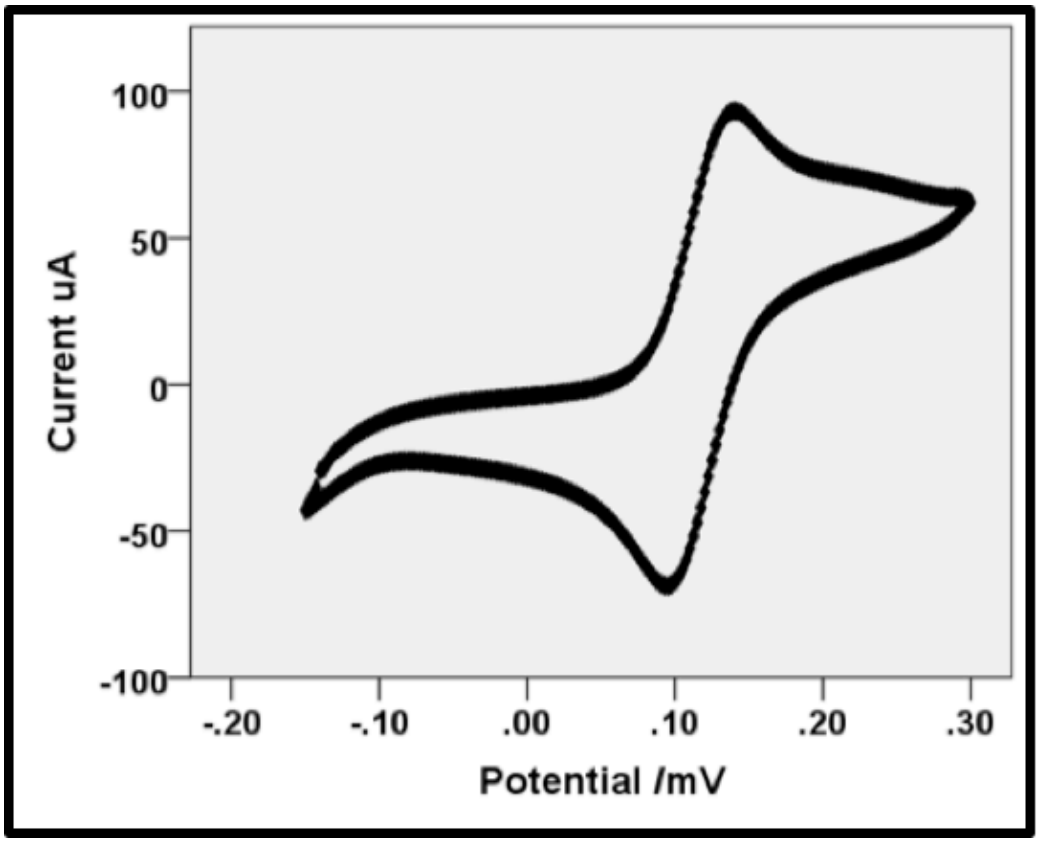


Figure 4-11 the typical CV for 1mM FcMeOH in aqueous solution (Tris buffer pH9).2mm gold disk as a working electrode and sliver /sliver chloride as a reference electrode at 50mV scan rate

Additionally, the maximum current peaks $i_{p.a}$ was proportional to the square root of the scan rate $mV^{1/2}$ as it can be seen from Figure 4-12 indicating that the mass transfer of FcMeOH to the electrode surface was diffusion- controlled. This is a good indicator of the good electroactivity of the FcMeOH.

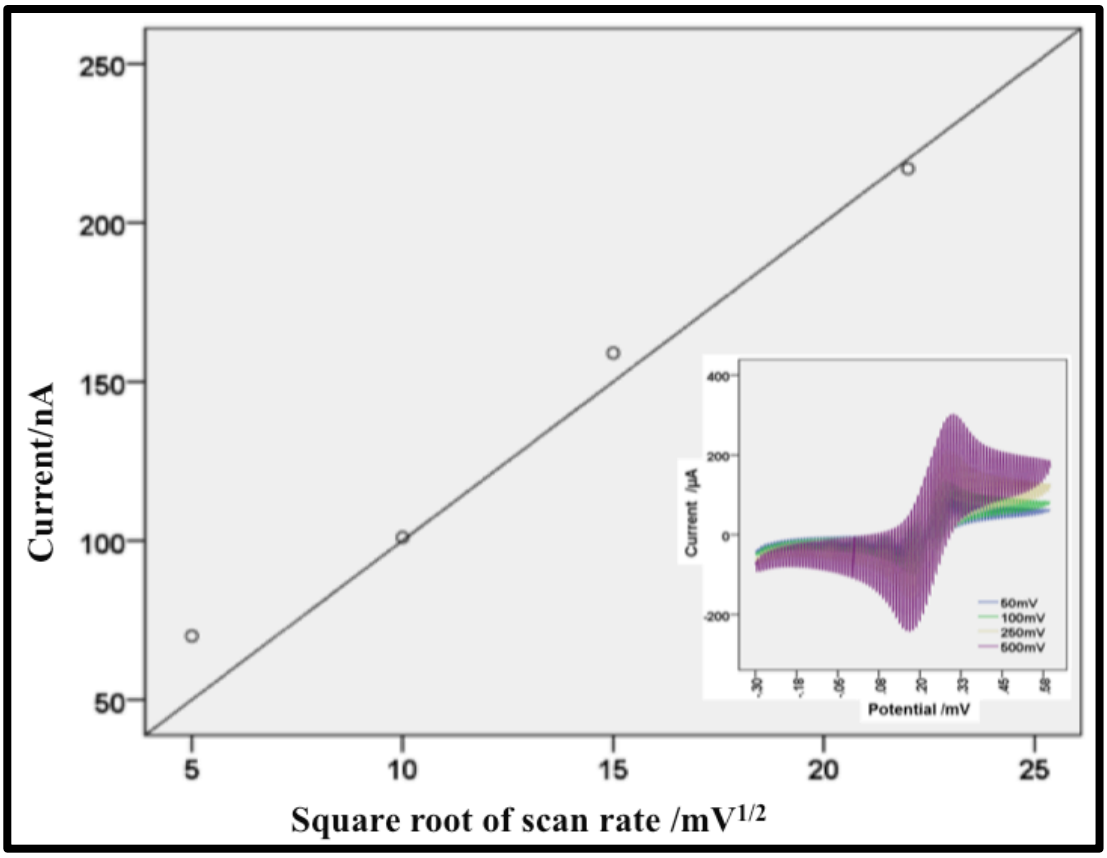


Figure 4-12 the linear respond of the maximum current peak against the square root of the scan rate for 1mM FcMeOH in aqueous solution.

Similarly the electroactivity of Methylene blue was determined by cyclic voltammetry for 1mM in aqueous solution as shown in **Figure 4-13** and the linear responds was also obtained from plotting the maximum current against the square root for range of scan rate (50mV-500mV) as it can be seen from the Figure 4-14.

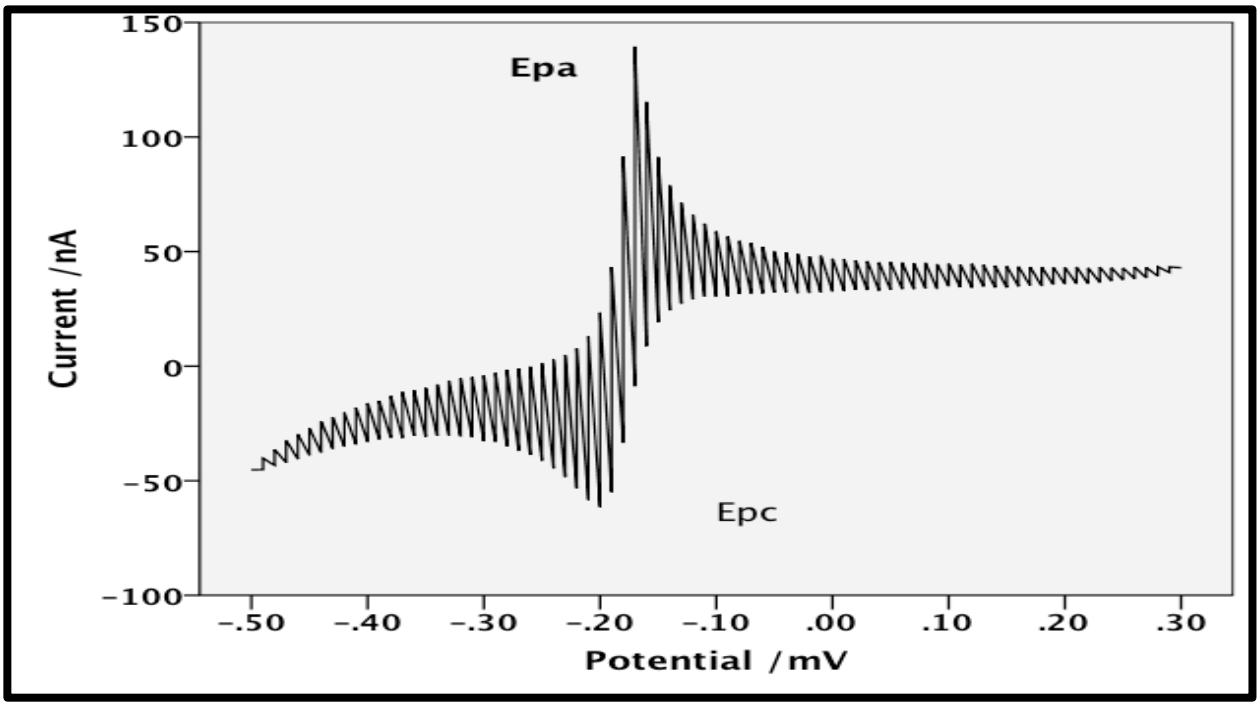


Figure 4-13 The typical CV of 1mM of Mb in aqueous solution tris pH9. 2mm gold disk was used as working electrode and silver/silver chloride as a reference electrode at 50mV scan rate.

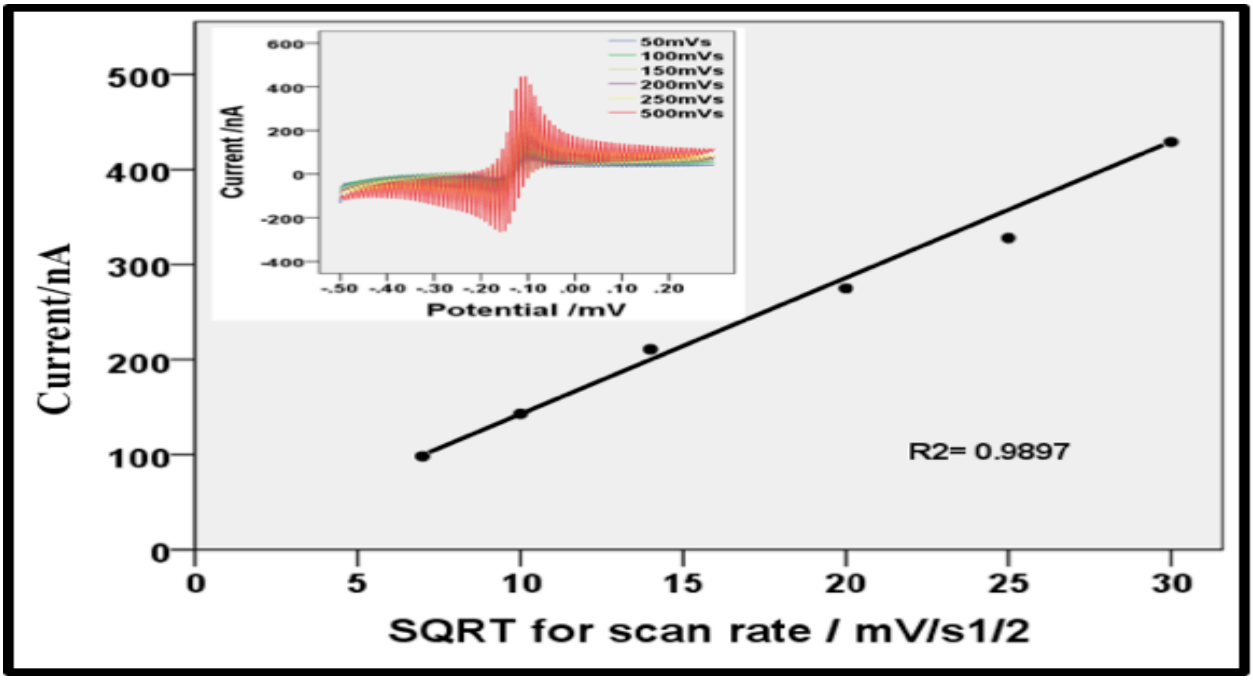


Figure 4-14 the linear respond of the maximum current peak against the square root of the scan rate of 1mM of Mb in aqueous solution.

4.6 Discussion

The development of an electrochemical lateral flow assay requires nanoparticles to be able to efficiently entrap redox active molecule. Several methods for PNPs synthesis have been described, including double emulsion and film ultrasonic dispersion and nanoprecipitation. The limitation of the first method is it can be used only for hydrophilic compounds while the second method it is quite complicated and time consuming to perform. Therefore, nanoprecipitation was chosen since it is a rapid method and it has successfully been used for loading many different compounds. Despite the fact that nanoprecipitation is an easy method for synthesising (substance-loaded) particles, a limitation comes from the possibility of particle aggregation, which increases the particles size and also reduces the encapsulation efficiency. Synthesis of 150-200 nm nanoparticles by nanoprecipitation is possible using the suggested conditions.

Table 4-5 Nanoprecipitation conditions to synthesis (150-250nm)-particles

Material	**Suggested composition (Ref.98)**	**Conditions used in this thesis**
Active substance	10-25mg	130μmol
Polymer	0.1-0.5% of solvent	2.6%
Oil	1-5 % of solvent	0%
Surfactant	0.2-5% of solvent	0%
Solvent	25ml	11ml
Stabilizer agent	0.2-5% of non-solvent	2% w/v
Non-solvent	50ml	50ml

In the work described in this thesis, the conditions of nanoprecipitation were controlled as closely as possible. However, a significant difference in size, among PNPs encapsulating different redox active molecules, was observed. The particle size was in the range from 200nm to 5000nm. The difference in particles size might be associated with the redox probes .It appears that smaller - sized particles were obtained when either methylene blue or hydroxylmethyl ferrocene was encapsulated. Whereas the larger-sized particles were observed for the control (no redox probe) and $K_3[Fe(CN)_6]$,($[Ru(NH_3)_6]cL_3$ and Ru $(BPY)_3$were present. As well as the size, zeta potential of the particles was also measured. The Mb-PNPs and FcMeOH-PNPs have a negative surface charge. In contrast, the zeta potential for the control and the large-sized PNPs are around 0, apart from K_3 $[Fe(CN)_6]$,which has a high negative zeta potential, which might be related to the probe' charges itself. Another important characteristic, which was studied was the loading efficiency, two techniques were used by either absorbance (UV/Vis) spectroscopy or square wave voltammetry. Both of these methods were based on an estimation of the entrapped probe, which was calculated indirectly from the supernatants immediately after the synthesis. Approximately 50% of FcMeOH was encapsulated (measured by absorbance), and this percentage was also confirmed by the electrochemical measurement suggesting very efficient FcMeOH encapsulation. About 70% of Mb was entrapped as estimated in the same fashion. For $[Ru(NH_3)_6]Cl_3$ the encapsulation was almost 50%. It was difficult to calculate the loading efficiency for Ru $(BPY)_3$ since it gave a poor voltammetric calibration curve. Thus, this probe was eliminated from further study since it doesn't exhibit good electrochemical behaviour compared to the remaining probes. This chapter has shown that a variety of redox probes can be entrapped in eudragit S-100 particles by nanoprecipitation. In the following chapter the pH dependent release of those probes is described.

Chapter 5 Release of entrapped redox probes as a function of increased pH

The dependence of the particles' solubility on increased pH is a result of ionization of the carboxyl groups. This resulted in increased electrostatic repulsion between the polymer chains **(**Figure 5-1**).** There are two ways that were achieved. One was by adding alkali and the other through the enzymatic reaction **(**Figure 5-2**).** Dissolution of the nanoparticles was expected to result in the release of encapsulated probes from the PNPs. For dissociation the PNPs under alkaline conditions, 100 µl of Tris at pH9 was added to 400 µl of the PNPs suspension at pH5. A 2 mm gold disk was used as the working electrode, silver/silver chloride as a reference electrode and platinum as a counter electrode. After the voltammetric measurements the pH was confirmed using a pH glass electrode.

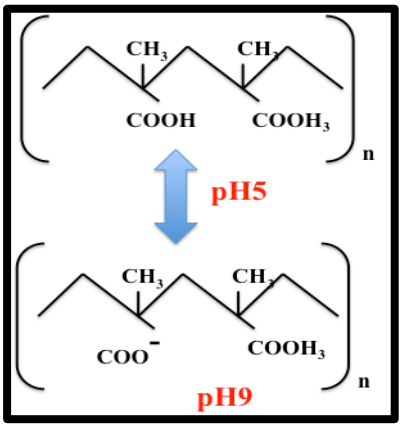


Figure 5-1 the chemical structure of Eudragit S-100 under alkaline and acetic condition

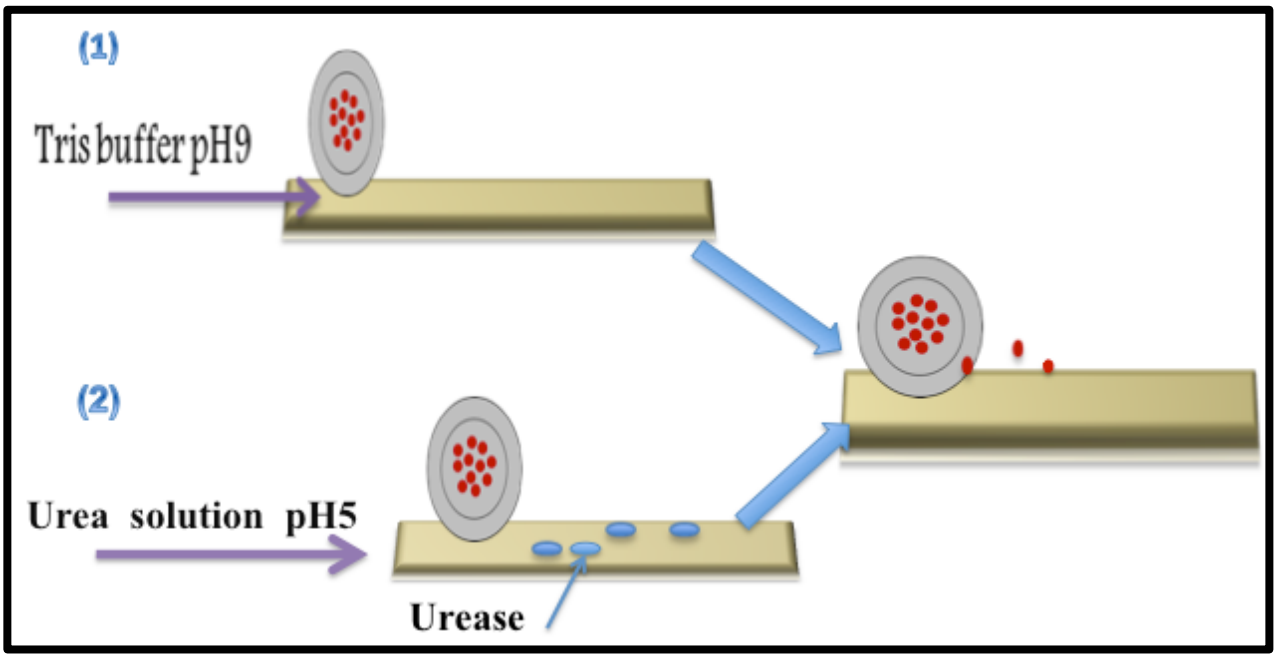


Figure 5-2 The dissociation of the PNPs and releasing of the encapsulated probe occurred under two different mechanisms. The first one was through the enzymatic reaction in particular, between urea and urease, while the second one was by the addition of alkali to the PNPs.

5.1 Release of redox probes under alkaline conditions

Based on our data, hydroxylmethyl ferrocene and methylene blue-PNPs showed good release of their redox probe cargos under alkaline condition as shown in the Figure 5-3 and Figure 5-4**.** While $[Ru(NH_3)_6]CL_3$ and $Ru(BPY)_3$ did not show constant behaviour from batch to batch (Figure 5-5 and Figure 5-6**)**. However, the redox potential of the ruthenium complex is very high (>0.9V) and so would be prone to interference. In contrast $K_3[Fe(CN)_6]$-PNPs did not give a measurable current (Figure 5-7). This may be due to very poor incorporation during the entrapment step or the $[Fe(CN_6]^{-3}$ associated with the polymer even after the latter had been sold. The latter explanation is less likely as both soluble polymer and $[Fe(CN)_6]_{-3}$ are negatively charged. Based in these data, the last three probes were eliminated from further characterizations, whilst only two probes were found to be good candidatures for further investigations. These selected probes are hydroxylmethyl ferrocene and methylene blue. Therefore, a cyclic voltammetry beside the SWV were performed to investigate the release of these probes. It can be seen from that the reversible cyclic voltammograms were obtained from the released FcMeOH under alkaline conditions. Additionally; the linear response to the maximum current with the

square root of scan rate was also obtained as it can be seen from the Figure 5-8 and Figure 5-9**.** The dissolution of the PNPs encapsulated FcMeOH and Mb was also carried out both with suspended particles and on nitrocellulose membrane in order to mimic the LFA environment as it can be seen from. Likewise the releasing behaviours and the electroactivity of Mb were also investigated and showing good electrochemical behaviour as shown in Figure 5-10 and Figure 5-11**.**

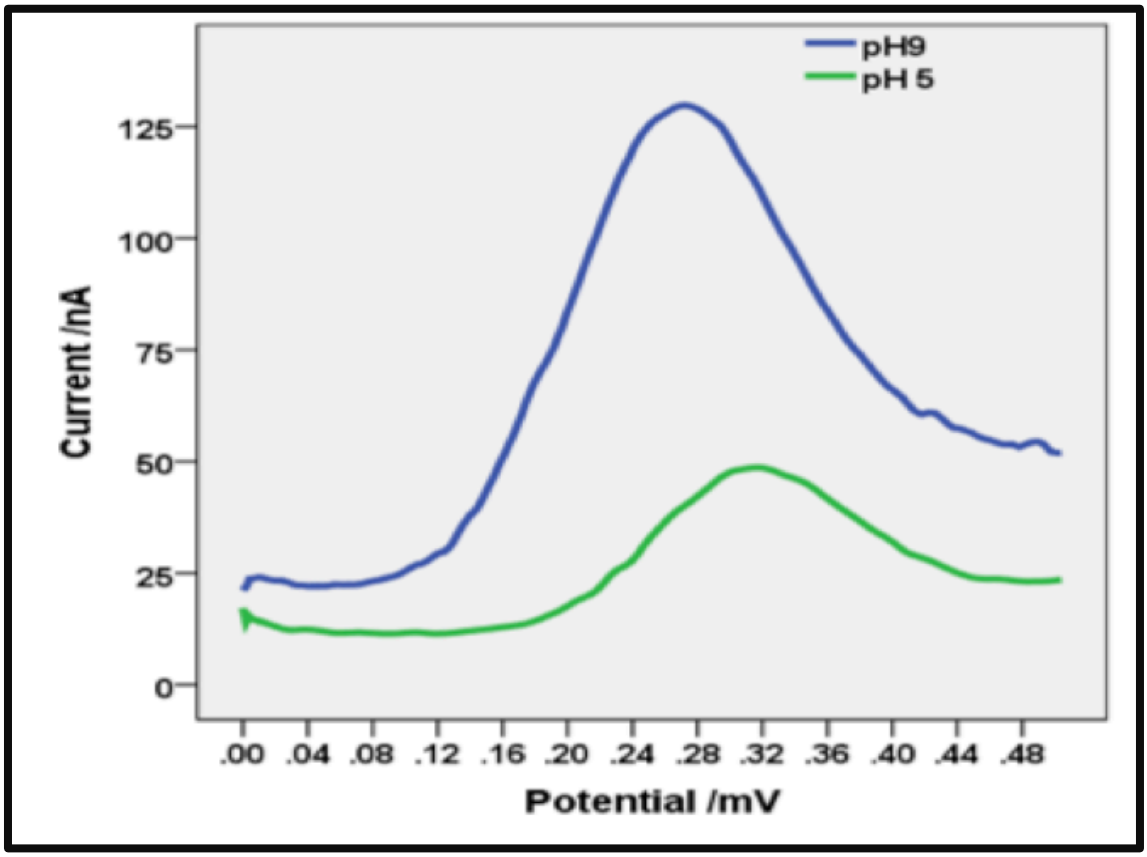


Figure 5-3 The dissociation of the PNPs occurred by adding alkali (Tris at pH9) to the suspension of the PNPs, which expects to release the encapsulate probe in this case, FcMeOH, which was electrochemically recorded using square wave voltammetry. Whilst keeping the PNPs suspension in acetate buffer (pH5), keeps the PNPs insoluble and as the results no FcMeOH will detect (control sample). However, the small current value from the control sample indicates some leakage from the probe, which is acceptable).

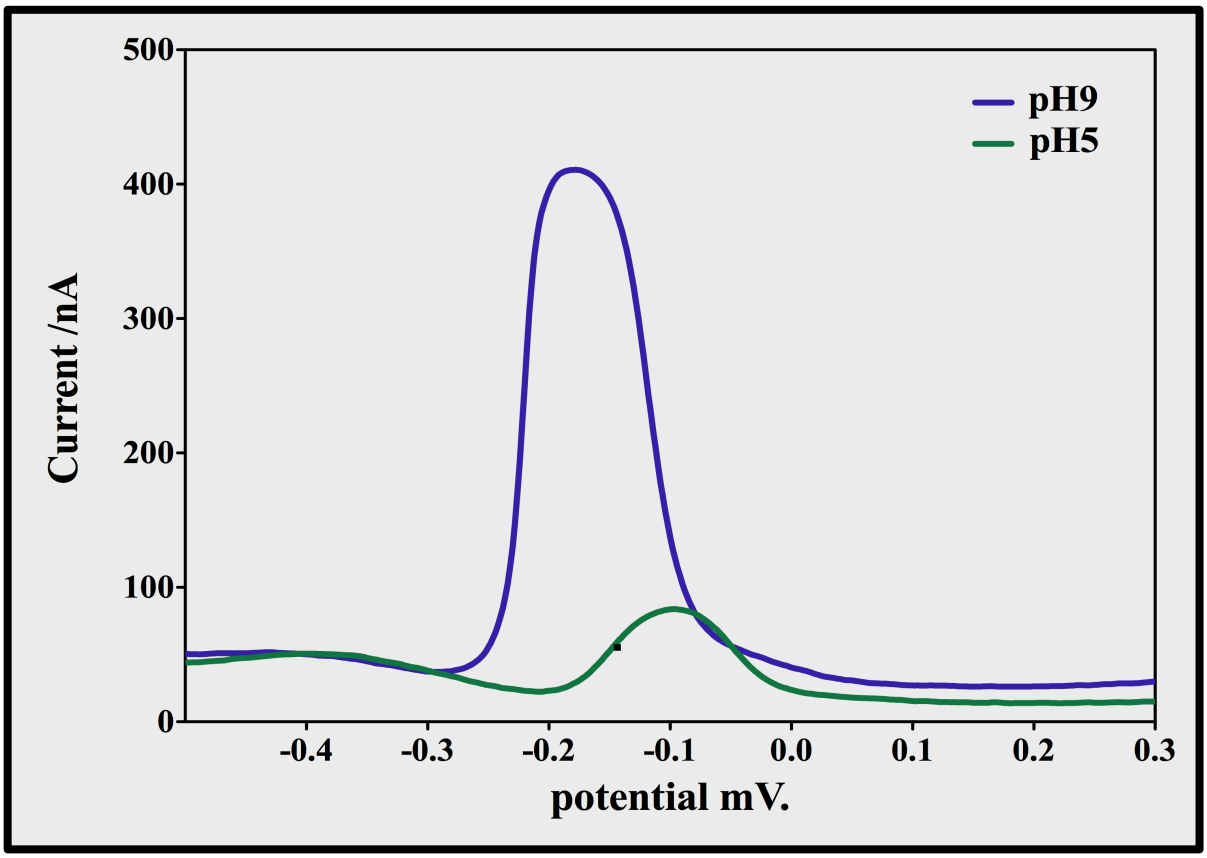


Figure 5-4 The dissociation of the PNPs occurred by adding alkali (Tris at pH9) to the suspension of the PNPs, which expects to release the encapsulate probe in this case, Mb, which was electrochemically recorded using square wave voltammetry. Whilst keeping the PNPs suspension in acetate buffer (pH5), keeps the PNPs insoluble and as the results no Mb will detect (control sample). However, the small current value from the control sample indicates some leakage from the probe, which is acceptable).

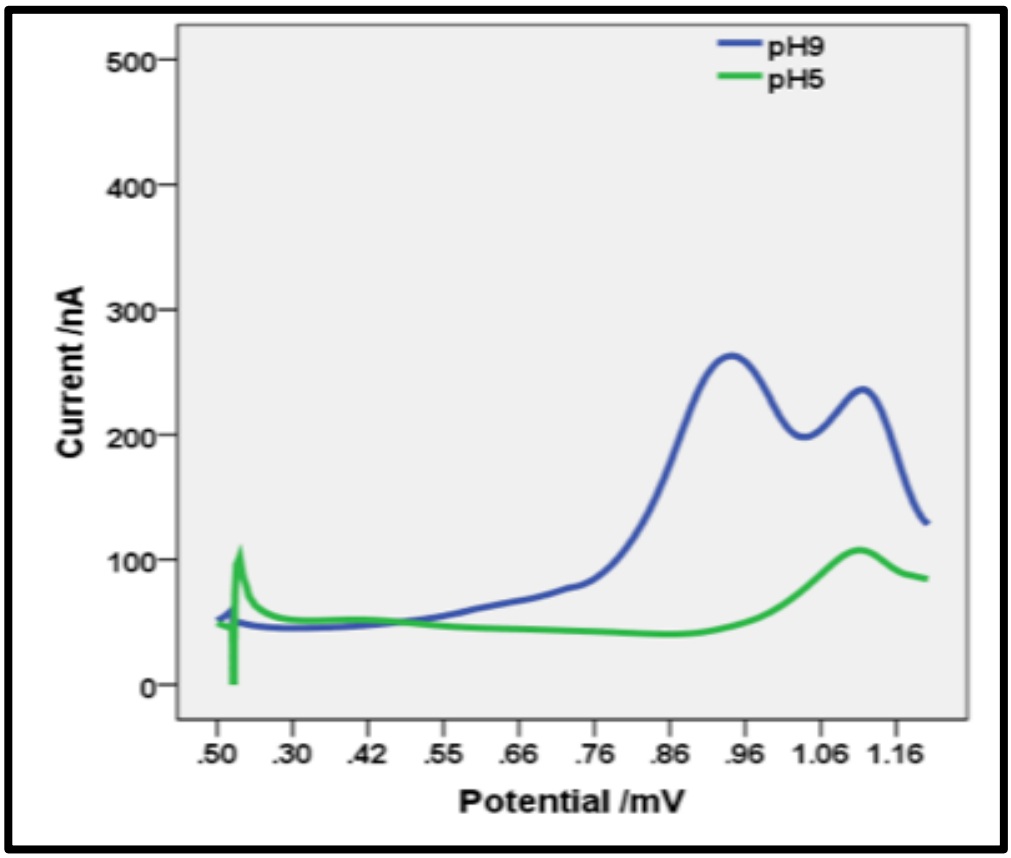


Figure 5-5 The dissociation of the PNPs occurred by adding alkali (Tris at pH9) to the suspension of the PNPs, which expects to release the encapsulate probe in this case, Ru $(BPY)_3$ at, which was electrochemically recorded using square wave voltammetry. Whilst keeping the PNPs suspension in acetate buffer (pH5), keeps the PNPs insoluble and as the results no Ru $(BPY)_3$ at will detect (control sample). However, the small current value from the control sample indicates some leakage from the probe, which is acceptable).

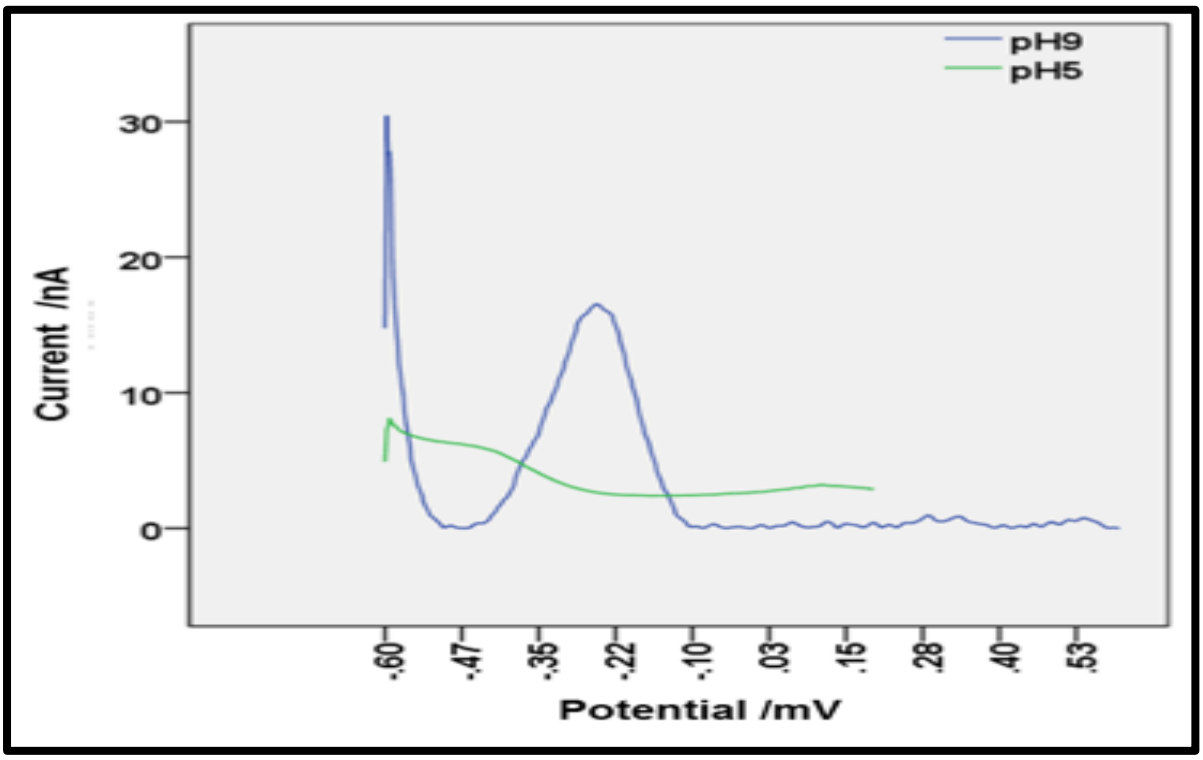


Figure 5-6 The dissociation of the PNPs occurred by adding alkali (Tris at pH9) to the suspension of the PNPs, which expects to release the encapsulate probe in this case, Ru $(NH_3)_6]$ CL_3 at, which was electrochemically recorded using square wave voltammetry. Whilst keeping the PNPs suspension in acetate buffer (pH5), keeps the PNPs insoluble and as the results no Ru $(NH_3)_6]$ CL_3 at will detect (control sample). However, the small current value from the control sample indicates some leakage from the probe, which is acceptable).

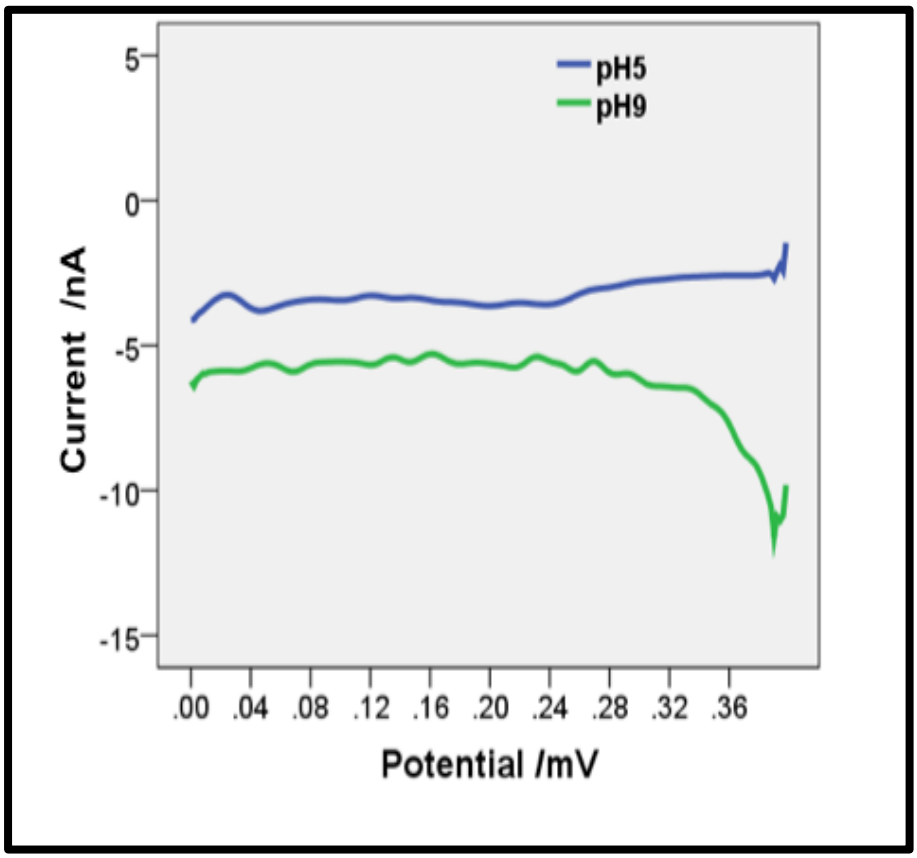


Figure 5-7 The dissociation of the PNPs under alkaline condition doesn't result in releasing the encapsulated $K_3[Fe(CN)_6$ as expected and show similar electrochemical behaviour .

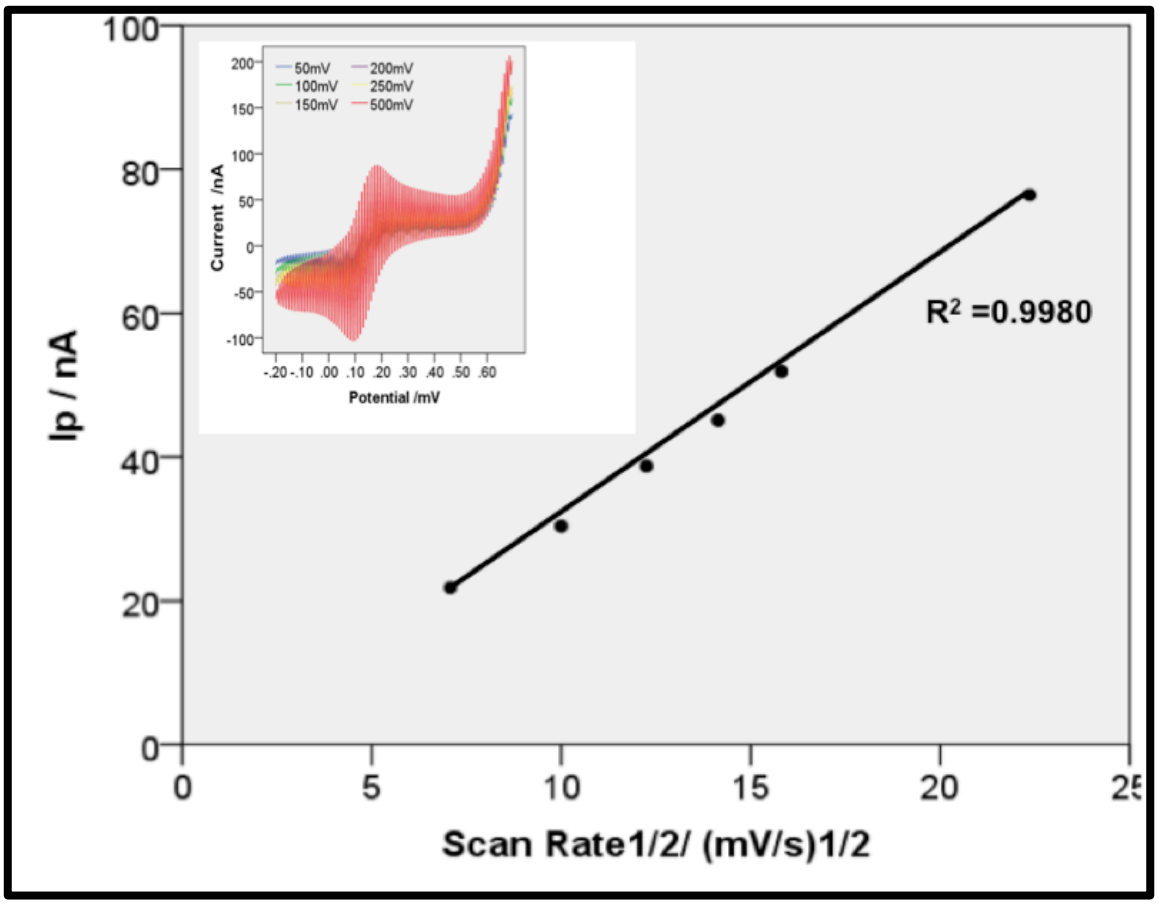


Figure 5-8 The linear response obtained by plotted the maximum current peak ($i_{p.a}$) against the square root of the scan rate ($mV^{1/2}$) of FcMeOH which was released from NPs by pH change under alkaline condtion and detected by cyclic voltammter

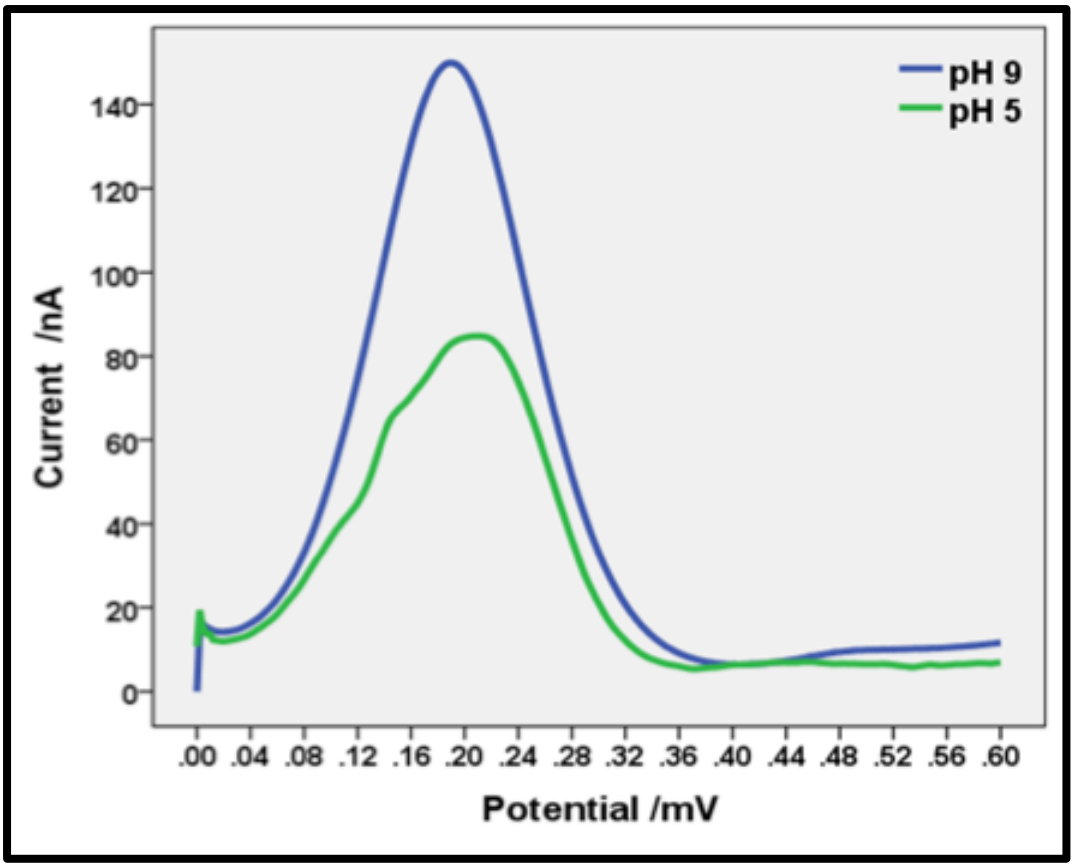


Figure 5-9 The dissociation of the PNPs occurred by adding alkali (Tris at pH9) to PNPs on nitrocellulose membrane NC to create a similar LFA condition, the addition of alkali expects to release the encapsulated probe in this case, FcMeOH, which was electrochemically recorded using square wave voltammetry (the higher current value). While adding the acetate solution (pH5) on immobilized PNPs, keeps the PNPs insoluble and as the results no FcMeOH will detect (control sample). However, the small current value from the control sample indicates some leakage from the probe, which is acceptable).

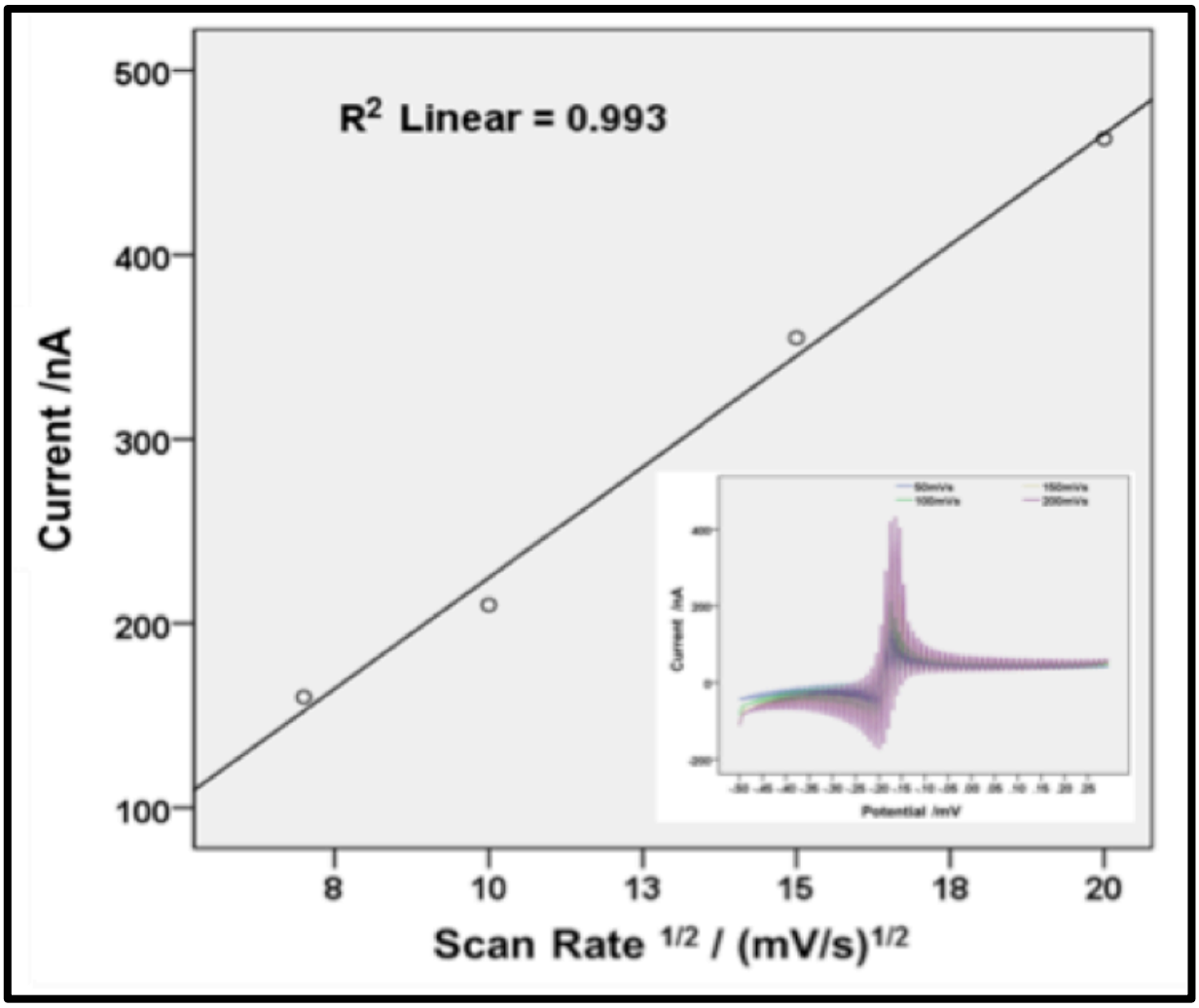


Figure 5-10 The linear response obtained by plotted the maximum current peak ($i_{p.a}$) against the square root of the scan rate ($mV^{1/2}$) of Mb, which was released from NPs by pH change under alkalin condtion and detected by cyclic voltammtery.

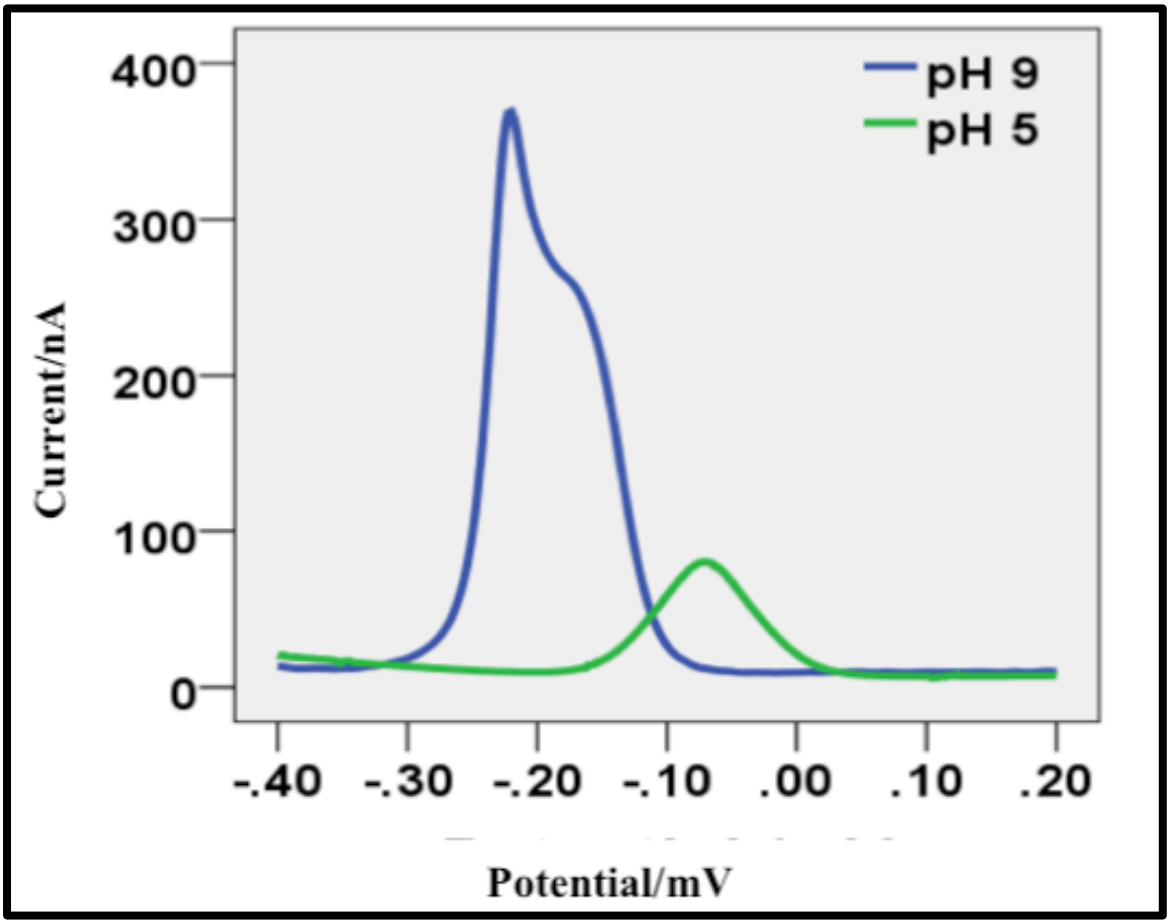


Figure 5-11 The dissociation of the PNPs occurred by adding alkali (Tris at pH9) to PNPs on nitrocellulose membrane NC to create a similar LFA condition, the addition of alkali expects to release the encapsulated probe in this case, Mb, which was electrochemically recorded using square wave voltammetry (the higher current value). While adding acetate solution (pH5) on immobilized PNPs, keeps the PNPs insoluble and as the results no Mb will detect (control sample). However, the small current value from the control sample indicates some leakage from the probe, which is acceptable).

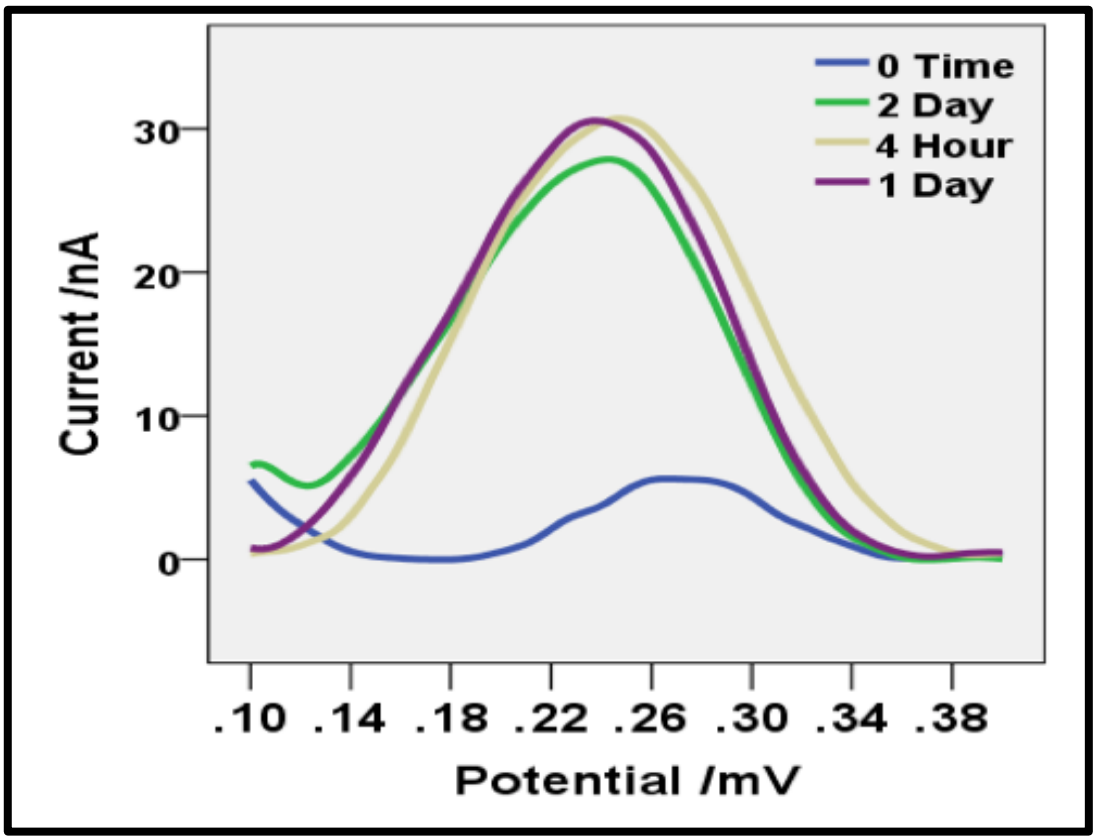


Figure 5-12 square wave voltammetry of FcMeOH-PNPS at pH5 at different interval time to investigate probe leakage.

It is clear from our control results (the PNPs suspended on pH5 solution) that there is some leakage from the PNPs at low pH. Therefore, the leakage was investigated with FcMeOH-PNPs and the square wave voltammetry was performed for PNPs in pH5 solution over days. The results presented in Figure 5-12 confirm the leakage of the hydroxylmethyl ferrocene from PNPs over the time. This is not likely to be a big issue for developing ELFA since the format of the assay will involved the PNP dried on NC membrane.

5.2 Dissociation of PNPs via the enzymatic reaction

The ability of the PNPs to release the encapsulate probes was investigated under alkaline condition in both solution phase and on the NC membranes, the next step was to establish the increase in pH through an enzymatic reaction. There are numerous literature reports that increased pH, as a result of ammonia occurs by the urea-urease reaction.

$$CO(NH_2)_2 + H_2O \longrightarrow CO_2 + 2NH_3$$

Therefore, 20 µl of 10mg/ml of urease was immobilized on NC membrane and then 200 µl of PNPs encapsulated probe were placed as a second layer at the top of the first one, before 70 µl of urea was added. The Figure 5-13 and Figure 5-14 show that PNPs encapsulate hydroxylmethyl ferrocene are able to release successfully both FcMeOH. Also it can be seen from Figure 5-15 and Figure 5-15 that Mb is released successfully by though the enzymatic reaction when PNPs were immobilized on NC membrane.

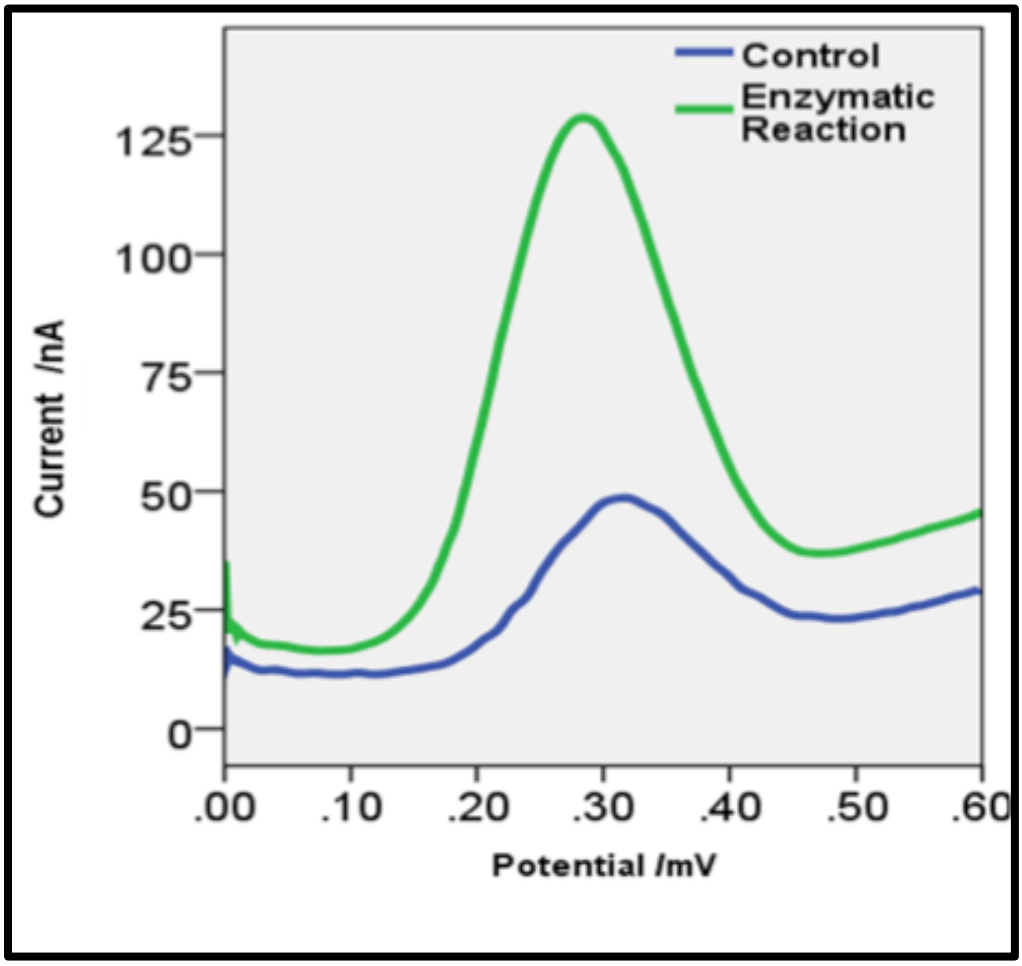


Figure 5-13 The dissociation of the PNPs occurred through the enzymatic reaction (Urease-urea system) to PNPs on nitrocellulose membrane NC to create a similar LFA condition, the enzyme was immobilized on NC membrane and the PNPs were immobilized as a second layer. By adding urea to NC membrane, the urease will hydrolysis urea and increase the pH which release of releasing the encapsulated probe in this case, FcMeOH, which was electrochemically recorded using square wave voltammetry (the higher current value). While adding the acetate solution (pH5) on immobilized PNPs, keeps the PNPs insoluble and as the results no FcMeOH will not detect (control sample). However, the small current value from the control sample indicates some leakage from the probe, which is acceptable).

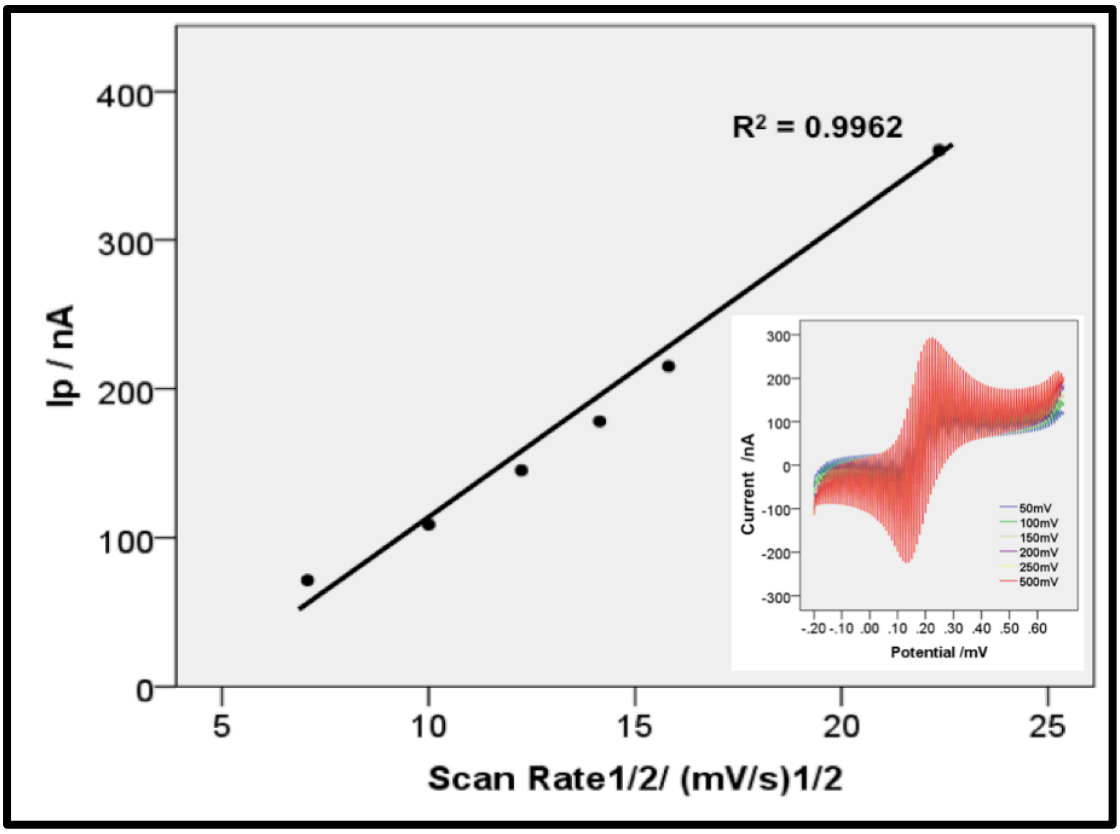


Figure 5-14 The linear response obtained by plotted the maximum current peak ($i_{p.a}$) against the square root of the scan rate ($mV^{1/2}$) of FcMeOH which was released from NPs by pH change though the enymatic reaction condtion and detected by cyclic voltammtery.The experiments were performed on NC membrane ,

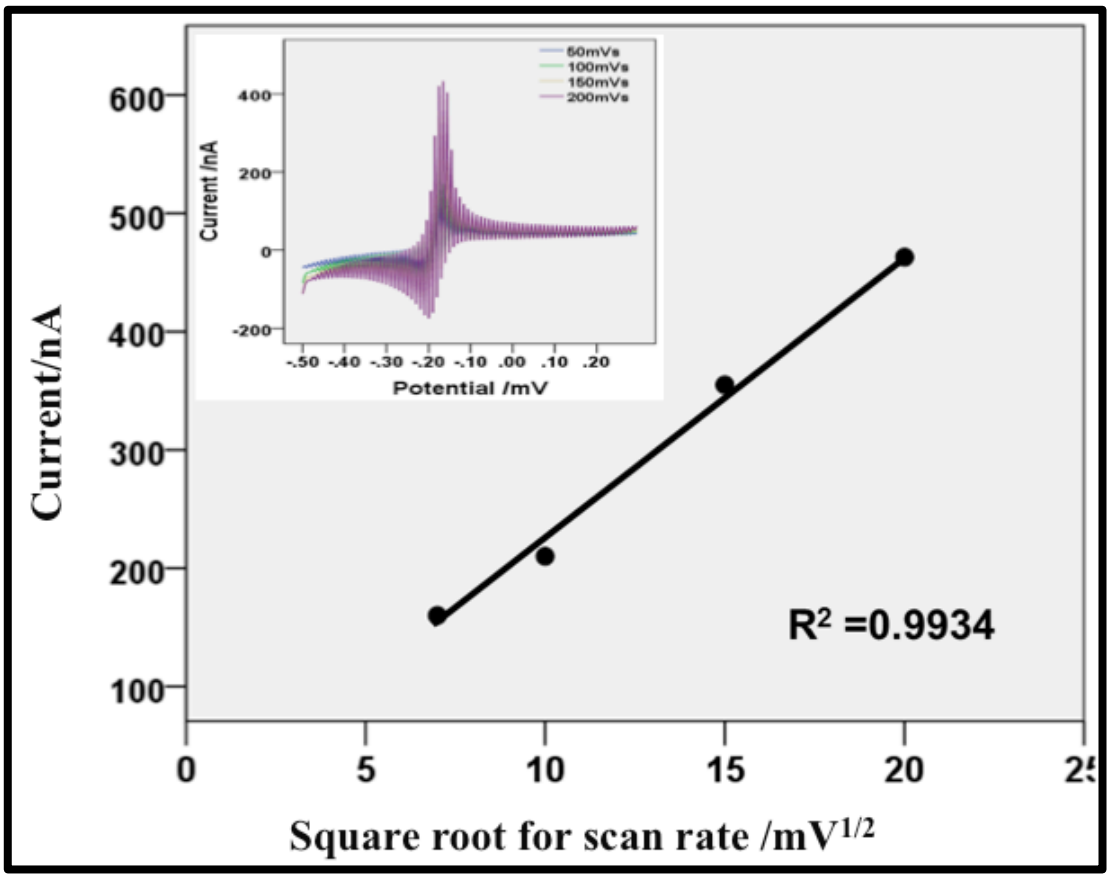


Figure 5-15 The linear response obtained by plotted the maximum current peak ($i_{p.a}$) against the square root of the scan rate ($mV^{1/2}$) of Mb which was released from NPs by pH change though the enymatic reaction condtion and detected by cyclic voltammtery.

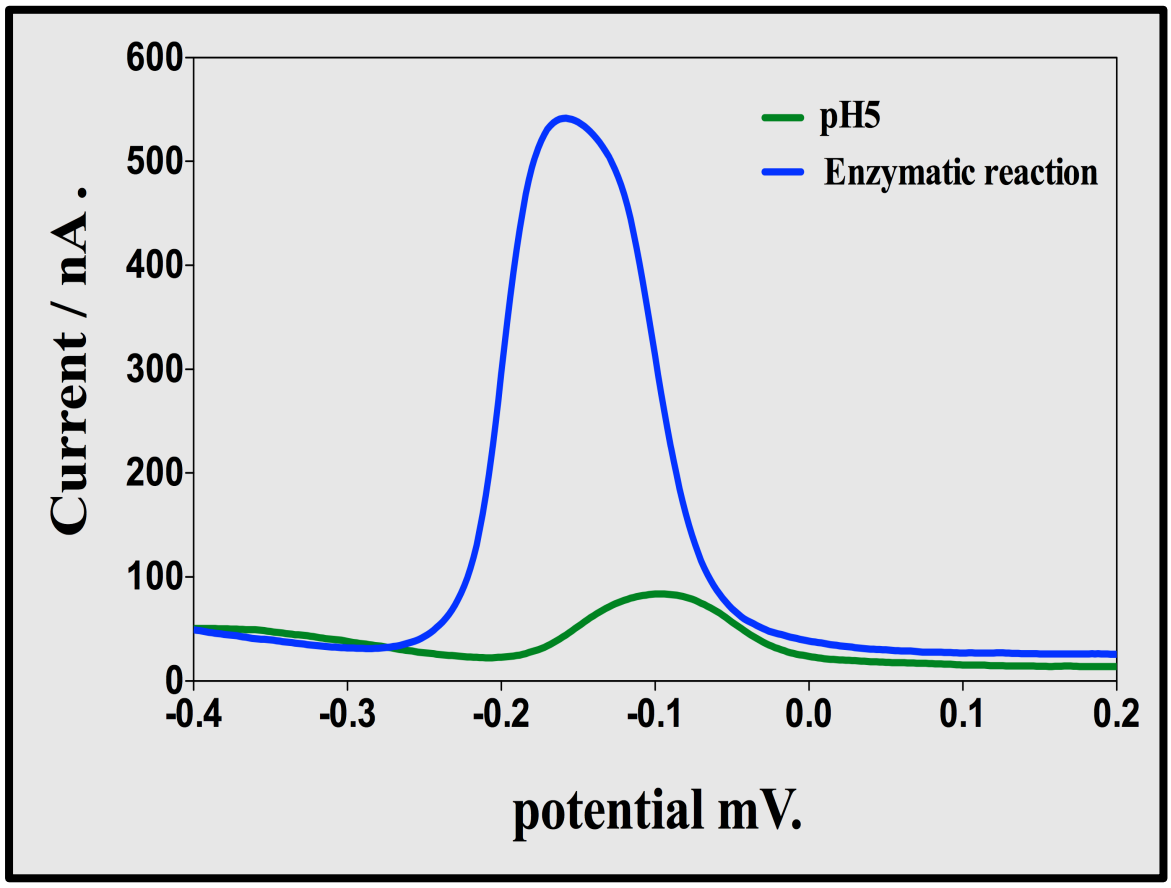


Figure 5-16 The dissociation of the PNPs occurred through the enzymatic reaction (Urease-urea system) to PNPs on nitrocellulose membrane NC to create a similar LFA condition, the enzyme was immobilized on NC membrane and the PNPs were immobilized as a second layer. By adding urea to NC membrane, the urease will hydrolysis urea and increase the pH which release of releasing the encapsulated probe in this case, Mb, which was electrochemically recorded using square wave voltammetry (the higher current value). While adding the acetate solution (pH5) on immobilized PNPs, keeps the PNPs insoluble and as the results no Mb will not detect (control sample). However, the small current value from the control sample indicates some leakage from the probe, which is acceptable).

5.3 Discussion

The characterization of the PNPs encapsulate probes under investigation ended with select both hydroxylmethyl ferrocene and methylene blue as good redox probes to be encapsulated with PNPs in particular ES-100. The nanoprecipitation under previously reported condition was able to synthesis small-sized particles (nm) and with greater than 50% of the probes was entrapped. The focused in this chapter was in investigating the releasing efficiency from the PNPs under two conditions, alkaline and enzymatic reaction in both solution phase and on NC membrane. However, the desired format is to release the encapsulated probes from the PNPs under enzymatic reaction since urease is immobilized on NC membrane just before the test line as well urea can be provided from the sample (urine) or by immobilizing on NC membrane. However, the selected probes showed good releasing behaviours under these conditions in either solution phase or on NC membrane. Our data indicate that the PNP were dissolved at increased pH and can be electrochemical detected (higher obtained current), compared to the control where the PNPs still insoluble in acidic conditions pH5 (lower obtained current). The PNPs encapsulate redox probe is now ready to move toward the next stage of developing an electrochemical lateral flow assay. In particular, conjugation with anti-hCG antibody via adsorption and to run lateral flow assay as presented in the next chapter.

Chapter 6 An electrochemical lateral flow assay (ELFA) and screen printing technology

This chapter presents the key result of this work, which demonstrates the electrochemical lateral flow assay for the detection of hCG. Also, the initial step of employing screen-printing on a nitrocellulose (NC) membrane is presented to realize the design of the POC device.

6.1 An electrochemical lateral flow assay (ELFA)

The optimization work, previously described in Chapter 5, led us to choose hydroxylmethyl ferrocene as a suitable redox active molecule to investigate the ELFA. The assay was run on a NC membrane as illustrated in the Figure 6-1 and explained as follows: Initially, on a NC membrane (1.5.cm width and 10 cm length), 20 µl of biotinylated antibody was placed by drop casting as the first reagent. On the test line, 20 µl of streptavidin was placed just before the test line and overlapping with it, 20 µl of 100 mg/ml of urease was placed. The gold disk a working electrode was placed on the test line and a silver/silver electrode a reference electrode was placed slightly "upstream" of the test line. The hCG concentration in the sample solutions was varied and square wave voltammetry was used in order to detect released hydroxylmethyl ferrocene at the test line. This release occurs due to the hydrolysis of urea by urease and the rise in pH dissolved the PNPs. Formation of the immune complex occurred during the migration through NC membrane occurred and the strong binding between the biotin on the biotinylated antibody and the streptavidin at the test line gave maximum capture of the PNPs' hydroxylmethyl ferrocene. The sample applied to the membrane was composed of the antibody-nanoparticles conjugate biotinylated antibody, hCG and 100mM urea in 10mM acetate buffer. As both antibodies were in molar excess compared to hCG all of the latter should be present as the immune complex and small variations in the exact amounts of the two antibodies should not affect the result.

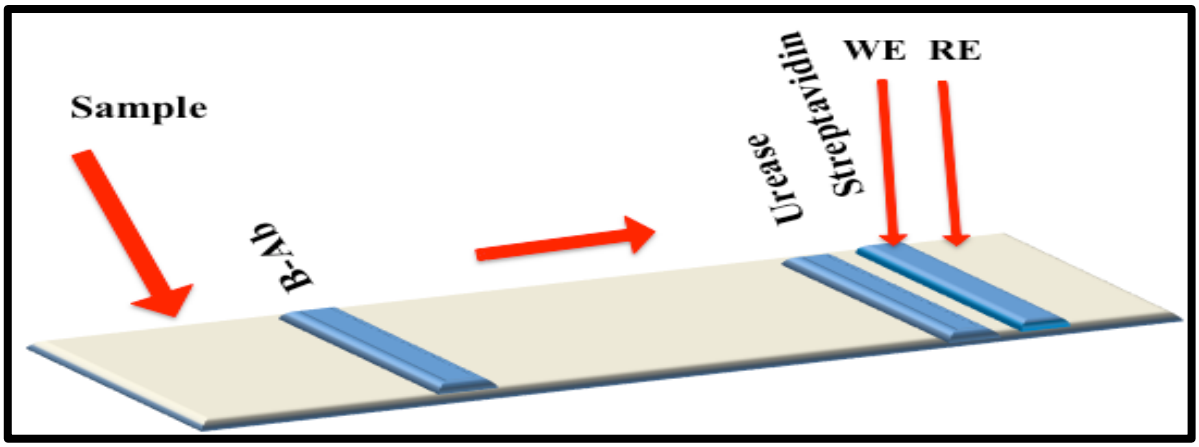


Figure 6-1 the layout of an electrochemical lateral flow assay (ELFA), the sample is the urea solution, which contains antibody-PNPs encapsulated hydroxylmethyl ferrocene. Streptavidin is placed at the test line while the urease is just before the test line, which helps to hydrolysis urea and produce ammonia to increase the pH environment. WE; is the working electrode, which is placed at the test line and RE is placed close to the working electrode.

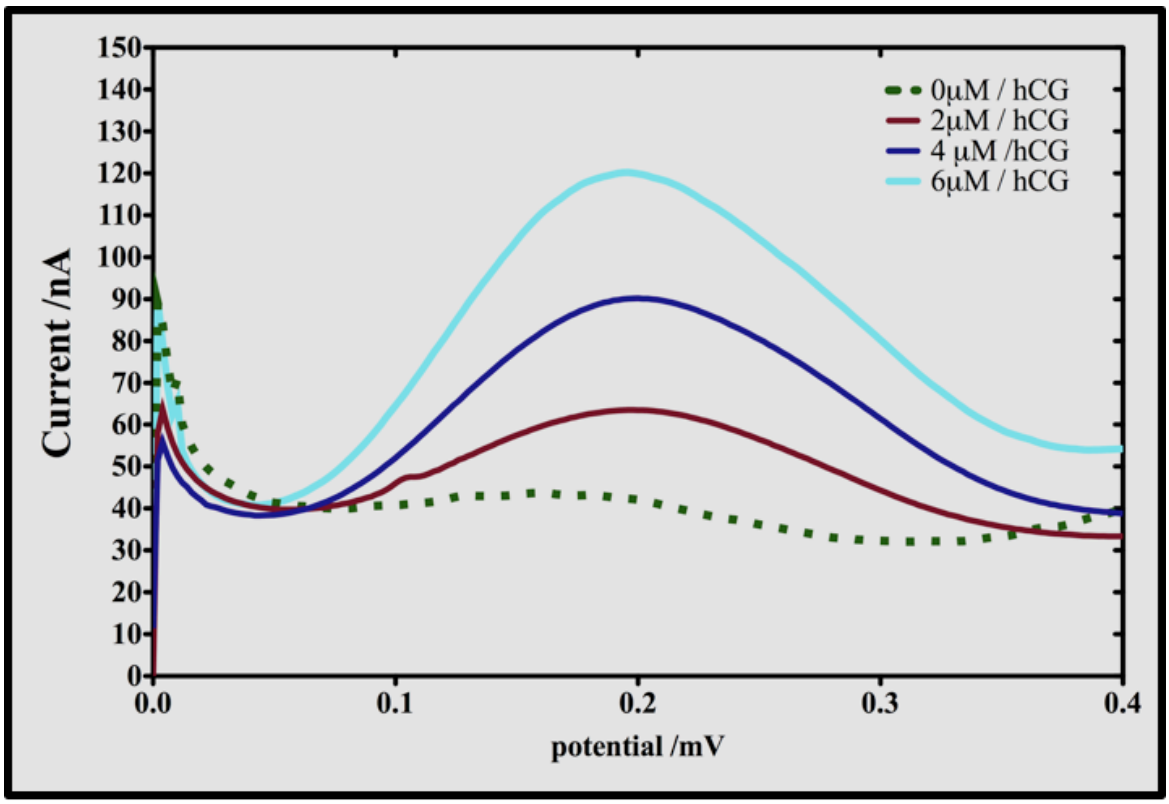


Figure 6-2 an electrochemical lateral flow assay was performed on NC membrane in the presence (varied concentration) and the absence of hCG. Square wave voltammetry was performed to detect the release of FcMeOH at the test line.

As can be seen in Figure 6-2 a low current is observed from the control sample (absence of hCG), whilst, higher currents are obtained in the presence of increasing hCG concentration.

6.2 Discussion

As described in the previous chapter, the release of an entrapped redox probe in PNPs could be triggered by an increased in pH generated through the hydrolysis of urea by urease. To use this system in an electrochemical immunoassay, it was necessary to separate the formation of a complex between the analyte (hCG) and the PNP labelled antibody from the PNP dissolution and detection of released redox probe. Lateral flow method is a suitable way to achieve this separation. A solution of the analyte is placed on the membrane and the immune 'sandwich' forms during the flow of this solution. Upstream of the sample addition are two immobilized protein lines, one of them is urease, which hydrolyses the urea in the (urine) sample and so produces a localized increase in pH. Immediately adjacent to the urease line is a streptavidin line, which captures the immune complex of a biotinylated antibody with hCG and PNP labelled antibody, allowing release of the redox probe at the site of the pH increase. An electrode on the streptavidin line then detects the released redox probe.

The dynamics of this system involve several steps:

1. Binding of antibodies to hCG during the flow.
2. Hydrolysis of urea at the urease line.
3. Binding of the immune sandwich to the streptavidin line.
4. Dissolution of the bound PNPs at the streptavidin line.
5. Flow of unbound PNPs, antibody conjugate past to the electrode.

If the limit of detection of the assay is to be high then the background hydrolysis of PNPs before binding to the streptavidin line should be minimal and the capture of the immune sandwich should be essentially quantitative, during the flow over the streptavidin line. This means there is an optimum flow rate, if the flow rate is too fast then the immune sandwich is not given enough time to bind to the SA line and so the signal is reduced. On the other hand if the flow rate is too slow then significant dissolution of the PNPs will occur before those not in the immune sandwich are carried post the electrode by the flow, this will result in a high background. In addition the rate of urea hydrolysis will depend on the amount of urease on

the membrane and the urea concentration in the sample, the latter is not controlled in urine samples however, because urea concentrations in urine are typically 20X the Vim of urease, the enzyme is saturated and therefore the rate of hydrolysis is independence of the urea concentration. This is a critical aspect of the assay, if the enzyme was not operating under saturating conditions then the currents would depend on both the hCG and urea concentrations and so determination of the former would be much more difficult. The rate of urea hydrolysis will however, depend on the amount of urease deposited and the rate of dissolution of the PNPs will depend on their composition, these two factors can be manipulated to maximize the signal to background ratio and hence the limit of detection. The signal shown in Figure 6-2 in the absence of hCG is therefore due to the dissolution of the PNP`s whilst flowing past the electrode. However, the increase in current in the presence of hCG is consistent with PNPs being bound and hence releasing more hydroxylmethyl ferrocene.

6.3 Screen printed NC membranes

Screen-printing technology is widely used to make electrochemical devices and after ELFA was clearly demonstrated in term of its feasibility. It was decided to use screen-printing on NC membranes. First, the compatibility of the carbon ink with NC membranes was tested before starting the final device design. Initially, the carbon inks deposited by drop casting and oven drying, the results shown in the Figure 6-3. In the first experiments, carbon was used on both a working and pseudo-reference electrodes. Using the same material for both electrodes has been shown to work successfully in glucose sensor.



Figure 6-3 Deposition carbon ink on NC membrane to crate working and reference electrodes

Cyclic voltammetry was used to test this arrangement. Although it did not generate reproducible voltammograms, it showed that it is possible to deposit carbon ink on a NC membrane. The results are shown in **Figure 6.4.**

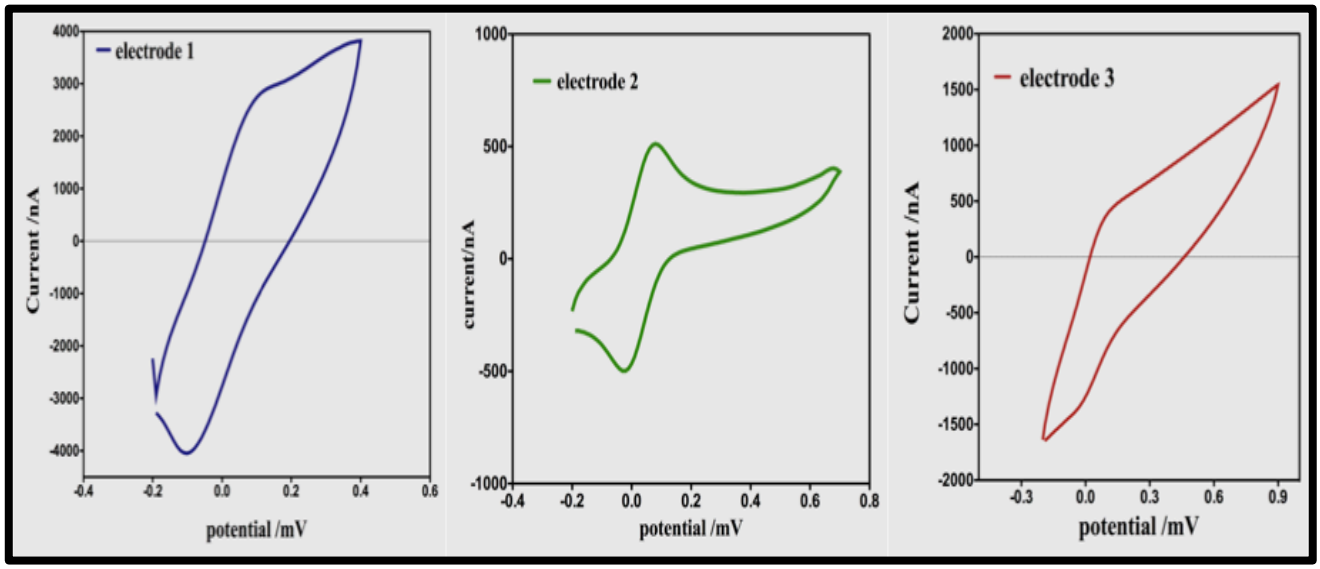


Figure 6-4 Three different electrodes were tested by applying the cyclic voltammetry (50mV scan rate) of 1mM hydroxylmethyl ferrocene. Tow carbon ink were screen-printed on NC membrane as working and reference electrode.

Based on Figure 6-4, the three electrodes gave quite different currant-voltage curves, in electrodes 1 and 3, there is a large resistance as seen by the upward sloping voltammograms, in addition there are substantial capacitance currents and the peaks separations are quite large (~150mV). In contrast electrode 2 shows more a well-behaved voltammetric response with smaller capacitive and resistive features and narrower peak separation (100mV). Although the reasons for the different voltammograms were not established, the manual deposition method is likely to have resulted in different thickness and different contacts between the ink particles due to lack of pressure control during deposition.

6.4 Discussion

The performance of ELFA was successfully demonstrated as shown in last chapter However, it was difficult to achieve reproducible results as showed a lot of experimental variation due to the difficultly of placing the electrodes on the membrane as it seen from the Figure 6-5. For

this reason it was important to design a more robust platform. It was decided to consider screen-printed technologies on the nitrocellulose membrane.

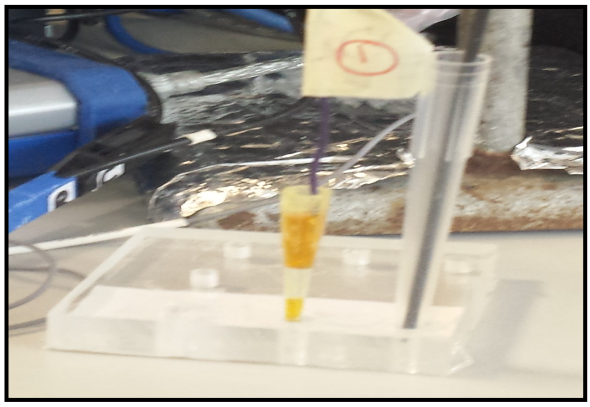


Figure 6-5 The platform system of the electrochemical measurements, which consist of working electrode and reference electrode placed on the top of NC membrane via two separated holes on the top of glass holder close to each other on one side of the glass, on the other side there is another hole used to apply the sample though.

As a first step, it was necessary to investigate the computability of carbon inks and sliver/sliver inks on NC. Thus a commercially printed membrane was obtained from Gwent electronic material as it can be seen from Figure 6-6. This is a template, which worth trying as a second stage to set the electrochemical platform for ELFA to reduce the experimental variation and to realize the final POC device.

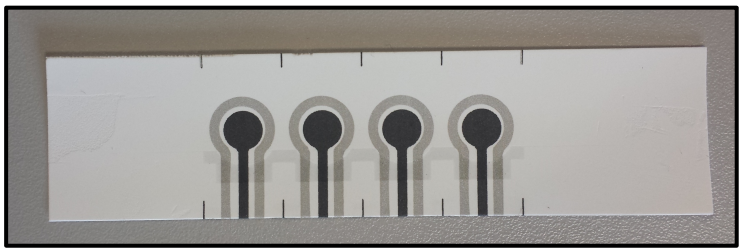


Figure 6-6 The screen-printed NC template, which was designed by Gwent electrode material (carbon ink and silver/silver electrodes**).**

Chapter 7 Conclusion and recommendation for the future work

In this thesis, two electrochemical assays have been presented as approaches to develop a quantitative pregnancy test based on the measurements of hCG. The first approach was an aptasensor using an anti-hCG RNA aptamer, while the second one was an electrochemical lateral flow assay (ELFA) based on dissolvable polymer nanoparticles. The main goal of this chapter is to summarize the project findings so far and to suggest the next stages in ELFA approach as well as to suggest alternative possible directions for the aptasensor.

7.1 Conclusion

With the purpose of developing a novel approach of a highly sensitive pregnancy test, the main aim of this project is to explore point of care to quantitative pregnancy detection based on hCG levels. Hence two different assays have been studied; the first one was the development of an aptasensor using an anti-hCG aptamer, while the second one was an electrochemical lateral flow assay (ELFA). Both approaches have their advantages and limitations. For instance, working with an aptamer for pregnancy test has several advantages over antibodies. Aptamers are a promising tool for diagnosis as they are cheaper (per mole) and more stable (thermal). Whereas, the ELFA concept is advantageous since it provides an amplification step (PNPs) and also a direct electrical signal (current) is generated. In principle, it could be adapted to any sandwich immunoassay and if the sample is not urine, the urea could be supplied via a reagent dried into the membrane. Alternatively different enzyme/substrate combinations could be used to generate a high pH. As the initial stage in developing the aptasensor, it was necessary to characterize the previously reported anti hCG-RNA aptamer and study the binding affinity toward its target (hCG). It was decided to choose an ELONA assay to determine the K_D because this method is an accurate, well established and simple analytical technique. The ELONA requires biotinylation of RNA, which was performed in two ways. The first of these methods is site-specific chemical biotinylation at the 3` end and the second one is the incorporation of biotin in UTPs during transcription. Although, both ways shown to be successful, the chemical modification had the better performance. From our ELONA data, we can confirm that RNA aptamer dose bind to hCG with a calculated K_D of 60 nM. However, much variation from batch to batch in preparing the aptamer was observed. This variation is very problematic when developing an aptasensor,

since it will result in a similarly variable performance. To confirm the binding between RNA and hCG, a CD spectra suggested that the RNA secondary structure is a Hairpin (A-form) with internal sequence mismatched. An alternative approach was the amplification of nanoparticles encapsulated redox-probe as the key feature of developing ELFA. Since this step is the main key feature of the development of ELFA, five different probes were investigated. The main property to select the probe is to have good electrochemical behaviour. The polymer should also have important characteristics that include: efficient encapsulation and release of the encapsulated probes and no adsorption to the electrode surface during the electrochemical measurements. Moreover, synthesis of a small particle (200nm) is required since it enhances the probe's loading. Additionally, a negatively charged particle helps to better conjugate the antibody. All these considerations were kept in mind when synthesising the PNPs. For these reasons, nanoprecipitation was chosen, as it is a good technique, which is able to produce PNPs with this desired feature. The choice was based on previously reported literature (as mentioned previously in this thesis). Among the probes under study, PNPs with encapsulated hydroxylmethyl ferrocene and methylene blue met all the desired criteria. These make them suitable for developing the ELFA.

7.1 Future work

7.1.1 Aptasensor

Select and characterize a DNA aptamer specific to hCG. Label aptamer with redox reporter ground and establish limit of detection and specificity of aptasensor.

7.1.2 An electrochemical lateral flow assay

Applying the screen-printing application on NC membrane to finalize the POC device is the next stage, which requires

1. Electrochemical characterisation of screen-printed electrode on NC membrane.
2. Establish printing conditions for all ELFA reagents.
3. Using comutes simulation to better understand the dynamics of the ELFA device.
4. Vary loading of urease to maximise signal to background.
5. Complete system generation and validation.
6. Extend to other analytes.

Bibliography

(1) Clerc, O.; Greub, G. Clinical Microbiology and Infection **2010**, 16, 1054-1061.

(2) Drain, P. K.; Hyle, E. P.; Noubary, F.; Freedberg, K. A.; Wilson, D.; Bishai, W. R.; Rodriguez, W.; Bassett, I. V. Lancet Infectious Diseases **2014**, 14, 239-249.

(3) Gubala, V.; Harris, L. F.; Ricco, A. J.; Tan, M. X.; Williams, D. E. Analytical Chemistry **2012**, 84, 487-515.

(4) Pai, N. P.; Peeling, R. W.; Smith, B. D.; Dowdy, D. AIDS research and treatment **2014**, 2014.

(5) Chan, C. P. Y.; Sum, K. W.; Cheung, K. Y.; Glatz, J. F. C.; Sanderson, J. E.; Hempel, A.; Lehmann, M.; Renneberg, I.; Renneberg, R. Journal of Immunological Methods **2003**, 279, 91-100.

(6) Greene, D. N.; Schmidt, R. L.; Kamer, S. M.; Grenache, D. G.; Hoke, C.; Lorey, T. S. Clinica Chimica Acta **2013**, 415, 317-321.

(7) Yang, H.; Yuan, R.; Chai, Y.; Su, H.; Zhuo, Y.; Jiang, W.; Song, Z. Electrochimica Acta **2011**, 56, 1973-1980.

(8) Xuan Viet, N.; Chikae, M.; Ukita, Y.; Maehashi, K.; Matsumoto, K.; Tamiya, E.; Hung Viet, P.; Takamura, Y. Biosensors and Bioelectronics **2013**, 42, 592-597.

(9) Hu, J.; Wang, S.; Wang, L.; Li, F.; Pingguan-Murphy, B.; Lu, T. J.; Xu, F. Biosensors & Bioelectronics **2014**, 54, 585-597.

(10) Sun, J.; Xianyu, Y.; Jiang, X. Chemical Society Reviews **2014**, 43, 6239-6253.

(11) Ramachandran, S.; Fu, E.; Lutz, B.; Yager, P. Analyst **2014**, 139, 1456-1462.

(12) Chin, C. D.; Linder, V.; Sia, S. K. Lab on a Chip **2012**, 12, 2118-2134.

(13) Yeo, C. P.; Ngo, A.; Ng, W. Y.; Lim, S. H. Proc Singap Healthc **2011**, 20.

(14) Yetisen, A. K.; Akram, M. S.; Lowe, C. R. Lab on a Chip **2013**, 13, 2210-2251.

(15) Warsinke, A. Analytical and Bioanalytical Chemistry **2009**, 393, 1393-1405.

(16) Araci, I. E.; Brisk, P. Current Opinion in Biotechnology **2014**, 25, 60-68.

(17) Hart, R. W.; Mauk, M. G.; Liu, C.; Qiu, X.; Thompson, J. A.; Chen, D.; Malamud, D.; Abrams, W. R.; Bau, H. H. Oral Diseases **2011**, 17, 745-752.

(18) Gervais, L.; Delamarche, E. Lab on a Chip **2009**, 9, 3330-3337.

(19) Xu, Y.; Liu, Y.; Wu, Y.; Xia, X.; Liao, Y.; Li, Q. Analytical Chemistry **2014**, 86, 5611-5614.

(20) Karakus, C.; Salih, B. A. Journal of immunological methods **2013**, 396, 8-14.

(21) Mansfield, M. A. Drugs of Abuse: Body Fluid Testing **2005**, 71-85.

(22) Ngom, B.; Guo, Y.; Wang, X.; Bi, D. Analytical and Bioanalytical Chemistry **2010**, 397, 1113-1135.
(23) Liu, C.; Jia, Q.; Yang, C.; Qiao, R.; Jing, L.; Wang, L.; Xu, C.; Gao, M. Analytical chemistry **2011**, 83, 6778-6784.
(24) Cho, J. H.; Paek, E. H.; Cho, I. H.; Paek, S. H. Analytical Chemistry **2005**, 77, 4091-4097.
(25) Xia, X.; Xu, Y.; Zhao, X.; Li, Q. Clinical Chemistry **2009**, 55, 179-182.
(26) Parolo, C.; de la Escosura-Muñiz, A.; Merkoçi, A. Biosensors and Bioelectronics **2013**, 40, 412-416.
(27) Martinez, A. W.; Phillips, S. T.; Whitesides, G. M.; Carrilho, E. Analytical Chemistry **2010**, 82, 3-10.
(28) Nie, Z.; Nijhuis, C. A.; Gong, J.; Chen, X.; Kumachev, A.; Martinez, A. W.; Narovlyansky, M.; Whitesides, G. M. Lab on a Chip **2010**, 10, 477-483.
(29) MacKay, S.; Wishart, D.; Xing, J. Z.; Chen, J. Biomedical Circuits and Systems, IEEE Transactions on **2014**, 8, 4-14.
(30) Haarburger, D.; Pillay, T. S. Journal of Clinical Pathology **2011**, 64, 546-548.
(31) Ghalioungui, P.; Khalil, S.; Ammar, A. Medical history **1963**, 7, 241-246.
(32) Cha, J.; Sun, X.; Dey, S. K. Nature Medicine **2012**, 18, 1754-1767.
(33) Muzzio, D.; Zygmunt, M.; Jensen, F. Frontiers in endocrinology **2014**, 5.
(34) Bansal, A. S.; Bora, S. A.; Saso, S.; Smith, J. R.; Johnson, M. R.; Thum, M.-Y. Expert Review of Clinical Immunology **2012**, 8, 747-753.
(35) Baldrich, E.; Restrepo, A.; O'Sullivan, C. K. Analytical Chemistry **2004**, 76, 7053-7063.
(36) Wang, A. Z.; Farokhzad, O. C. Journal of Nuclear Medicine **2014**, 55, 353-356.
(37) Ellington, A. D.; Szostak, J. W. Nature **1990**, 346, 818-822.
(38) Geiger, A.; Burgstaller, P.; vonderEltz, H.; Roeder, A.; Famulok, M. Nucleic Acids Research **1996**, 24, 1029-1036.
(39) Wallis, M. G.; Vonahsen, U.; Schroeder, R.; Famulok, M. Chemistry & Biology **1995**, 2, 543-552.
(40) Germer, K.; Leonard, M.; Zhang, X. International journal of biochemistry and molecular biology **2013**, 4, 27.
(41) Cass, A. E.; Zhang, Y. Faraday discussions **2011**, 149, 49-61.
(42) Luzi, E.; Minunni, M.; Tombelli, S.; Mascini, M. TrAC Trends in Analytical Chemistry **2003**, 22, 810-818.

(43) Drolet, D. W.; Moon-McDermott, L.; Romig, T. S. Nature biotechnology **1996**, 14, 1021-1025.
(44) Faraji, A. H.; Wipf, P. Bioorganic & medicinal chemistry **2009**, 17, 2950-2962.
(45) Hans, M.; Lowman, A. Current Opinion in Solid State and Materials Science **2002**, 6, 319-327.
(46) Mohanraj, V.; Chen, Y. Tropical Journal of Pharmaceutical Research **2007**, 5, 561-573.
(47) Kumar, A.; Srivastava, A.; Galaev, I. Y.; Mattiasson, B. Progress in Polymer Science **2007**, 32, 1205-1237.
(48) Roy, I.; Gupta, M. N. Chemistry & biology **2003**, 10, 1161-1171.
(49) Davis, S.; Wilding, E.; Wilding, I. International journal of pharmaceutics **1993**, 94, 235-238.
(50) Nordström, P. **2011**.
(51) Wiseman, M. E.; Frank, C. W. Langmuir **2012**, 28, 1765-1774.
(52) Renedo, O. D.; Alonso-Lomillo, M.; Martínez, M. A. Talanta **2007**, 73, 202-219.
(53) Rawat, M.; Saraf, S.; Saraf, S. AAPS pharmscitech **2007**, 8, 289-297.
(54) Champion, J. A.; Katare, Y. K.; Mitragotri, S. Journal of Controlled Release **2007**, 121, 3-9.
(55) Xu, R. Particuology **2008**, 6, 112-115.
(56) Dogan-Topal, B.; Ozkan, S. A.; Uslu, B. The Open Chemical and Biomedical Methods Journal **2010**, 3, 56-73.
(57) Lu, Y.; Shi, W.; Qin, J.; Lin, B. Analytical chemistry **2009**, 82, 329-335.
(58) Liana, D. D.; Raguse, B.; Gooding, J. J.; Chow, E. Sensors **2012**, 12, 11505-11526.